# A NUMERICAL STUDY OF POROUS-FLUID COUPLED FLOW SYSTEMS WITH MASS TRANSFER

**BAI HUIXING**

**NATIONAL UNIVERSITY OF SINGAPORE**

**2011**


# A NUMERICAL STUDY OF POROUS-FLUID COUPLED FLOW SYSTEMS WITH MASS TRANSFER

**BAI HUIXING**

(B. Eng., M. Eng., Dalian University of Technology, China)

**A THESIS SUBMITTED**

**FOR THE DEGREE OF DOCTOR OF PHILOSOPHY**

**DEPARTMENT OF MECHANICAL ENGINEERING**

**NATIONAL UNIVERSITY OF SINGAPORE**

**2011**

# ACKNOWLEDGEMENTS

I would like to express my deepest gratitude to my Supervisors, Associate Professor Low Hong Tong and Associate Professor S. H. Winoto for their invaluable guidance, supervision, encouragement, patience and support throughout my PhD studies.

Moreover, I would like to thank Dr. P. Yu, Dr. Y. Zeng, Dr. X. B. Chen and Dr. Y. Sui who helped me a lot during my research period. I also want to thank all the staff members and students in Fluid Mechanics laboratory and Bio-fluids Laboratory for their valuable assistance during my research work. I also wish to express my gratitude to the National University of Singapore (NUS) for providing me a Research Scholarship and an opportunity to pursue my PhD degree.

My sincere appreciation will go to my wife, Zhao Wei, my parents, my sisters and brothers. Their love, concern, support and continuous encouragement really help me to complete this PhD study. I would like to give my special appreciation to my angels, my son Bai Leyang and my daughter Bai Siyang. They are the gifts that God specially give me. Their birth gives me more responsibilities and never ceased driving force to perform my duties and help poor people, especially children all over the world.

Finally, I would like to thank all my friends and teachers who have helped me in different ways during my whole period of study in NUS.

# TABLE OF CONTENTS

# SUMMARY

This thesis concerns the study of coupled flow systems which compose of a porous medium layer and a homogenous fluid layer. The study consists of three parts: channel partially filled with a porous medium, fluid-porous domains coupled by interfacial stress jump, microchannel reactors with porous walls. The low Reynolds number flow is studied in present work.

The flow through a channel partially filled with fibrous porous medium was analyzed to investigate the interfacial boundary conditions. The fibrous medium was modeled as a periodic array of circular cylinders, in a hexagonal arrangement, using the boundary element method. The area and volume average methods were applied to relate the pore scale to the representative elementary volume scale. The permeability of the modeled fibrous medium was calculated from the Darcy's law with the volume-averaged Darcy velocity. The slip coefficient, interfacial velocity, effective viscosity and shear jump coefficients at the interface were obtained with the averaged velocities at various permeability or Darcy numbers.

Next, a numerical method was developed for flows involving an interface between a homogenous fluid and a porous medium. The numerical method is based on the lattice Boltzmann method for incompressible flow. A generalized model, which includes Brinkman term, Forcheimmer term and nonlinear convective term, was used to govern the flow in the porous medium region. At the interface, a shear stress jump that includes the inertial effect was imposed for the lattice Boltzmann equation, together with a continuity of normal stress. The present method was

implemented on three cases each of which has a porous medium partially occupying the flow region: channel flow, plug flow and lid-driven cavity flow. The present results agree well with the analytical and/or the finite-volume solutions.

Finally, a two-dimensional flow model was developed to simulate mass transfer in a microchannel reactor with a porous wall. A two-domain approach, based on the lattice Boltzmann method, was implemented. For the fluid part, the governing equation used was the Navier–Stokes equation; for the porous medium region, the generalized Darcy–Brinkman–Forchheimer extended model was used. For the porous-fluid interface, a stress jump condition was enforced with a continuity of normal stress, and the mass interfacial conditions were continuities of mass and mass flux. The simplified analytical solutions are deduced for zeroth order, Michaelis-Menten and first order type reaction, respectively. Based on the simplified analytical solutions, generalized results with good correlation of numerical data were found based on combined parameter of effective channel distance. The effects of Damkohler number, Peclet number, release ratio and Mechaelis-Menten constant were studied. Effectiveness factor, reactor efficiency and utilization efficiency were defined. The generalized results could find applications for the design of cell bioreactors and enzyme reactors with porous walls.

# NOMENCLATURE

| | |
|---|---|
| $a$ | Release ratio (release rate over absorb rate) |
| $A$ | Cross-section area |
| $c$ | Lattice velocity $\Delta x/\Delta t$; substrate concentration |
| $c_{bot}$ | Concentration at bottom |
| $c_{in}$ | Concentration at inlet |
| $c_{\text{int}}$ | Concentration at interface |
| $\overline{c}_{out}$ | Average concentration at outlet |
| $c_s$ | Speed of sound |
| $C$ | Non-dimensional concentration |
| $C_{bot}$ | Non-dimensional concentration at bottom |
| $C_F$ | Forchheimer coefficient |
| $C_{in}$ | Non-dimensional concentration at inlet |
| $C_{\text{int}}$ | Non-dimensional concentration at interface |
| $C_q$ | Contour of $qth$ particle |
| $d$ | Diameter of the circular cylinder |
| $Dam$ | Damkohler number |
| $Dam_{fa}$ | Damkohler number for absorption cell in fluid region |
| $Dam_{fr}$ | Damkohler number for release cell in fluid region |
| $Dam_{pa}$ | Damkohler number for absorption cell in porous region |
| $Dam_{pr}$ | Damkohler number for release cell in porous region |
| $Da$ | Darcy number, $K / H^2$ |

| | |
|---|---|
| $D$ | Diffusivity in plain fluid region |
| $Deff$ | Effective diffusivity |
| $\boldsymbol{e}_i$ | Particle velocity vector along direction $i$ |
| $f_i$ | Particle distribution function |
| $f_i^D$ | Disturbance component of the hydrodynamic traction |
| $f_i^{\mathrm{eq}}$ | Equilibrium particle distribution function |
| $g$ | Gravity constant |
| $G$ | Body force |
| $h$ | Height of porous region |
| $H$ | Height of fluid region |
| $H_1$ | Height of homogeneous fluid region |
| $H_2$ | Height of fluid-saturated porous medium region |
| $k$ | Carman-Kozeny constant |
| $k_m$ | Half-saturation parameter, Michaelis-Menten constant |
| $K_m$ | Non-dimensional Michaelis-Menten constant |
| $K$ | Permeability |
| $l_1, l_2$ | Representative element volume cell dimensions |
| $l_e$ | Ratio of the cylinder radius to the cell radius |
| $l_n$ | Ratio of half the center spacing divided by the cylinder radius |
| $L$ | Length |
| $\vec{n}$ | Unit vector normal to the interface |
| $p$ | Intrinsic average pressure |
| $p^*$ | Local average pressure $p^* = \varepsilon p$ |
| $P_r$ | Prandtl number |
| $Pe$ | Peclet number |

| | |
|---|---|
| $Pe_f$ | Peclet number for fluid region |
| $Pe_p$ | Peclet number for porous region |
| $Q$ | Flow rate |
| $Ra$ | Rayleigh number |
| $Re$ | Reynolds number |
| $Sc$ | Schmidt number |
| $T$ | Temperature |
| $u, v$ | Velocity at x-coordinate and y-coordinate |
| $u_0$ | Lid driven top lid velocity |
| $u_a$ | Mean velocity |
| $u_D$ | Darcy velocity |
| $u_{f\_av}$ | Average flow velocities in fluid region |
| $u_{\text{int}}$ | Interface velocity |
| $u_n$ | Velocity component normal to the interface |
| $u_{p\_av}$ | Average flow velocities in porous region |
| $u_t$ | Velocity component parallel or tangential to the interface |
| $U, V$ | Dimensionless velocity, $u / u_D$ |
| $\vec{v}_{\text{int}}$ | Interface velocity vector |
| $v_f$ | Volume fraction of the fibrous medium |
| $V_m$ | Maximum substrate uptake or release rate per cell |
| $V_{ma}$ | Maximum substrate uptake rate for absorption |
| $V_{mr}$ | Maximum substrate release rate for release |
| $x, y$ | Cartesian coordinates |
| $y'$ | Distance at y-coordinate to calculate volume averaged interface velocity |

| | |
|---|---|
| $X, Y$ | Dimensionless Cartesian coordinates, $x/H$ and $y/H$ |

**Greek Symbols**

| | |
|---|---|
| $\alpha$ | Slip coefficient |
| $\beta_C$ | Stress jump coefficient in Chandesris & Jamet's model |
| $\beta, \beta_O, \beta_1$ | Stress jump coefficient in Ochoa-Tapia & Whitaker's model |
| $\gamma$ | Cell density |
| $\gamma_a$ | Cell density of absorption cell |
| $\gamma_r$ | Cell density of release cell |
| $\varepsilon$ | Porosity |
| $\eta$ | Reactor efficiency |
| $\eta_u$ | Utilization efficiency (or conversion rate) |
| $\lambda$ | Reaction rate parameter |
| $\mu, \mu_f$ | Fluid dynamic viscosity |
| $\mu_{eff}$ | Brinkman effective viscosity |
| $\nu$ | Fluid kinematic viscosity |
| $\nu_e$ | Effective (Brinkman) kinematic viscosity |
| $\xi$ | Local effectiveness factor |
| $\rho$ | Mass density of the fluid |
| $\omega_i$ | Weight coefficients for the equilibrium distribution function |

**Superscripts**

| | |
|---|---|
| $D$ | Disturbance component |
| eq | Local equilibrium |
| $\infty$ | Far-field incident component |

| | |
|---|---|
| $\bar{}$ | Average value along cross section / outlet / inlet etc. |

**Subscripts**

| | |
|---|---|
| a | Substrate absorption |
| bot | Bottom position |
| D, *Da* | Darcy |
| eff | Effective property |
| f | Fluid side property |
| fluid | Fluid side property |
| i | Component in direction $\mathbf{e}_i$ |
| in | Inlet position |
| int | Interface position |
| n | Direction normal to the interface |
| out | Outlet position |
| p | Porous side property |
| porous | Porous side property |
| r | Substrate release |
| t | Direction parallel or tangential to the interface |
| $y = 0$ | Position in y-coordinate at $y = 0$ |
| 0 | Initial state |
| + | Upper side of interface |
| – | Below side of interface |
| $\_av$ | Average value |

**Abbreviations**

| | |
|---|---|
| 2-D | Two-dimensional |
| 3-D | Three-dimensional |
| BEM | Boundary element method |
| D2Q5 | Two-dimensional five speed |
| D2Q9 | Two-dimensional nine speed |
| EDF | Equilibrium distribution function |
| FDM | Finite difference method |
| FEM | Finite element method |
| FVM | Finite volume method |
| GLBM | Generalized Lattice Boltzmann method |
| LBE | Lattice Boltzmann equation |
| LBM | Lattice Boltzmann method |
| LTE | Local thermal equilibrium |
| OUR | Oxygen uptake rate |
| REV | Representative elementary volume |
| SUR | Substrate uptake rate |
| TDF | Temperature distribution function |

# LIST OF FIGURES

# LIST OF TABLES

# Chapter 1 Introduction

## 1.1 Background

The study of flow systems, which consists of porous media and homogenous fluids, is relevant to a wide range of industrial and environmental applications. Examples of practical applications are drug delivery with porous microspheres, fuel cells, drying process, electronic cooling and ceramic processing, and bioreactors with porous scaffolds. The porous matrix in the bioreactor provides opportunities for the cells to grow into three-dimensional spaces, and thus maintain their normal functional activities. Another interesting application is enzyme reactors which have porous silicon etched along the walls in the microchannels. Glucose oxidase was immobilized on the porous structure and the enzyme activity was monitored following a colorimetric assay.

To analyze flow in a domain partially filled with a porous medium, it is needed to couple the flow equations of the fluid and porous regions by using the interfacial boundary conditions. The interfacial conditions will also influence the heat and mass transfer across the interface. To investigate the interfacial boundary conditions, simple models of flow through a channel partially filled with a porous medium have been considered. These studies can be classified into three types according to scales: the pore scale, the representative elementary volume (REV) scale, and the domain scale.

In the pore scale, the fluid in the pores of the medium have been directly studied. In this scale, the detailed flow characteristics in the pores can be obtained, and these characteristics can be used to predict the values of the parameters and flow properties for the domain scale and REV scale. In the pore scale, the pore structures are always irregular and difficult to be averaged over a representative elementary volume (REV). Numerical simulation of porous media with heterogeneous or non-homogeneous elements will need finer mesh which will definitely greatly increase the computation cost. For some large scale application scenarios, pore scale study is almost impossible based on present hardware and simulation technologies. Hence the application of pore scale studies in complex engineering problems present challenging problems.

The representative elementary volume (REV) is a statistical representation of typical material properties. It is defined as a smallest volume over which a measurement of characteristics can be made that will yield a value representative of the flow region. Below REV, the parameter is not defined and the material cannot be treated as a continuum. The REV scale is much larger than the pore scale but much smaller than the domain scale. The main advantages of the REV scale are its high computational efficiency and easy of application compared with the pore scale. Many studies have been done in the REV scale in the past several decades for porous material with homogeneous elements. Several important volume averaged parameters of porous media, such as permeability, effective viscosity, velocity and pressure, can only be predicted from REV scale experiment or numerical analysis.

In the domain scale, the whole porous media flow domain was considered as homogeneous in every grid point inside the porous media. One set of governing

equations was implemented in each selected domain. The literature review for domain scale study will be presented in Section 1.2.2.

The judgment of whether a material is homogeneous or heterogeneous depends on how large the scale is. In the present work, the material will be homogeneous if its properties can be represented by volume averaged values over a selected REV.

## 1.2 Literature Review

### 1.2.1 Porous flow modeling in pore and REV scale

For the porous medium, an important parameter is permeability. Theoretical and numerical predictions of permeability have been made based on approximations over the REV scale volume average. Kozeny et al. (1927) approximated the porous medium by tortuous capillaries to develop an expression for the permeability. In the Carman-Kozeny model (Carman 1937), a hydraulic diameter is defined from the specific surface area and porosity of the packed bed of particles. By applying the Poiseuille equation, the permeability is obtained in terms of the particle diameter, porosity, and a Carman-Kozeny constant. The Carman-Kozeny model has been commonly used for granular porous media.

For fibrous media, due to its anisotropy, it is more appropriate to model them by arrays of cylinders. The solid volume fraction of the fibrous medium is a fraction of the volume of cylinders over the total volume, between 0-1. On the contrary, the porosity is a fraction of the volume of void spaces over the total volume. The permeability is obtained from the drag resistance across the cylinders. Two extreme

cases were considered to obtain a closed form solution for the whole range of porosity: closed packed and widely spaced cylinders.

The lubrication theory by Keller (1964) is used for low porosities when the cylinders are closely packed. The pressure drop over the small gap between cylinders can be calculated analytically to give the permeability of the array (Happel 1959):

$$\frac{K}{d^2} = \frac{1}{12}\frac{\left(1-l_n^2\right)^2}{l_n^3}\left[3l_n\frac{\arctan\left[\sqrt{\frac{1+l_n}{1-l_n}}\right]}{\sqrt{1-l_n^2}}+\frac{1}{2}l_n^2+1\right]^{-1} \tag{1.1}$$

where $d$ is the cylinder diameter, $K$ is the permeability of the porous medium and $l_n$ is the ratio of half the center spacing divided by the cylinder radius and can be expressed by the volume fraction as:

$$l_n^2 = \frac{4}{\pi}v_f \tag{1.2}$$

where $v_f$ is the volume fraction of the fibrous medium.

The unit cell model is used for high porosities when the cylinders are widely spaced. It assumes that the cylinders are spaced far away so that the region can be divided into independent cells. Thus the arrangement of the fibers has no effects on the solution. Typically a circular cell is adopted with the cylinder located in the centre, whose radius depends on the porosity. From the drag on the cylinder the permeability can be obtained (Happel 1959):

$$\frac{K}{d^2} = -\frac{l_e^2}{16}\left[\ln\left(l_e\right)-\frac{3}{4}+l_e^{-2}-\frac{l_e^4}{4}\right] \tag{1.3}$$

where $l_e$ is the ratio of the cylinder radius to the cell radius and is related to volume fraction of the porous medium by:

$$l_e^2 = \frac{1}{v_f} \tag{1.4}$$

where $v_f$ is the volume fraction of the fibrous medium.

Different mathematical treatments have been used in the cell model based on Stokes flow. For example, there are the free-surface models of Happel (1959) with zero drag force and Kuwabara (1959) with vorticity free boundary condition. There are also methods using Fourier series to calculate the drag force of the cylinder in the cell model, for example those of Hasimoto (1959), and Sangani and Acrivos (1982a 1982b). The method of singularities was used by Lord Rayleigh (1892) and Drummond and Tahir (1984). Wang (1996, 1999 and 2001) used the eigenfunction expansion method.

In addition to methods for the extreme cases, there is a hybrid model of Bruschke and Advani (1993) which attempts to predict the permeability over the full porosity range. The approach combines functions from both the lubrication and cell models. Weighting functions, which depend on the porosity, are used to make the solution tends asymptotically to the extreme cases of lubrication or cell models. The asymptotic model gives a smooth transition from lubrication to cell model, which covers the middle range of porosity. The asymptotic model is given in terms of the porosity (Bruschke and Advani 1993):

$$\frac{K}{d^2} = \frac{1}{16(1-\varepsilon)}\left[\ln\left(\sqrt{\frac{1}{1-\varepsilon}}\right) - \frac{3}{4} + (1-\varepsilon) - \frac{(1-\varepsilon)^2}{4}\right] \tag{1.5}$$

where $\varepsilon$ is the porosity.

### 1.2.2 Porous flow modeling in domain scale

The velocity in a porous medium is related to the pressure gradient by the Darcy's law (Vafai, 2000):

$$u = -\frac{K}{\mu}\frac{\partial p}{\partial x} \tag{1.6}$$

where $p$ is the interstitial pressure, $u$ is the mean filter velocity, $\mu$ is the dynamic viscosity of the fluid, $K$ is the permeability of porous media.

Darcy's law is valid only when the flow is of the seepage type and the fluid is homogeneous. The Darcy's law can be considered valid in situations where the flow is of creeping type (Greenkorn, 1981) or when the porous medium is densely packed with small enough permeability (Rudrauah and Balachandra, 1983), so that the pore Reynolds number based on the local volume averaged speed is less than unity. However, Darcy's law neglects the boundary and inertial effects of the fluid flow due to the small porosity associated with the medium. When the velocity gradient is high, viscous effects cannot be taken into account in this law, especially in the presence of a solid wall, due to its low order accuracy. When the fluid Reynolds number is large enough, it will over predict the actual fluid motion and the other effects (for example, inertial, viscous and convective effects) cannot be neglected (Vafai and Tien, 1981; Hsu and Cheng, 1990).

Non-Darcian effects have been incorporated to account for the other effects in porous flow. Forchheimer (1901) suggested a modification to the previous models to

account for inertia effect. This was due to the rather high speed of the flow in some porous media, which was neglected in Darcy's law. Lapwood (1948) and Yin (1965) added the unsteady term in the Darcy's law to account for temporal acceleration. Brinkman (1947a, 1947b) introduced a viscous term by examining the flow past a spherical particle to account for the viscous shear stresses that acted on the fluid element. An effective fluid viscosity inside the porous domain was used in his formulation.

When all the unsteady, inertia and viscous effects are taken into consideration, Vafai and Tien (1981), Hsu and Cheng (1990) derived the generalized Darcy-Brinkman-Forchheimer extended model, given as:

$$\nabla \cdot \vec{u} = 0 \tag{1.7}$$

$$\underbrace{\rho \frac{\partial \vec{u}}{\partial t}}_{\text{Unsteady Term}} + \underbrace{\nabla \cdot \left( \frac{\rho \vec{u} \vec{u}}{\varepsilon} \right)}_{\text{Convective Term}} = - \underbrace{\nabla \left( \varepsilon p^* \right)}_{\text{Pressure Term}} + \underbrace{\mu \nabla^2 \vec{u}}_{\text{Brinkman Term}} - \underbrace{\frac{\mu \varepsilon}{K} \vec{u}}_{\text{Darcy Term}} - \underbrace{\frac{\rho \varepsilon C_F \left| \vec{u} \right|}{\sqrt{K}} \vec{u}}_{\text{Forchheimer Term}} \tag{1.8}$$

where Equation (1.7) is the mass continuity equation; Equation (1.8) is the momentum conservation equation; $\varepsilon$ is porosity; $K$ is the permeability; $\vec{u}$ the local average velocity vector (Darcy velocity); $t$ is time; $\rho$ is the fluid density; $\mu$ is the fluid dynamic viscosity; $p^*$ is the intrinsic average pressure; and $C_F$ is Forchheimer coefficient. The local average and intrinsic average can be related by the Dupuit-Forchheimer relationship, for example, $p = \varepsilon p^*$.

Equation (1.7) and (1.8) were derived using local averaging technique. In this approach, a macroscopic variable is defined as an appropriate mean over a sufficiently large representative elementary volume (REV) (Figure 1.1). This operation yields the value of that variable at the centroid of REV (Vafai and Tien,

1981, Larson and Higdon 1987, Sahraoui and Kaviany 1992, Whitaker 1999 and Bai et al. 2009a). It is assumed that the result is independent of the size of the REV. The length scale of the REV is much larger than the pore scale, but smaller than the length scale of the macroscopic domain scale.

It should be noted that the above Equations (1.7 and 1.8) are the most general equations governing the flow of a viscous fluid in porous media. They can recover the standard Navier-Stokes equations when the porosity approaches unity and Darcy number goes to infinity. This characteristic facilitates its use for flow problems with porous/fluid coupled domains, based on a one domain approach, as reviewed later in Section 1.2.4.

### 1.2.3 Heat and mass transfer modeling

There are two kinds of models for heat transfer in porous media. One is the local thermal equilibrium (LTE) model, which is widely accepted and used in various analytical and numerical studies on transport phenomena in porous media. It is assumed that both the fluid and solid phases are at the same temperature (Vafai and Tien, 1981; Hsu and Cheng, 1990; Nithiarasu et al., 1997 and 2002), due to the high conductivity value of the solid parts in porous media. Under the assumption of LTE, many investigators have used one unique set of equation to obtain temperature distributions in a porous medium because an analysis based on the one-equation model is simple and straightforward. The other model is local thermal non-equilibrium (LTNE) model, where two sets of energy equations are used to treat the solid phase and the fluid phase separately (Khashan et al., 2006; Haddad et al., 2007).

This model is employed when temperature difference between the two phases is considered as a crucial design parameter.

## 1.2.4 Porous and fluid coupled systems

From the modeling point of view, three different approaches can be used to represent transport phenomena in coupled fluid and porous domains: domain scale, REV scale and pore scale. Domain scale studies can be classified as: one-domain and two-domain approaches. The detailed comparison of one-domain and two-domain approaches has been given out by Goyeau et al. (2003) and here their main differences are discussed. Table 1.1 lists classifications for modeling of coupled fluid and porous medium system.

### 1.2.4.1 Domain scale modeling

In the one-domain approach, the porous region is considered as a pseudo-fluid and the whole regions including fluid and porous domains are treated as a continuum. One set of general governing equations is applied for the whole domain (Mercier et al. 2002, Jue 2004, Silva and Lemos 2003, Costa et al. 2004, Goyeau et al. 2003). The transition from the fluid to the porous medium, such as the abrupt change of permeability and porosity values across the interface, is achieved through a continuous spatial variation of properties. In this case, the explicit formulation of boundary condition is avoided at the interface and the transitions of the properties between the fluid and porous medium are achieved by certain artifacts (Goyeau et al.

2003), as the matching conditions are automatically implicitly satisfied. Thus this approach has been extensively used in previous numerical computations dealing with natural convection (Bennacer et al., 2003; Gobin et al., 2005), forced convection problems (Zhang and Zhao, 2000; Abu-Hijleh, 1997 and 2000) in coupled fluid and porous domains.

However, in the one-domain approach attention should be paid to the abrupt jump of permeability and porosity along the interface which may result in numerical instabilities (Basu and Khalili, 1999). It may be overcome by unphysical numerical techniques (Basu and Khalili, 1999). Thus, its physical representation of momentum conservation at the interfacial region depends on the relevance of the discretization scheme (Goyeau et al., 2003). Although the one-domain approach is relatively easy to implement, the flow behavior at the interface depends on how the code is structured (Nield 1997, Yu et al. 2007) and hence it is not a good choice to solve coupled flow and porous domains.

In the two-domain approach, two sets of conservation governing equations are applied to describe the flow in the two domains separately and additional boundary conditions are applied at the interface to couple the two sets of equations. Interfacial boundary conditions for flow and heat transfer at the porous-fluid interface have been proposed previously and summarized in Tables 1.2 and 1.3.

*Slip and non-slip interface conditions*

The earliest study on the interfacial conditions is that by Beavers and Joseph (1967). In their approach, the flows in a homogeneous fluid and a porous medium are governed by the Navier-Stokes and Darcy equations respectively. The governing equations are of different orders in the different regions. Thus a semi-empirical slip boundary condition was proposed at the interface to couple the equations, where the slip coefficient depends on the local microstructure geometry of the interface. The interface condition contained a jump in both stress and velocity. To make the governing equations of the same order, Neale and Nader (1974) introduced the Brinkman term in the Darcy equation for the porous medium. The continuity of both stress and velocity was proposed at the interface. An analytical solution of this model was deduced by Vafai and Kim (1990). Another interfacial boundary condition involving continuous stress was proposed by Kim and Choi (1996) who used the effective viscosity in the porous medium.

Alternatively, Brinkman correction to Darcy's law (Brinkman, 1947a, 1947b) can be used to meet the second order requirement in the porous region. Therefore, continuity of both velocity and shear stress can be satisfied at the interface. However, stress jump conditions can also be written in order to account for the heterogeneity of the interfacial region (Ochoa-Tapia and Whitaker, 1995a). In the two-domain approach, the involved adjustable parameters (slip coefficient, stress jump coefficient) are difficult to predict and need further practical experiments to validate their values (Ochoa-Tapia and Whitaker, 1995b).

*Stress-jump interface conditions*

The non-continuity of both velocity gradient and shear stress has been developed by Ochoa-Tapia and Whitaker (1995a, 1995b). The development was based on the non-local form of the volume averaged Stokes' equation. The length-scale constraint was that the radius of the averaging volume is much smaller than the height of the fluid channel. Under these assumptions, the volume-averaged equations in the homogeneous fluid regions are equivalent to the point equations; and the analysis of jump condition is greatly simplified because a single volume-averaged transport equation is used in both fluid and porous regions. The jump condition links the Darcy law, with Brinkman's correction, to the Stokes equation. The analysis produced a jump in the stress but not in the velocity. The normal component of jump condition simply reduced to continuity of pressure. The function for the jump coefficient indicates dependence on permeability and porosity and was complex to solve. The coefficient was expected to be of order one, and may be either positive or negative. It was noted that the parameter depends on $\sqrt{K}/\delta$ where $\delta$ is the thickness of the boundary region.

Subsequently, Ochoa-Tapia and Whitaker (1998b) developed another stress jump condition which includes the inertial effects. Though inertial effects may be negligible in homogeneous regions of channel flow, it is not negligible in the boundary between the porous and fluid regions. Outside the boundary regions, the non-local form of the volume-averaged momentum equation reduces to the Forchheimer equation with Brinkman correction and the Navier Stokes equation. Two

coefficients appear in this jump condition: one is associated with an excess viscous stress and the other is related to an excess inertial stress.

The stress jump parameter (associated with an excess viscous stress) was derived by Goyeau et al. (2003) as an explicit function of the effective properties of a transition layer between the fluid and porous regions. The parameter is also related to the variations of the velocity in the transition layer, which is an unknown in the problem. Recently, Chandesris and Jamet (2006) presented a model in which the shear jump is built on fluid stress rather than effective stress. An explicit function for the stress jump coefficient was obtained which only depends on the characteristics of the porous medium (porosity and permeability) in the transition zone.

*Heat and mass transfer interfacial conditions*

For heat transfer interface conditions, usually continuities of temperature and heat flux are required (Neale and Nader, 1974; Vafai and Thiyagaraja, 1987; Ochoa-Tapia and Whitaker, 1997; Jang and Chen, 1992; Kim and Choi, 1996; Kuznetsov, 1999). However, other types of interfacial conditions are also possible. Ochoa-Tapia and Whitaker (1998a) proposed a jump condition for heat flux to account for its production or consumption at the interface. Another hybrid interfacial condition, continuity of heat flux but non-continuity in temperature, was proposed by Sahraoui and Kaviany (1994).

For mass transfer interface conditions, Valencia-Lopez et al. (2003) developed a mass jump condition that representing the excess surface accumulation, convection,

diffusion adsorption and a nonequilibrium source, in addition to a term representing the exchange with the surrounding region. Recently, the closure problem has been derived by Valdes-Parada et al (2006 and 2007b) to predict the jump coefficient as a function of the microstructure of the porous layer.

*Numerical techniques for coupled fluid and porous domains*

Numerical solutions for the coupled viscous and porous flows have been attempted by many researchers with the two-domain approach (Gartling et al., 1996; Costa et al., 2004; Betchen et al., 2006). Costa et al. (2004) proposed a control-volume finite element method to simulate the problems of coupled viscous and porous flows. A continuity of both velocity and stress at the interface was assumed and no special or additional procedure was needed to impose the interfacial boundary conditions. Betchen et al. (2006) developed a finite volume model, also based on continuity of both velocity and stress, but special attention was given to the pressure-velocity coupling at the interface.

The implementation of the numerical methodology on the stress jump condition based on Ochoa-Tapia and Whitaker (1995a, 1995b) can be found in the work of Silva and de Lemos (2003). They used the finite volume method with an orthogonal Cartesian coordinate system which is not easy to apply for complex geometries. The jump in shear stress was considered and there was no special treatment on velocity derivatives. Alazmi and Vafai (2001) proposed different types of interfacial

conditions between a porous medium and a homogenous fluid, and found that interfacial conditions have pronounced effects on the velocity field.

Recently, Yu et al. (2007) developed a numerical method based on finite volume method with a collocated variable arrangement to treat the stress jump condition given by Ochoa-Tapia and Whitaker (1998), which includes the inertial effects. Yu et al. (2007) used body-fitted and multi-block grids to treat the fluid and porous regions. Their method is effective for the coupled problems in homogeneous fluid and porous medium regions with complex geometries.

The main drawback of the stress jump condition is that its parameters are unknown. This closure problem has been investigated by many researchers recently (Goyeau et al., 2003; Chandesris and Jamet, 2006; Valdes-Parada et al., 2007; Chandesris and Jamet, 2007) and derivations have been proposed to evaluate the first stress-jump parameter which is viscous related.

#### 1.2.4.2 Pore and REV scale modeling

In the pore and REV scale approach, there were a few studies giving solutions which describe the interfacial flow for fibrous porous media. Most studies were modeled by flow in a channel partially filled with an array of cylinders. Usually the volume averaged slip velocity and the volume averaged effective viscosity were investigated. There were very few attempts on analysis of stress jump coefficients.

Larson and Higdon (1987) analyzed the shear flow near the surface of a porous medium, as modeled by cylindrical array, using boundary integral method. The volume averaged slip velocity and dimensionless effective viscosity were presented

as function of solid-volume fraction. The slip coefficient was found to be sensitive to the definition of the interface which they defined to be at the centre of the outermost cylinder.

Sahraoui & Kaviany (1992) also modeled the porous medium by cylindrical arrays and used finite difference method to study the interfacial boundary conditions. The flow characteristics were volume averaged over selected REV. The volume averaged slip coefficient was presented in terms of Reynolds number and the distribution of the local effective viscosity was given. Their results of volume averaged slip coefficient agree well with the experiments of Beavers and Joseph (1967).

James and Davis (2001) used a singularity method to solve the flow field for cylindrical arrays of large porosity (greater than 0.9). Their calculations showed that the external flow penetrated the porous medium very little. The volume averaged slip velocity was found to be about 0.4 of that predicted from the Brinkman model (based on effective viscosity).

## 1.2.5 Lattice Boltzmann method approach

### 1.2.5.1 Lattice Boltzmann modeling development for flow in porous media

Besides the above macroscopic methods, another mesoscopic method to simulate the porous fluid flow is to use the lattice Boltzmann method (LBM). The standard Lattice Boltzmann Equation (LBE) was revised by adding an additional term to account for the influence of the porous medium (Spaid and Phelan 1997 & 1998,

Dardis and McCloskey 1998, Freed 1998, Martys 2001 and Kang et al. 2002). In this method, the detailed medium structure and direction is usually ignored, including the statistical properties of the medium into the model. Thus, it is not suitable to obtain detailed pore scale flow information. But the LBM with REV scale could be used for porous medium system of large size. Some examples of the models with REV scales are discussed below.

Dardis and McCloskey (1998) proposed a Lattice Boltzmann scheme for the simulation of flow in porous media by introducing a term describing the no-slip boundary condition. By this approach, the loss of momentum resulting from the solid obstacles is incorporated into the evolution equation. A number ordered parameter of each lattice node related to the density of solid scatters is used to represent the effect of porous medium solid structure on the hydrodynamics. Their method removes the need to obtain spatial averaging and temporal averaging, and avoid the microscopic length scales of the porous media.

Spaid and Phelan (1997) proposed a SP model of LBM which is based on the Brinkman equation for single component flow in heterogeneous porous media. The scheme uses a hybrid method in which the Stokes equation is applied to the free domains and the Brinkman equation is used to model the flow through the porous structures. The particle equilibrium distribution function was modified to recover the Brinkman equation. Through this way, the magnitude of momentum at specified lattice nodes is reduced and the momentum direction is kept.

Freed (1998) proposed a similar approach by using an additional force term to simulate flows through a resistance field. An extension term was implemented to

modify the standard lattice BGK model (LBGK), which results in a local resistance force appropriate for simulating the porous medium region. Results of the simulation for uniform flow confirmed that the LBGK algorithm yields the satisfied and precise macroscopic behaviors. Also, it was observed that the fluid compressibility simulated by LBM influences its ability to simulate incompressible porous flows.

Later the SP model was combined with a multi-component Lattice Boltzmann algorithm to extend for multi-component system (Spaid and Phelan 1998). The method was developed by introducing a momentum sink to simulate the multi-component fluid flow of a fiber system. It was confirmed that the model is useful to simulate the multi-component fluid flow system. By using the LBM, the complex interface between two immiscible fluids can be easily dealt with without special treatment of the interface by tracking algorithm.

Shan and Chen (1993) combined the Stokes/Brinkman LBM with the algorithm to model the multi-component infiltration of the fiber microstructure. The developed LBM is suitable to simulate flows containing multiple phases and multi-components immiscible fluids of different masses in constant temperature. One of the main improvements of this model is to include a dynamical temperature. The component equilibrium state can have a non-ideal gas state equation at a given temperature showing phase transitions of thermodynamics.

The SP model was improved to generalize the LBM by introducing an effective viscosity into the Brinkman equation to improve the accuracy and stability (Martys 2001). The approach can describe the general case when fluid viscosity is not the same as the effective viscosity. By implementing the dissipative forcing term into a

linear body force term, the validity of the Brinkman equation is extended to a larger range of forcing and effective viscosity. This model eliminates the second order errors in velocity and improves stability over the SP model. It also improves the accuracy of other applications of the model, such as fluid mixtures.

The discussed Brinkman model and improved models have been shown to be an easily implemented and computationally efficient method to simulate fluid flows in porous media. However, these models are based on some relatively simple semi-empirical models such as Darcy or Brinkman models. Therefore they have some intrinsic limitations. Vafai and Kim (1995) pointed out that if there is no convective term, the driving force of the flow field does not exist. Since Brinkman model does not contain the nonlinear inertial term, it is only suitable for low-speed flows.

Recently, a generalized lattice Boltzmann method called GLBM (Guo and Zhao 2002) was developed for isothermal incompressible flows. It is used to overcome the limitations of the Darcy or Brinkman model for flows in porous media. GLBM could automatically deal with the interfaces between different media without applying any additional boundary conditions. This enables the GLBM suitable to model flows in a medium with a variable porosity. The GLBM is based on the general Navier–Stokes model and considered the linear and nonlinear matrix drag components as well as the inertial and viscous forces. The inertial force term of GLBM is based on a recently developed method (Guo et al. 2002), and the newly defined equilibrium distribution function is modified to simulate the porosity of the medium. Because the GLBM is very close to the standard LBM, the GLBM solvers for the generalized Navier-Stokes equations are similar to the standard LBM solvers for the Navier-Stokes equations.

Furthermore, the force term in GLBM was used to simulate the interaction between the fluid and the media. It was equivalent to implementing an effective boundary condition between the fluid and the solid (Guo and Zhao 2002). The relationship between GLBM with pore scale and GLBM with REV scale could be built through the drag force term derived directly from the boundary rules. The results also showed that the nonlinear drag force due to the porous media is important and could not be neglected for high-speed flows. The numerical results agreed well with the analytical or the finite difference solutions.

#### 1.2.5.2 Lattice Boltzmann modeling development for heat and mass transfer in porous media

For heat transport problem, the internal energy evolution equation was first given by He et al. (1998) using the two dimensional nine speed (D2Q9) lattice Boltzmann method (LBM). Later, Guo and Zhao (2005) revised the model of He et al. (1998) and presented one simpler temperature distribution function (TDF) and equilibrium temperature distribution function (ETDF). They also successfully extended their new model to porous medium flow and heat transfer. There are also many other studies in heat transfer using LBM (Peng et al. 2003, Zhang 2008, Chen et al. 2009 etc.).

For mass transfer problem, the distribution function is similar to that of heat transfer problem because the governing equations are the convection and diffusion equation, which are similar for heat or mass transfers. For example, Chen et al. (2007) simulated corrosion behavior and oxygen transport in the natural convection lead-

alloy flow. There is no novelty in their temperature and mass distribution functions; their models are similar to that of Guo and Zhao (2005). Chen (2007) also used the same model of Guo and Zhao (2005) to simulate oxygen transfer in an enhanced forced convection system.

As for the heat source or mass source problems, Zhang (2008) presented a lattice Boltzmann model for Pennes bioheat equation, which includes a temperature-dependent heat source term. Yamamoto et al. (2005) presented a LBM formula for temperature and mass concentration, which contains the source term due to chemical reaction.

#### 1.2.5.3 Lattice Boltzmann modeling development for coupled system

Martys (2001) used the lattice Boltzmann method (LBM) to model the flow through and over a partial porous medium in a channel. The study assumed continuation of both velocity and shear stress at the interface, by defining an effective viscosity term. The Stokes and Brinkman equations were used for fluid and porous flow respectively. Through a Chapmann-Enskog procedure, these governing equations can be transformed into lattice Boltzmann equations (LBE). A body force term caused by the porous medium was incorporated into the LBE as a linear first order or second order Hermite polynomials.

Later, Guo and Zhao (2002) extend the study by using the generalized Navier-Stokes equation and Darcy-Brinkmann-Forchheimer equation for the fluid and porous medium respectively. They also assumed continuation of both velocity and shear stress at the interface using the effective viscosity. In their study, the porosity was

included into the equilibrium distribution function, and a body force term was added to the LBE to account for the linear and nonlinear drag forces caused by the porous medium.

In the existing LBM models for coupled flow with fluid and porous media, the assumed boundary condition is based on the continuation of shear stress at the interface through the use of the effective viscosity. However, as described earlier, there are other suitable boundary conditions, for example the stress jump conditions, which was derived under consideration of the Brinkman term and inertial term; and may be of importance to practical applications in mechanical, chemical and biological engineering. It would be of interest to examine how the stress jump conditions can be incorporated into the LBM model.

At the domain scale, the LBM approach has the following advantages over the traditional CFD methods: easy implementation, natural for parallel computing and easy to treat complex boundary (Martys 2001, Guo et al. 2004). Besides the application of the LBM at the domain scale, the LBM is also capable of resolving porous media flow at the REV scale and pore scale. However, the LBM implementations of heterogeneous porous media at the pore scale demand very large lattice sizes, and both the operations and storage of the full lattices are needed; thus substantial computational and memory requirements are needed. To overcome waste of computational memory, Hou et al. (1995) presented a two-stage implementation which used a sparse lattice representation to store only the fluid cells. But their methods still have the following drawbacks (Guo et al. 2002): load imbalance, lack of nearest subdomain communication and complex communication pattern. Later, Wang

et al. (2000) contributed a cell-based domain-decomposition method for parallel lattice Boltzmann simulation of flow in porous media. Their method recovers the interfaces rather than the load balance and there was no need for iteration. The limitation of their method is assumption that all cells are either fluid or solid. However for the real porous media, the solid structure is very complex and either the fluid cells or solid cells may be of irregular shape.

### 1.2.6 Mass transfer in reactors with porous media

Numerical simulation can be a very useful tool for design of tissue engineering bioreactors with controlled mass transfer parameters. Martin et al. (2004) pointed out that computational fluid dynamics (CFD) could be used to optimize flow conditions rather than using a trial-and-error approach. Several researchers had implemented CFD methods to study fluid dynamics and mass transfer parameters in scaffolds and bioreactors. Based on the dimension scale of porous scaffolds, these studies can be classified into three different types: at a pore or/and REV scale for the analysis of fluid dynamics inside the idealized or realistic 3D micro pore structure of the scaffolds (Boschetti et al. 2006, Galbusera et al. 2007, Cioffi et al. 2006, Raimondi et al. 2002, 2004, Porter et al. 2005 and Cantini et al. 2009) and at a domain scale for the analysis of the homogeneous porous scaffolds using domain scale (Williams et al. 2002, Sengers et al. 2005, Dhanasekharan et al. 2005, Dvir et al. 2006, Ma et al. 2007, Zeng et al. 2006, 2007, 2008, Yu et al. 2009, Chen et al. 2010).

For bioreactors with porous media, experimental research has been conducted previously. Dusting et al. (2006) experimentally investigated, using particle image

velocimetry technique, the flow field and shear stress outside a scaffold in a spinner-flask bioreactor. It was found that vortex breakdown may still occur and relatively large stresses occur along the edge of scaffold protruding into the boundary of the vortex breakdown region. A perfusion bioreactor was designed (Ma et al., 1999; Zhao and Ma, 2005) with fibrous matrix walls in the channels, for tissue engineering of trophoblast and mesenchymal stem cells.

Mathematical modeling and numerical simulations have also been carried out and used to explain experimental results or cast light on research directions for mass transfer in reactors with porous media. Porter et al. (2005) applied the lattice-Boltzmann method to simulate the flow of culture media through scaffolds in a bioreactor. Micro-computed tomography imaging was used to define the micro-architecture of the scaffold for the simulations. The local shear stress was estimated from velocity derivatives at various media flow rates. Boschetti et al. (2006) developed a computational fluid dynamic model of the flow through a three dimensional scaffold of homogeneous geometry. The scaffold was idealized as composing of many subunits which were obtained by subtracting a solid sphere from a concentric solid cube.

In both of the above two approaches, a large number of elements were needed to describe the microstructure of the scaffolds. Herein the pore / REV scale study of mass transfer in porous media is limited by high end requirements of computing resources.

#### 1.2.6.1 Bioreactors with porous media

Vafai and Tien (1982) used the volume averaging technique for macroscopic conservation equations to study sucrose concentration in the porous matrix. Chung et al. (2007) investigated the perfusion bioreactor with culture media flow perpendicular to the cellular construct. Finite element method was implemented to solve the Navier-Stokes equations for the fluid domain and Brinkman's equation for the porous scaffold domain. The porosity and permeability varied with cell growth time. Numerical results showed that cells penetrated to a great extend into the scaffold with a more uniform distribution. Zhao et al. (2007) investigated a perfusion bioreactor with parallel flow to the porous scaffold. Lattice-Boltzmann method was used to solve the coupled flow system with the Stokes' equations in fluid region and the Brinkman's equation in the porous scaffold region.

However, in the above studies, the details for the bioreactor design, for example, concentration distribution for cell growth, reaction effectiveness, reactor efficiency, critical channel length and critical inlet concentration, were not systematically and parametrically investigated.

Recently, numerical modeling of a micro-channel flat-plate bioreactor with cells distributed along the bottom wall was carried out. The results were correlated by use of combined parameters for applications in bioreactors with single-culture cells (Zeng et al., 2006), co-culture cells (Zeng et al., 2007) and micro-patterning cells (Zeng et al., 2008). The critical channel length and critical inlet concentration were investigated, which was essential for bioreactor design to avoid oxygen hypoxia. The results were presented systematically and parametrically.

However the studies of Zeng et al. (2006, 2007 and 2008) were limited to two dimensional cell growth since the cells were attached to the bottom wall. There is limited previous study on co-culture type bioreactor with a porous scaffold. The porous scaffold provides a structure for attachment of the cells which allows them to grow in a three dimensional way like that in their natural environment. Porous scaffolds improve cell growth and function.

#### 1.2.6.2 Enzyme reactors with porous media

For enzyme reactors with a porous wall, several experimental studies have been conducted. Drott et al. (1997 and 1999) fabricated a microstructured enzyme reactor with flow-through cells comprising 32 channels in silicon by anisotropic wet etching. Their method increased the enzyme matrix surface by using high-aspect-ratio silicon and hence the enzyme activity was greatly improved by a factor of 100. A 3-D modeling of enzyme reactor was done by Stefan et al. (2003). The reactor consists of a container filled with 20 spherical enzyme carriers. Each of these carriers is covered by an active surface layer where the reaction happens. The effect of substrate transport velocity on the catalytic process was investigated. In addition, the reaction effectiveness with varying of inlet concentration and Reynolds number was also studied. Melander et al. (2005) immobilized endoglucanases in micro-immobilized enzyme reactors made of porous silicon. The characteristics of the micro-immobilized enzyme reactors were investigated by studying the product formation with variation of the concentration flow rate, temperature and pH of the substrate solution. Later, Melander et al. (2006) continued to experimentally study hydrolysis in microreactors

with porous parallel channels made by silicon wafer. Besides the effects of concentration flow rate, temperature, PH and concentration, the conversion efficiency was also measured and the long term stability of the reactor was tested.

## 1.3 Objectives and Scope of Study

### 1.3.1 Motivations

The interfacial conditions (stress jump coefficients, effective viscosity and slip coefficient) are difficult to predict and need further experiments to validate their predicted values (Ochoa-Tapia and Whitaker, 1995b). Several researchers (Larson and Higdon 1987, Sahraoui & Kaviany 1992, James and Davis 2001) have tried to study the interfacial conditions using the REV scale and pore scale numerical experiments, but their studies were only limited to slip velocity and effective viscosity. No previous work has ever been attempted to investigate and validate stress jump conditions in REV scale.

For numerical simulations of heat and mass transfer in porous/fluid coupled domains, the stress jump interfacial conditions (Ochoa-Tapia and Whitaker, 1998b) have not been incorporated with heat or mass transfer. The generalized Darcy-Brinkman-Forchheimer extended model has not been implemented and there is no sufficient work to investigate mass transfer in a reactor partially filled with porous media. There is also no systematic or parametrical study on a microchannel reactor with a porous wall that examines the influence of flow and geometric parameters on mass transfer behavior.

The implementation of stress jump interfacial condition has not been attempted for lattice Boltzmann method, which is a novel numerical method and has several advantages over traditional CFD methods as described in many previous studies (Martys 2001, Guo et al. 2004).

### 1.3.2 Objectives

One of the main objectives was to consider the boundary conditions at the interface between fluid layer and porous medium. Such boundary conditions included the slip coefficient, interfacial velocity, effective viscosity and stress jump coefficients. Another objective was to extend the lattice Boltzmann method (LBM) to coupled-flow problems with fluid layer and porous medium layer by using the stress jump interfacial boundary conditions. It involved the treatments of the velocity, temperature/concentration and distribution functions at the interface. The modeling included the viscous and inertial effects as studied by using the Navier-Stokes equation for fluid region and Darcy-Brinkman-Forchheimer equation for porous region. Another major objective was to investigate the flow and mass transfer in a microchannel reactor partially filled with a porous wall. The investigation included correlation of numerical results using combined non-dimensional parameters for a systematic and parametrical analysis.

### 1.3.3 Scope

The major challenges of pore scale and REV scale studies are time-consuming mesh generation and high computational effort in complex geometries for three-dimensional problems. For REV scale numerical experiments, porous media can be modeled as arrays of granular particles or cylinders. In the current study the array of cylinders was used because it can be simplified as a two dimensional (2D) case. This simplification saves much computational time and resources. There are traditionally four methods for solving the flow through an array of cylinders: Finite Difference method (FDM), Finite Volume method (FVM), Finite Element method (FEM) and Boundary Element method (BEM). FDM, FVM and FEM all need to mesh the whole flow domain including the pores between the cylinders and the boundaries of the cylinders. Thus when the diameters of the cylinders are changed, much time is needed to regenerate the meshes for the whole flow domain. This mesh regenerating problem can be overcome by the BEM since it only needs to mesh the boundaries of the cylinders for the whole domain. Thus, when the diameters of the cylinders are changed, BEM can easily regenerate the meshes. Also, since the BEM is almost like an analytical method, the results for flow through an array of cylinders are very accurate. Due to the above advantages, the BEM was used in this work to solve the flow through an array of cylinders.

The lattice Boltzmann method (LBM) was implemented for domain scale study of coupled flow systems including plain fluid and porous medium. The porous medium was considered to be rigid, homogeneous and isotropic; and saturated with the same single-phase fluid as that in the homogenous fluid region. For heat transfer,

local thermal equilibrium (LTE) model was assumed. For the shear stress jump parameters, to demonstrate the implementation of current numerical method and to test their effects, their values ranged from -0.7 to +0.7 in the present study. For normal stress, temperature, heat flux, mass and mass flux, the continuity conditions were imposed.

The study of mass transfer in the microchannel reactor with a porous wall was carried out in the range relevant to practical applications. The fluid Damkholar numbers is one order smaller than the porous Damkholar numbers; thus the mass transfer was not limited by convection except for long reactor length. The Darcy number was small so that in the porous medium, the diffusion is relatively dominant. The reaction was based on the Michaelis Menten model.

## 1.4 Organization of the Thesis

In Chapter 2, the BEM and the LBM are developed to simulate the coupled flow and mass transfer problems based on pore/REV scale and domain scale respectively. A novel treatment of interfacial conditions using LBM is presented. The validation is presented for the LBM model.

In Chapter 3, the simplified analytical solutions for microchannel reactors with a porous wall are deduced. Several dimensionless combined parameters are defined to correlate the numerical data. The definition of the effectiveness factor, reactor efficiency and utilization efficiency are given.

In Chapter 4, the pore scale/REV scale investigation of the interfacial flow behaviors and interfacial conditions is presented. The various interfacial condition models are evaluated.

In Chapter 5, the LBM is extended to the coupled-flow systems with stress jump interfacial conditions. A novel treatment of the interfacial boundary conditions is used which is developed and validated in Chapter 2.

In Chapter 6, the mass transfer in microchannel reactors with porous wall is investigated by the lattice Boltzmann method. The results are correlated with the use of several combined dimensionless parameters; the effectiveness factor, reactor efficiency and utilization efficiency are investigated; and the critical channel length and critical inlet concentration are also calculated.

In Chapter 7, a summary of the main conclusions that can be drawn from this work and the recommendations for future research work are presented.

Table 1.1 Classifications for modeling of coupled fluid and porous medium system

| Scale | Type | Sub classification | Reference |
|---|---|---|---|
| Domain scale | One domain approaches | | Bennacer et al., 2003<br>Gobin et al., 2005<br>Zhang and Zhao, 2000<br>Abu-Hijleh, 1997 and 2000 |
| | Two domain approaches | Slip on model<br>Continuous stress model<br>Stress jump model | Beavers and Joseph, 1967<br>Taylor 1971<br>Neale and Nader 1974,<br>Vafai and Thiyagaraja 1987<br>Vafai and Kim, 1990<br>Kim and Choi, 1996<br>Ochoa-Tapia and Whitaker, 1995a and II, 1998<br>Goyeau et al. 2003<br>Chandesris and Jamet 2006 |
| Pore scale and REV scale | | | Larson and Higdon 1987<br>Sahraoui and Kaviany, 1994.<br>James and Davis 2001<br>Bai et al. 2009a |

Table 1.2 Interface boundary conditions between porous medium and homogenous fluid domains

| Model | Velocity | Velocity Gradient | Reference |
|---|---|---|---|
| 1 | | $\left.\frac{\partial u}{\partial y}\right\|_{\text{fluid}} = \frac{\alpha}{\sqrt{K}}\left(u\|_{\text{int}} - u_D\right)$ | Beavers and Joseph, 1967<br>Taylor 1971 |
| 2 | $u\|_{\text{porous}} = u\|_{\text{fluid}}$ | $\left.\frac{\partial u}{\partial y}\right\|_{\text{porous}} = \left.\frac{\partial u}{\partial y}\right\|_{\text{fluid}}$ | Neale and Nader, 1974 |
| 3 | $u\|_{\text{porous}} = u\|_{\text{fluid}}$ | $\nu_{eff}\left.\frac{\partial u}{\partial y}\right\|_{\text{porous}} = \nu\left.\frac{\partial u}{\partial y}\right\|_{\text{fluid}}$ | Neale and Nader 1974,<br>Vafai and Thiyagaraja 1987<br>Kim and Choi, 1996;<br>Vafai and Kim, 1990 |
| 4 | $u\|_{\text{porous}} = u\|_{\text{fluid}}$ | $\frac{1}{\varepsilon}\left.\frac{\partial u}{\partial y}\right\|_{\text{porous}} - \left.\frac{\partial u}{\partial y}\right\|_{\text{fluid}} = \frac{\beta}{\sqrt{K}} u\Big\|_{\text{int}}$ | Ochoa-Tapia and Whitaker, 1995a and II<br>Goyeau et al. 2003 |
| 5 | $u\|_{\text{porous}} = u\|_{\text{fluid}}$ | $\frac{1}{\varepsilon}\left.\frac{\partial u}{\partial y}\right\|_{\text{porous}} - \left.\frac{\partial u}{\partial y}\right\|_{\text{fluid}} = \frac{\beta}{\sqrt{K}} u\Big\|_{\text{int}} + \frac{\beta_1}{\nu} u^2\Big\|_{\text{int}}$ | Ochoa-Tapia and Whitaker, 1998 |
| 6 | $u\|_{\text{porous}} = u\|_{\text{fluid}}$ | $\left.\frac{\partial u}{\partial y}\right\|_{\text{porous}} - \left.\frac{\partial u}{\partial y}\right\|_{\text{fluid}} = \frac{\beta_C}{\sqrt{K}} u\Big\|_{\text{int}}$ | Chandesris and Jamet 2006 |

Table 1.3 Heat transfer boundary conditions at interface between porous and fluid domains.

| Model | Temperature | Temperature Gradient | References |
|---|---|---|---|
| 1 | $\langle T \rangle\big\|_{\text{porous}} = T\big\|_{\text{fluid}}$ | $k_{eff} \left.\frac{\partial \langle T \rangle}{\partial y}\right\|_{\text{porous}} = k_f \left.\frac{\partial T}{\partial y}\right\|_{\text{fluid}}$ | Neale and Nader, 1974; Vafai and Thiyagaraja, 1987; Ochoa-Tapia and Whitaker, 1997; Jang and Chen, 1992; Kim and Choi, 1996; Kuznetsov, 1999. |
| 2 | $\langle T \rangle\big\|_{\text{porous}} = T\big\|_{\text{fluid}}$ | $k_{eff} \left.\frac{\partial \langle T \rangle}{\partial y}\right\|_{\text{porous}} = k_f \left.\frac{\partial T}{\partial y}\right\|_{\text{fluid}} + \phi$ | Ochoa-Tapia and Whitaker, 1998 I. |
| 3 | $\left.\frac{dT}{dy}\right\|_{\text{fluid}} = \frac{\alpha_T}{\lambda}(T\big\|_{\text{fluid}} - \langle T \rangle\big\|_{\text{porous}})$ | $k_{eff} \left.\frac{\partial \langle T \rangle}{\partial y}\right\|_{\text{porous}} = k_f \left.\frac{\partial T}{\partial y}\right\|_{\text{fluid}}$ | Sahraoui and Kaviany, 1994. |

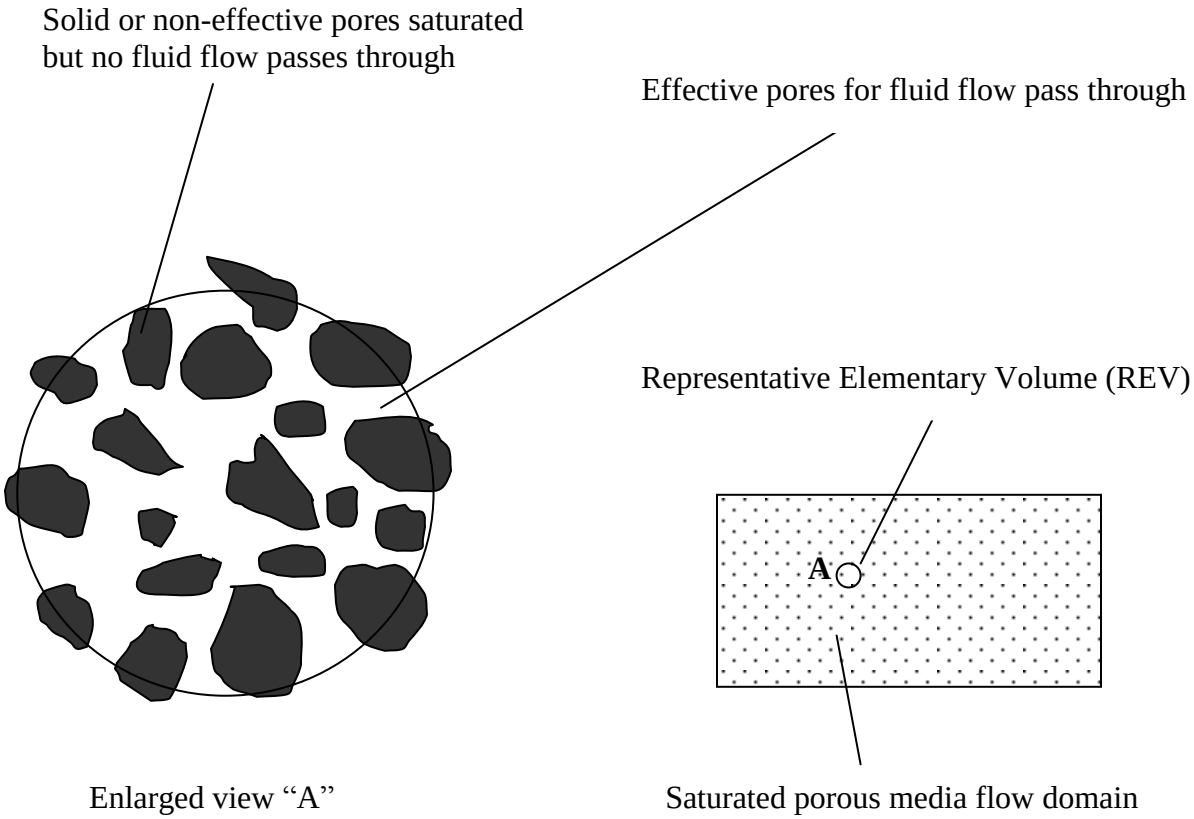


Figure 1.1 A representative elementary volume (REV) for saturated porous media

# Chapter 2 Numerical Methods*

## 2.1 Numerical Methods for Pore and REV Scales

### 2.1.1 Boundary element method for Stokes equation

For steady incompressible slow viscous flow in fibrous media, the flow may be governed by the Stokes equation:

$$\mu\nabla^2 u - \nabla p = 0 \tag{2.1}$$

where $\mu$ is the fluid dynamic viscosity, $u$ is the velocity and $p$ is the pressure.

The boundary element method (BEM) is used to solve the Stokes equation for the flow through the fibrous porous media modeled as an array of cylinders. The BEM has several advantages which are discussed in Section 1.3.3. The cylinders are discretized into boundary elements of circular arcs.

The boundary integral equations of two-dimensional Stokes flow for velocity are given by Pozrikidis (1992 and 2002):

$$u_j(x_0) = u_j^{\infty}(x_0) - \frac{1}{4\pi\mu}\sum_{q=1}^{N_p}\int_{C_q} G_{ji}(x_0, x)\, f_i^D(x)\, dl(x)$$

$$-\frac{1}{4\pi}\sum_{q=1}^{N_p}\int_{C_q} u_i^{\infty}(x, x_0) T_{ijk}(x, x_0) n_k(x)\, dl(x) \tag{2.2}$$

where the subscript $C_q$ is the contour of *qth* particle, $N_p$ is the number of particles, $n$ is the unit normal vector pointing into the fluid, $f_i^D$ is the disturbance component

*Parts of this chapter have been published in Bai et al., *International Journal for Numerical Methods in Fluids 60, 691-708, 2009*

of the hydrodynamic traction and $G_{ji}$ is the unidirectional periodic Green's function for flow in a channel bounded by two parallel planes. Polar coordinate integral method is used to avoid the integral singularity. The open source BEM code of Pozrikidis (1992 and 2002) was tested and used to solve two-dimensional Stokes flow through fibrous array in present work.

### 2.1.2 Volume averaged method

For the channel flow partially filled with porous medium modeled as an array of circular cylinders, the two-dimensional array is spatially periodic in x-direction. For such kind of theoretical modeling, the definition of the averaging volume has been discussed in previous studies (Larson and Higdon 1987, Sahraoui and Kaviany 1992, Alazmi and Vafai 2001). To relate the pore scale variations to the REV scale behavior, area and volume averages must be taken.

For periodic array of cylinders, the length scale constraint has been discussed by Whitaker (1999) and Kaviany (1991). The volume average methods are valid when the following length-scale constraint is satisfied:

$$l_1 \cdot l_2 \ll L^2 \tag{2.3}$$

where $L$ is the channel characteristic length and $l_1$, $l_2$ are the cell dimensions as defined in Figure 4.1 of Chapter 4, where the point *(x, y)* is at the cell center, $l_1$ is the cell dimension in *x* direction and $l_2$ is the cell dimension in *y* direction.

A justification of the present representative elementary volume is necessary to establish whether the length constraint is satisfied. In the present study there were 16 rows of cylinders in the $y$ direction and $l_1 = l_2/\sqrt{3}$ . Thus $l_1 \cdot l_2 / H^2 \approx 1/15\sqrt{3} = 0.051 \ll 1$ and length constraint is satisfied in present study.

To enforce the length constraint more rigorously, a larger number of rows of cylinders are needed, which would require more computation resources. For comparison, James and Davies (2001) used 5–20 rows of cylinders in their study.

Taking the velocity for example, the area average is defined as (Sahraoui and Kaviany 1992):

$$\langle u \rangle_A (y) \equiv \frac{1}{l} \int_0^l u(x, y)\, dx \tag{2.4}$$

where $l$ is the cell dimension, the bracket $\langle\ \rangle_A$ represents area average. The interfacial velocity is defined as the area average velocity at the selected interface position $y_i$:

$$\langle u \rangle_{A,i} = \langle u \rangle_A (y_i) \tag{2.5}$$

In present study, the interface is defined at the position of $y = 0$, which is tangent to outermost edge of first row of cylinders. The volume average velocity is defined as (Sahraoui and Kaviany 1992):

$$\langle u \rangle_V (y) \equiv \frac{1}{l_1 \cdot l_2} \int_{x-l_1/2}^{x+l_1/2} \int_{y-l_2/2}^{y+l_2/2} u(x, y)\, dy dx \tag{2.6}$$

where the bracket $\langle\ \rangle_V$ represents volume average, which is independent of $x$ as the array is periodic in the $x$ direction.

To calculate the velocity gradients near the interface, the averaging volume must be carefully chosen so that the velocity variations near the interface can be reflected accurately. Furthermore, the averaging volume should guarantee that the volume averaged interfacial velocity and Darcy velocities are in agreement with those of the area averaged values.

Sahraoui and Kaviany (1992) proposed that for any point $y$ located between 0 and $-l_2/2$, the averaging volume is taken as $-2yl_1$ (see Figure 4.1c, note $y$ is negative), and the volume averaged velocity is defined as:

$$\langle u \rangle_V (y) \equiv \frac{-1}{2yl_1} \int_{-2y}^{0} \int_{x-l_1/2}^{x+l_1/2} u(x, y')\, dx dy' \tag{2.7}$$

The permeability in the porous region is then calculated using Darcy's law:

$$\frac{dP}{dx} = \frac{\mu}{K} u_D \tag{2.8}$$

where $dP/dx$ is the pressure gradient, $\mu$ is the fluid dynamic viscosity and $u_D = \langle u \rangle_V (y \to -\infty)$ is the Darcy velocity which is a volume averaged velocity over a local REV positioned deep into the porous medium. Noted that in the following parts, all the velocity $u$ represents area or volume averaged velocities.

## 2.2 Governing Equations and Boundary Conditions

For steady incompressible viscous flow, the governing equations for a homogenous fluid region can be expressed as:

$$\nabla \cdot \vec{u} = 0 \tag{2.9}$$

$$\nabla \cdot (\vec{u}\vec{u}) = -\frac{1}{\rho}\nabla p + \nu \nabla^2 \vec{u} \tag{2.10}$$

The governing equations for porous medium flow based on Darcy-Brinkman-Forchheimer extended model are expressed in the vector form (Vafai and Tien 1981, Hsu and Cheng 1990, Guo and Zhao 2002, Yu et al. 2007, Bai et al. 2009b):

$$\nabla \cdot \vec{u} = 0 \tag{2.11}$$

$$\underbrace{\nabla \cdot \left(\frac{\vec{u}\vec{u}}{\varepsilon}\right)}_{\text{Convective Term}} = \underbrace{-\frac{1}{\rho}\nabla(\varepsilon p)}_{\text{Pressure Term}} + \underbrace{\nu_e \nabla^2 \vec{u}}_{\text{Brinkman Term}} - \underbrace{\frac{\nu\varepsilon}{K}\vec{u}}_{\text{Darcy Term}} - \underbrace{\frac{\varepsilon C_F |\vec{u}|}{\sqrt{K}}\vec{u}}_{\text{Forchheimer Term}} \tag{2.12}$$

where $\vec{u}$ is the local average velocity vector (Darcy velocity); $\rho$ is the mass density of the fluid; $p$ is the intrinsic-average pressure; $\nu$ is the fluid kinematic viscosity; $\nu_e$ is the effective (Brinkman) kinematic viscosity; $\varepsilon$ is the porosity; $K$ is the permeability; and $C_F$ is the geometric function which is expressed as (Guo and Zhao 2002, Yu et al. 2007, Bai et al. 2009b):

$$C_F = 1.75 / \sqrt{150\varepsilon^3} \tag{2.13}$$

The nonlinear Forchheimer term and linear Darcy term are drag forces caused by the presence of the porous medium. The Brinkman term accounts for the force due to the solid boundary. The local average $p^*$ and the intrinsic average pressure $p$ can be linked by the Dupuit-Forchheimer relationship $p^* = \varepsilon p$.

The governing equations for heat transfer and mass transfer:

$$u\frac{\partial G_s}{\partial x} + v\frac{\partial G_s}{\partial y} = D_s\left(\frac{\partial^2 G_s}{\partial x^2} + \frac{\partial^2 G_s}{\partial y^2}\right) + \mathrm{Q_s} \qquad s = T,\ c \tag{2.14}$$

where $Q_s$ is the source term due to heat source/sink or chemical reaction; $T$ is temperature; $c$ is mass concentration and $D_s$ is the thermal diffusivity or mass diffusivity. Note that the governing equations for heat and mass transfer are similar. The heat source or reaction rate will determine the source term expressions.

At the interface between the homogeneous fluid layer and porous medium layer, additional boundary conditions must be applied to couple the flows in the two regions. The previous pore/REV scale studies had shown that there is a stress jump at the interface (Bai et al. 2009a, also see Chapter 4). In the present study, the stress jump condition (Ochoa-Tapia and Whitaker 1998, Bai et al. 2009a and 2009b) is applied:

$$\frac{1}{\varepsilon}\frac{\partial u_t}{\partial n}\bigg|_{\text{porous}} - \frac{\partial u_t}{\partial n}\bigg|_{\text{fluid}} = \frac{\beta}{\sqrt{K}} u_t\bigg|_{\text{interface}} + \frac{\beta_1 u_t^2}{\nu} \tag{2.15}$$

where in the porous medium region, $u_t$ is the Darcy velocity component parallel to the interface aligned with the direction $t$ and normal to the direction $n$; while in the homogenous fluid region $u_t$ is the fluid velocity component parallel to the interface; $\beta$ and $\beta_1$ are the stress jump parameters.

Ochoa-Tapia & Whitaker (Ochoa-Tapia and Whitaker 1998) derived analytical expressions for parameters $\beta$ and $\beta_1$ which indicate their dependence on permeability and porosity. They concluded that these two parameters are both of order one. Ochoa-Tapia & Whitaker (1995b) experimentally determined that $\beta$ varies from $-1.0$ to $+0.7$ for different materials with permeability varying from $15 \times 10^{-6}$ to $127 \times 10^{-6}$ in$^2$ and average pore size from 0.016 to 0.045 in. No experimental data is available for $\beta_1$. In the present study, both $\beta$ and $\beta_1$ vary in the range from

-1.0 to +0.7 . Bai et al. (2009a) investigated the interfacial boundary condition based on pore/REV scale studies and confirmed the presence of the stress jump (see Chapter 4). Their study found that the stress jump coefficients are order one, which agrees with Ochoa-Tapia and Whitaker 1995a and 1995b.

In addition to Equation (2.6), the continuity of velocity and normal stress prevailing at the interface is given by:

$$\vec{u}\big|_{\text{fluid}} = \vec{u}\big|_{\text{porous}} = \vec{u}_{\text{int}} \tag{2.16}$$

$$\frac{\nu}{\varepsilon}\frac{\partial u_n}{\partial n}\bigg|_{\text{porous}} - \nu\frac{\partial u_n}{\partial n}\bigg|_{\text{fluid}} = 0 \tag{2.17}$$

where in the porous medium region, $u_n$ is the Darcy velocity component normal to the interface; and in the homogenous fluid region, $u_n$ is the fluid velocity component normal to the interface; the subscript ' $_{\text{int}}$ ' represents the interface.

For the heat and mass transfer interfacial condition, continuities of the heat & mass and heat & mass flux are implemented as:

$$G_s\big|_{\text{fluid}} = G_s\big|_{\text{porous}} = G_{s,\text{int}} \tag{2.18}$$

$$D_{s,eff}\frac{\partial G_s}{\partial n}\bigg|_{\text{porous}} - D\frac{\partial G_s}{\partial n}\bigg|_{\text{fluid}} = 0 \tag{2.19}$$

where $s = T,\ c$; T is the temperature and $c$ is the mass concentration; the subscript ' $_{\text{int}}$ ' represents the interface; n represents the direction normal to the interface. By combining with the appropriate boundary conditions of the composite region, Equations (2.9) - (2.19) can be used to simulate the coupled flow, heat and mass transfer in a system composed of a porous medium and a homogenous fluid.

## 2.3 LBM for Domain Scale

### 2.3.1 Homogenous fluid domain

In the lattice Boltzmann method (LBM) the fluid flow field is modeled by a single-particle distribution function (DF) $f_i$. The quantity of $f_i(\vec{x},t,\vec{e})$ represents the probability of finding a particle in the vicinity of $\vec{x}$ at time $t$, that is moving with velocity $\vec{e}_i$. For the two-dimensional case, the lattice Boltzmann BGK equation is expressed as (Martys 2001, Guo and Zhao 2002, Hou et al. 1995, Shi et al. 2006):

$$f_i(\vec{x}+\vec{e}_i\delta_t,t+\delta_t)-f_i(\vec{x},t)=-\frac{f_i(\vec{x},t)-f_i^{eq}(\vec{x},t)}{\tau} \tag{2.20}$$

where $\delta_t$ is the time increment, $\tau$ is the non-dimensional relaxation time and $f_i^{eq}$ is the corresponding equilibrium state, which is the distribution that the system will evolve in the absence of forcing gradients. The equilibrium distribution function (EDF) is defined by (Guo and Zhao 2002):

$$f_i^{eq}=w_i\rho\left[1+\frac{\vec{e}\cdot\vec{u}}{c_s^2}+\frac{\vec{u}\vec{u}:(\vec{e}_i\vec{e}_i-c_s^2\mathrm{I})}{2c_s^4}\right] \tag{2.21}$$

where $w_i$ is the weight coefficient and $c_s$ is the sound speed. Here $c_s=c/\sqrt{3}$, $c=\delta_x/\delta_t$ and $\delta_x$ is the lattice spacing. In present study, $c$ is set to be 1.

For the D2Q9 (Guo and Zhao 2002, Hou et al. 1995, Guo et al. 2002) model (Fig. 2.1), the discrete velocities $(e_x, e_y)_i$ are defined as

$$\vec{e}_i = \begin{cases} (0,0) & i = 0 \\ \left(\cos\left[(i-1)\pi/2\right], \sin\left[(i-1)\pi/2\right]\right) & i = 1,2,3,4 \\ \sqrt{2}\left(\cos\left[(i-5)\pi/2+\pi/4\right], \sin\left[(i-5)\pi/2+\pi/4\right]\right) & i = 5,6,7,8 \end{cases} \tag{2.22}$$

The weight coefficients are given as

$$w_i = \begin{cases} \dfrac{4}{9} & i = 0 \\ \dfrac{1}{9} & i = 1,2,3,4 \\ \dfrac{1}{36} & i = 5,6,7,8 \end{cases} \tag{2.23}$$

The macroscopic mass density $\rho$ and velocity $\vec{u}$ are calculated from the distribution functions:

$$\rho = \sum_{i=0}^{8} f_i , \qquad \rho\vec{u} = \sum_{i=0}^{8} f_i \vec{e}_i \tag{2.24}$$

The pressure and the kinematic viscosity are defined as

$$p = \rho c_s^2 , \qquad \nu = c_s^2 (\tau - \frac{1}{2})\delta_t \tag{2.25}$$

Using the Chapman-Enskog expansion (Guo et al. 2004), the momentum Equation (2.4) can be recovered by performing a Taylor series expansion of the particle distribution function (2.11).

### 2.3.2 Porous medium domain

To solve the porous medium flow governed by the Darcy-Brinkman-Forchheimer extended model (Equation 2.12), Guo and Zhao (2002) introduced the porosity into the equilibrium distribution function, and added a force term $F_i$ to the standard lattice Boltzmann equation to account for the linear and nonlinear drag forces caused by the porous medium. Their model is expressed as:

$$f_i(\vec{x}+\vec{e}_i\delta_t, t+\delta_t) - f_i(\vec{x},t) = -\frac{f_i(\vec{x},t) - f_i^{eq}(\vec{x},t)}{\tau} + \delta_t F_i \tag{2.26}$$

$$f_i^{eq} = w_i \rho \left[ 1 + \frac{\vec{e}\cdot\vec{u}}{c_s^2} + \frac{\vec{u}\vec{u} : (\vec{e}_i\vec{e}_i - c_s^2 \mathrm{I})}{2\varepsilon c_s^4} \right] \tag{2.27}$$

in which the total force term $F_i$ is defined by

$$F_i = w_i \rho \left(1 - \frac{1}{2\tau}\right) \left[ 1 + \frac{\vec{e}\cdot\vec{F}}{c_s^2} + \frac{\vec{u}\vec{F} : (\vec{e}_i\vec{e}_i - c_s^2 \mathrm{I})}{\varepsilon c_s^4} \right] \tag{2.28}$$

where $\vec{F}$ is the total body force due to the presence of a porous medium and other external force fields. This total body force is expressed as

$$\vec{F} = -\frac{\varepsilon \nu}{K}\vec{u} - \frac{\varepsilon C_F}{\sqrt{K}}|\vec{u}|\vec{u} + \varepsilon \vec{g} \tag{2.29}$$

where $\vec{g}$ is the body force due to external force; and the fluid velocity is defined as

$$\rho\vec{u} = \sum_{i=0}^{8} \vec{e}_i f_i + \frac{\delta_t}{2}\rho\vec{F} \tag{2.30}$$

The nonlinear Equation (2.30) was solved by Guo and Zhao (2002) and expressed as:

$$\vec{u} = \frac{\vec{v}}{c_0 + \sqrt{c_0^2 + c_1|\vec{v}|}} \tag{2.31}$$

where $\vec{v}$ is an auxiliary velocity defined as:

$$\rho\vec{v} = \sum_{i=0}^{8} \vec{e}_i f_i + \frac{\delta_t}{2} \varepsilon\rho\vec{g} \tag{2.32}$$

The two parameters $c_0$ and $c_1$ in Equation (2.31) can be calculated by

$$c_0 = \frac{1}{2}\left(1 + \varepsilon \frac{\delta_t}{2} \frac{\nu}{K}\right) \qquad c_1 = \varepsilon \frac{\delta_t}{2} \frac{C_F}{\sqrt{K}} \tag{2.33}$$

Through the Chapman-Enskog expansion (Guo et al. 2004) the momentum Equation (2.12) can be deduced from the distribution function (2.26).

### 2.3.3 Heat and mass transfer equations

In the lattice Boltzmann method (LBM) the temperature and mass concentration fields are modeled by a single-particle distribution function (DF) $g_i$. The quantity of $g_i\left(\vec{x}, t, \vec{e}\right)$ represents the probability of finding a particle in the vicinity of $\vec{x}$ at time $t$ that is moving with velocity $\vec{e}_i$. For the two-dimensional case, the lattice Boltzmann equation is expressed as (Guo and Zhao 2005):

$$g_i(\vec{x} + \vec{e}_i\delta_t, t + \delta_t) - g_i(\vec{x}, t) = -\frac{g_i(\vec{x}, t) - g_i^{eq}(\vec{x}, t)}{\tau'} \tag{2.34}$$

where $\delta_t$ is the time increment, $\tau'$ is the non-dimensional relaxation time and $g_i^{eq}$ is the corresponding equilibrium state, which is the distribution that the system will evolve in the absence of thermal or mass concentration gradients.

The equilibrium distribution function (EDF) is defined by (Guo and Zhao 2005):

$$g_i^{eq} = w_i G_s \left[ 1 + \frac{\vec{e} \cdot \vec{u}}{c_s^2} \right] \qquad s = T, c \tag{2.35}$$

where $T$ is the temperature and $c$ is mass concentration; $c_s$ is sound speed.

For the model of heat source or mass concentration reaction term, one source term is added to the lattice Boltzmann equation as (Yamamoto et al. 2005):

$$g_i(\vec{x} + \vec{e}_i \delta_t, t + \delta_t) - g_i(\vec{x}, t) = -\frac{g_i(\vec{x}, t) - g_i^{eq}(\vec{x}, t)}{\tau'} + w_i Q_s \qquad s = T, c \tag{2.36}$$

where $Q_s$ is the source term due to heat source/sink or chemical/bio-reaction; $T$ is the temperature and $c$ is mass concentration.

### 2.3.4 Interface boundary conditions

The interfacial boundary condition must be chosen appropriately to couple the two lattice Boltzmann equations as given by Equations (2.20) and (2.26). As discussed in Chapter 4 and Chapter 5, Bai et al. (2009a) had shown the presence of stress jump at the interface based on pore/REV scale numerical experiment. Subsequently they successfully implemented the stress jump conditions in LBM modeling (Bai et al. 2009b). In the present study, the stress jump condition is also used. For traditional discretization methods, such as finite difference and finite volume method, the momentum flux is calculated by discretizing of the velocity field using finite difference. Thus implementation of appropriate velocity boundary conditions automatically guarantees correct momentum flux near the boundary.

However, in LBM, only the equations for $f_i$ are solved and the velocity boundary conditions are not enough to guarantee the strain field (Chen et al. 1996). Thus additional boundary conditions for $f_i$ must be correctly implemented to ensure correct momentum flux near the boundary (Bai et al. 2009b).

Fig. 2.1 shows a basic lattice for D2Q9 lattice Boltzmann model with lattice layer (E-O-A) just at the interface, lattice layer (D-C-B) at one lattice inside of the fluid, and lattice layer (F-G-H) at one lattice inside the porous medium. The interface is selected just at the lattice layer (E-O-A) so that the interfacial boundary conditions can be applied directly on the interfacial lattice points and there is no need to carry out the interpolation. Consider the stress jump condition as a case, the normal velocity-gradients at the interface can be calculated by using the backward second order difference approximation for porous side and forward second order difference approximation for fluid side:

$$\left.\frac{\partial u}{\partial y}\right|_{\text{porous}} = \frac{3u_{\text{int}} - 4u_{\text{int}-1} + u_{\text{int}-2}}{2\Delta y} \qquad \left.\frac{\partial v}{\partial y}\right|_{\text{porous}} = \frac{3v_{\text{int}} - 4v_{\text{int}-1} + v_{\text{int}-2}}{2\Delta y} \tag{2.37}$$

$$\left.\frac{\partial u}{\partial y}\right|_{\text{fluid}} = \frac{-3u_{\text{int}} + 4u_{\text{int}+1} - u_{\text{int}+2}}{2\Delta y} \qquad \left.\frac{\partial v}{\partial y}\right|_{\text{fluid}} = \frac{-3v_{\text{int}} + 4v_{\text{int}+1} - v_{\text{int}+2}}{2\Delta y} \tag{2.38}$$

where $u_{\text{int}}$ is the interfacial velocity in x-coordinate; $v_{\text{int}}$ is the interfacial velocity in y-coordinate; the subscript ‘$_{\text{int}}$’ represents the lattice points at the interface, ‘$_{\text{int-1}}$’ and ‘$_{\text{int-2}}$’ represent the lattice points which are one lattice and two lattices below the interface, respectively; ‘$_{\text{int+1}}$’ and ‘$_{\text{int+2}}$’ represent the lattice points which are one lattice and two lattices above the interface, respectively; and $\Delta y$ is the lattice spacing.

Combine Equations (2.15), (2.17), (2.37) and (2.38) as given in Bai et al. (2009b):

$$\frac{1}{\varepsilon}\frac{3u_{\text{int}}-4u_{\text{int}-1}+u_{\text{int}-2}}{2\Delta y}\bigg|_{\text{porous}}-\frac{-3u_{\text{int}}+4u_{\text{int}+1}-u_{\text{int}+2}}{2\Delta y}\bigg|_{\text{fluid}}=\frac{\beta}{\sqrt{K}}u_{\text{int}}+\frac{1}{\nu}\beta_1 u_{\text{int}}^2 \qquad (2.39)$$

$$\frac{1}{\varepsilon}\frac{3v_{\text{int}}-4v_{\text{int}-1}+v_{\text{int}-2}}{2\Delta y}\bigg|_{\text{porous}}-\frac{-3v_{\text{int}}+4v_{\text{int}+1}-v_{\text{int}+2}}{2\Delta y}\bigg|_{\text{fluid}}=0 \qquad (2.40)$$

The interfacial velocity $u_{\text{int}}$ and $v_{\text{int}}$ can be calculated from Equations (2.39) and (2.40), respectively.

After the interfacial velocity $u_{\text{int}}$ and $v_{\text{int}}$ are calculated from the above interfacial stress condition, the equilibrium distribution functions at the interface lattice points can be evaluated. For the one-domain approach, both the porous flow region and the fluid flow region are treated as one domain and thus there is no need to treat the interfacial boundary condition specially. The particle distribution functions can be evaluated according to the LBM Equation (2.26). However, for stress jump condition using two-domain approach, the porous side LBE and the fluid side LBE are different; thus a special treatment of the interfacial boundary condition is needed to link the two LBEs. Moreover, the stress jump has to be enforced over the interface. The LBM Equation (2.26) cannot satisfy the stress jump interfacial condition and the interface is treated as a special boundary. In the present study, the interfacial particle distribution along the directions 2, 5 and 6 move from the interface boundary to the fluid region, so they are calculated with the fluid LBM equations. Along the directions 4, 7 and 8 the interfacial distribution moves from the interface to the porous medium region, and are calculated with porous medium LBM equations. For directions 0, 1 and 3 along the interface, the interfacial distribution functions are calculated based on

interpolation of fluid and porous medium lattice Boltzmann models. The interfacial distribution functions can be expressed as (Bai et al. 2009b):

$$f_{\mathrm{i,\,int}}^{eq} = f_{\mathrm{i,\,int}}^{eq}\Big|_{\mathrm{fluid}} \qquad f_{i,\,\mathrm{int}} = f_{i,\,\mathrm{int}}\Big|_{\mathrm{fluid}} \qquad \text{for i=2, 5, 6} \tag{2.41}$$

$$f_{\mathrm{i,\,int}}^{eq} = f_{\mathrm{i,\,int}}^{eq}\Big|_{\mathrm{porous}} \qquad f_{i,\,\mathrm{int}} = f_{i,\,\mathrm{int}}\Big|_{\mathrm{porous}} \qquad \text{for i=4, 7, 8} \tag{2.42}$$

$$f_{\mathrm{i,\,int}}^{eq} = \frac{1}{2}\left( f_{\mathrm{i,\,int}}^{eq}\Big|_{\mathrm{fluid}} + f_{\mathrm{i,\,int}}^{eq}\Big|_{\mathrm{porous}} \right) \qquad f_{i,\,\mathrm{int}} = \frac{1}{2}\left( f_{i,\,\mathrm{int}}\Big|_{\mathrm{fluid}} + f_{i,\,\mathrm{int}}\Big|_{\mathrm{porous}} \right) \qquad \text{for } i = 0,\ 1,\ 3 \tag{2.43}$$

where the subscript '$i,\mathrm{int}$' represents the interfacial distribution at the direction '$i$'; $f_{\mathrm{i,\,int}}^{eq}\Big|_{\mathrm{fluid}}$ and $f_{\mathrm{i,\,int}}^{eq}\Big|_{\mathrm{porous}}$ can be calculated from Equations (2.21) and (2.27) respectively, and $f_{i,\,\mathrm{int}}\Big|_{\mathrm{fluid}}$ and $f_{i,\,\mathrm{int}}\Big|_{\mathrm{porous}}$ can be calculated from Equations (2.20) and (2.26) respectively.

For the two ends of the interface nodes, different treatments need to be imposed. Taking the left end as an example, the distribution functions along the directions of 1, 5 and 8 stream from the outside, which is unknown. For channel flow with periodic boundary condition in inlet and outlet, the periodic boundary condition is applied to calculate $f_1, f_5$ and $f_8$ at the interface $f_{in1} = f_{out1}$ $f_{in5} = f_{out5}$ $f_{in8} = f_{out8}$; where the subscript '$in$' and '$out$' represent inlet and outlet respectively. In the case of cavity flow, the no-slip boundary conditions are used for $f_1, f_5$ and $f_8$ at the left end of interface. Similar boundary conditions can be applied for the right end of the interface.

Note that when jump coefficients $\beta = 0$ and $\beta_1 = 0$, the interfacial boundary conditions are changed to continuity of stress. The implementation continuities of

temperature/mass concentration and heat/mass flux are similar but easier compared with stress jump condition.

### 2.3.5 Solution algorithm

The calculation procedure for the LBM is summarized below.

1. The computation of the flow field is started by assuming initial values for all the parameters.

2. The equilibrium distribution functions for the flow field, including those at the interface, are calculated. Then the collision step is carried out for all nodes, except the interfacial nodes where the velocity boundary conditions are enforced (in step 4) for the equilibrium distribution functions. After the collision step, the streaming step is executed for all nodes.

3. The macroscopic parameters, such as densities and velocities are calculated from the updated distribution functions.

4. The jump conditions are implemented by using Equations (2.39) and (2.40) to calculate the updated interfacial velocities. The velocities and distribution function boundary conditions are enforced, including the updated interfacial velocities.

5. Convergence is checked by using the following condition:

$$\frac{\sum_{ij}\left|u_{ij}^{(n)}-u_{ij}^{(n-100)}\right|}{\sum_{ij}\left|u_{ij}^{(n)}\right|}\le 10^{-9} \tag{2.44}$$

where $u_{ij}^{(n)}=u\left(x_i,y_j,n\Delta t\right)$. Equation (2.44) represents the sum of the nondimentional error over total grid nodes. If the Equation (2.44) is satisfied, the calculation is

stopped and the results are computed as output; if not, steps 2 to 5 are repeated till the Equation (2.44) is satisfied.

## 2.3.6 Code validation

In this section, the LBM numerical algorithms described in this Chapter are applied to simulate some well-studied cases: 1) Natural convection in a square cavity; 2) Channel flow partially filled with porous; 3) Mass transfer in a 2D flat-plate microchannel bioreactor with monolayer cells adheres to base plate. The numerical results are compared with published benchmark results to validate the accuracy of the present numerical method.

### 2.3.6.1 Natural convection in a square cavity

The natural convection in a square cavity can be simulated by solving the following non-dimensional 2-D Navier-Stokes equations:

$$\frac{\partial U}{\partial X}+\frac{\partial V}{\partial Y}=0 \tag{2.45}$$

$$\frac{\partial U}{\partial t}+U\frac{\partial U}{\partial X}+V\frac{\partial U}{\partial Y}=-\frac{\partial p}{\partial X}+\Pr\left(\nabla^2 U\right) \tag{2.46}$$

$$\frac{\partial V}{\partial t}+U\frac{\partial V}{\partial X}+V\frac{\partial V}{\partial Y}=-\frac{\partial p}{\partial Y}+\Pr\left(\nabla^2 V\right)+\Pr\bullet Ra\bullet T \tag{2.47}$$

$$\frac{\partial T}{\partial t}+U\frac{\partial T}{\partial X}+V\frac{\partial T}{\partial Y}=\nabla^2 T \tag{2.48}$$

where Pr and Ra are the Prandtl and Rayleigh numbers. The geometry and boundary conditions of the problem are given in Figure 2.2.

The physical boundary conditions are: velocity components $U,V$ and temperature $T$ are given at each boundary, which are:

at $X = 0, 0 \le Y \le 1$

$$U = 0, V = 0, T = 0 \tag{2.49}$$

at $X = 1, 0 \le Y \le 1$

$$U = 0, V = 0, T = 1 \tag{2.50}$$

at $Y = 0, 0 \le X \le 1$

$$U = 0, V = 0, \frac{\partial T}{\partial Y} = 0 \tag{2.51}$$

at $Y = 1, 0 \le X \le 1$

$$U = 0, V = 0, \frac{\partial T}{\partial Y} = 0 \tag{2.52}$$

where $U,V$ are non-dimensional velocities. Figure 2.3a, 2.3b and 2.3c show the temperature contour and velocity contour of the natural convection. The detailed comparisons of the present results with the benchmark solutions (de Vahl Davis, 1983) are shown in Table 2.1 and Table 2.2. The comparisons show that the present numerical results are in good agreement with the benchmark solutions (de Vahl Davis, 1983). It indicates that the present code is valid for the heat and mass transfer problems.

#### 2.3.6.2 Channel flow partially filled with porous medium

Figure 2.4 is the schematic of flow in a channel partially filled with saturated porous medium. The analytical solution of this model had been solved by Yu et al.

(2007) and Bai et al. (2009b). The comparisons of the present numerical solution and the analytical solution are presented in Figure 2.5. The comparisons show that the present numerical result is in good agreement with the analytical solution.

#### 2.3.6.3 Single cell culture bioreactor

In order to validate the present numerical model, a test was performed on the oxygen transfer in a 2D flat-plate microchannel bioreactor with uniform, constant flow and constant reaction rate at the base. The culture medium flows through the channel and the flow is assumed to be slug flow. A monolayer of hepatocytes attaches to the bottom of the channel and consumes oxygen from the culture medium at the maximum uptake rate. The configuration and the boundary conditions are shown in Figure 2.6. This model has been solved analytically by Carslaw and Jaeger (1959) and Tilles et al. (2001) as:

$$C_{bot} = 1 - \frac{x}{H}\frac{1}{Pe}Dam - \frac{Dam}{3} + \frac{2Dam}{\pi^2}\sum_{n=1}^{\infty}\frac{(-1)^n}{n^2}\cos(n\pi)\exp(-n^2\pi^2\frac{x}{H}\frac{1}{Pe}) \quad (2.53)$$

where $C_{bot}$ is non-dimensional bottom concentration at base plate, *Dam* is Damkohler number, *Pe* is Peclet number, H is channel height and x is distance along x-coordinate.

The oxygen concentration distribution on the bottom computed with the present numerical model is compared with the analytical solution (Carslaw and Jaeger, 1959; Tilles et al., 2001) at different conditions of *Pe* = 55.5, *Dam* = 0.083 and *Pe* = 17.6, *Dam* = 0.167. The comparison between the numerical results and the analytical solution is shown in Figure 2.7. The excellent agreement indicates that the present numerical model is satisfactory for mass transfer problem.

## 2.4 Conclusions

A LBM numerical method has been developed to investigate the fluid, heat and mass transfer in homogeneous fluid region, in porous medium region and in coupled flow regions with fluid and porous regions. For the porous medium flow, the governing equations based on a generalized model including the Darcy extended Brinkman and Forchheimer terms as well as the non-linear advection term (Hsu and Cheng, 1990; Gartling et al., 1996; Nithiarasu et al., 2002), which can recover the Navier-Stokes equations when the porosity approaches unity. The lattice BGK model based on the above Darcy extended Brinkman and Forchheimer terms as well as the non-linear advection term is used to solve the porous medium flow. The stress jump interfacial boundary conditions are implemented to LBE to solve the coupled plain fluid and porous medium system (Bai et al. 2009b). A variety of numerical experiments are performed to test the validation of the present code. The comparisons with the benchmark solutions are in good agreement and show that the present code can be used to calculate the two-dimensional, incompressible, steady, laminar fluid, heat and mass transfer problems for both fluid flow and porous medium flow.

Table 2.1Numerical results of natural convection in a square cavity for $Ra=10^3$

| | Benchmark | LBM | FV |
|---|---|---|---|
| Mesh size | 81×81 | 81×81 | 81×81 |
| $U_{\max}$ | 3.649 | 3.653 | 3.649 |
| y | 0.187 | 0.187 | 0.187 |
| $V_{\max}$ | 3.697 | 3.701 | 3.690 |
| x | 0.822 | 0.820 | 0.821 |
| $Nu_{ave}$ | 1.117 | 1.118 | 1.109 |
| $Nu_{\max}$ | | 1.508 | |
| y | | 0.087 | |

Table 2.2 Numerical results of natural convection in a square cavity for $Ra=10^4$

| | Benchmark | LBM | FV |
|---|---|---|---|
| Mesh size | 81×81 | 81×81 | 81×81 |
| $U_{\max}$ | 16.178 | 16.195 | 16.189 |
| y | 0.177 | 0.173 | 0.178 |
| $V_{\max}$ | 19.617 | 19.639 | 19.606 |
| x | 0.881 | 0.880 | 0.880 |
| $Nu_{ave}$ | 2.238 | 2.248 | 2.310 |
| $Nu_{\max}$ | | 3.543 | |
| y | | 0.140 | |

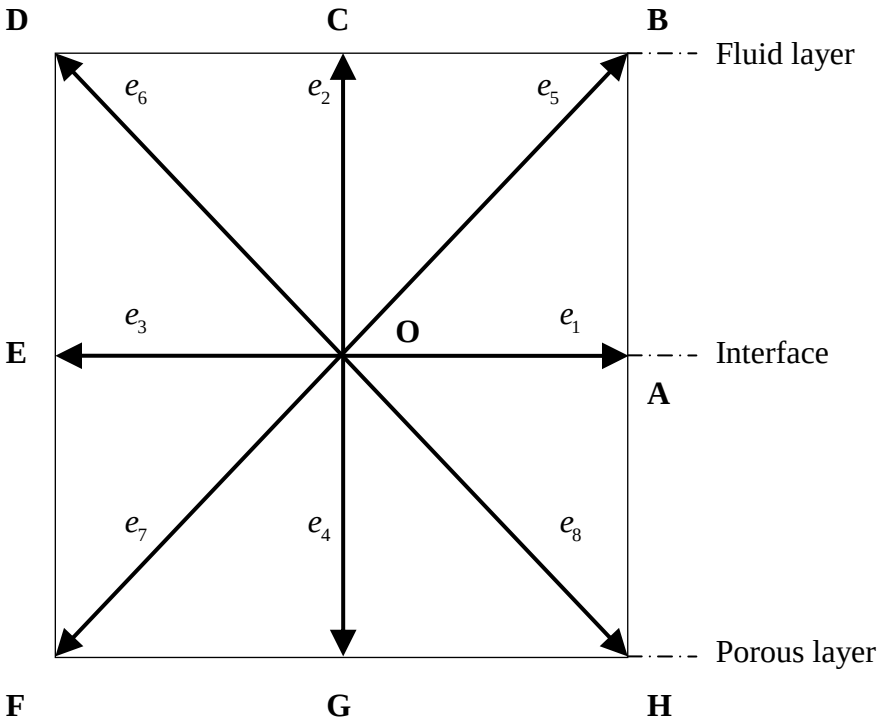


Figure 2.1 Basic lattice for the D2Q9 lattice Boltzmann model

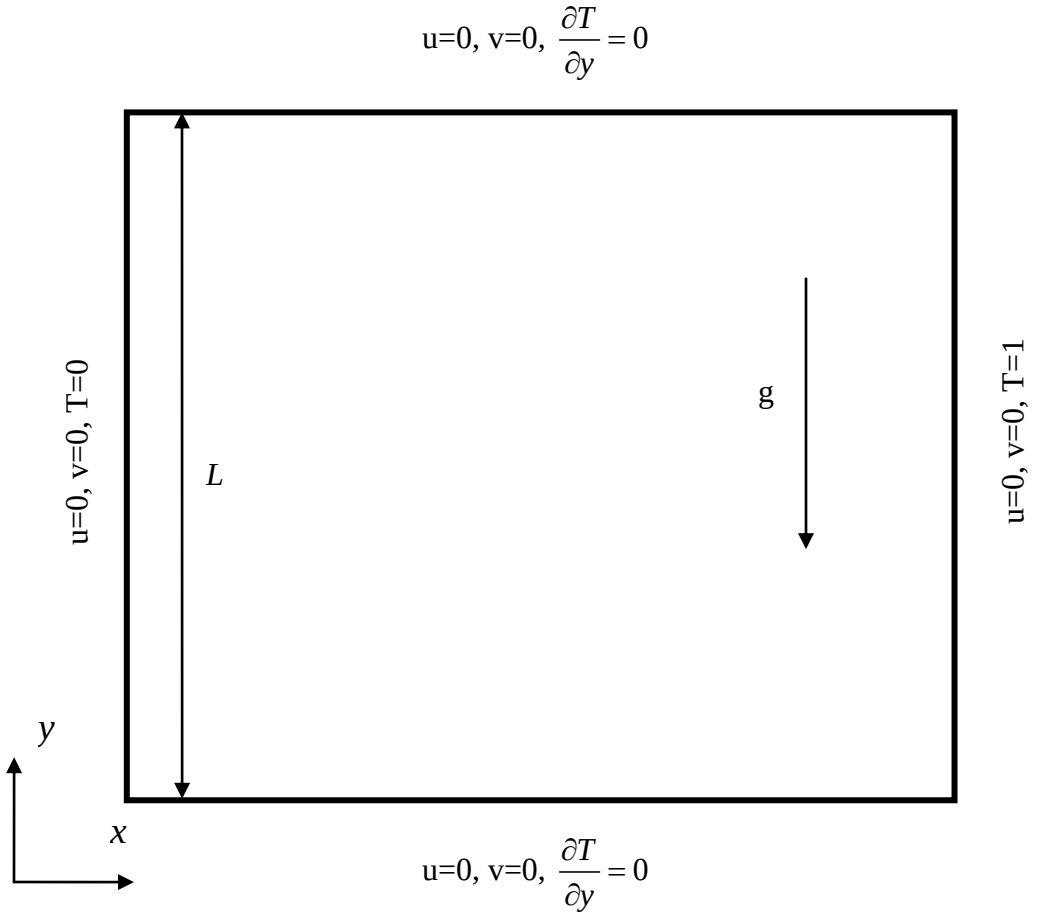


Figure 2.2 Schematic of natural convection in a square cavity

(a) Temperature

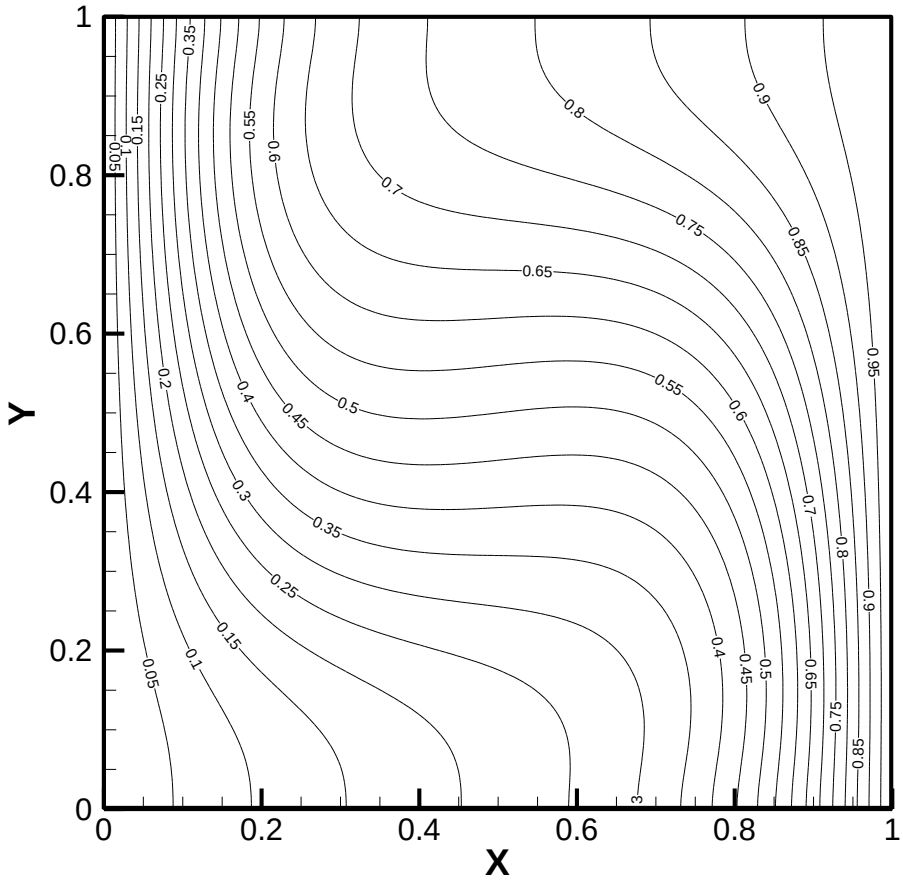

(b) Velocity U

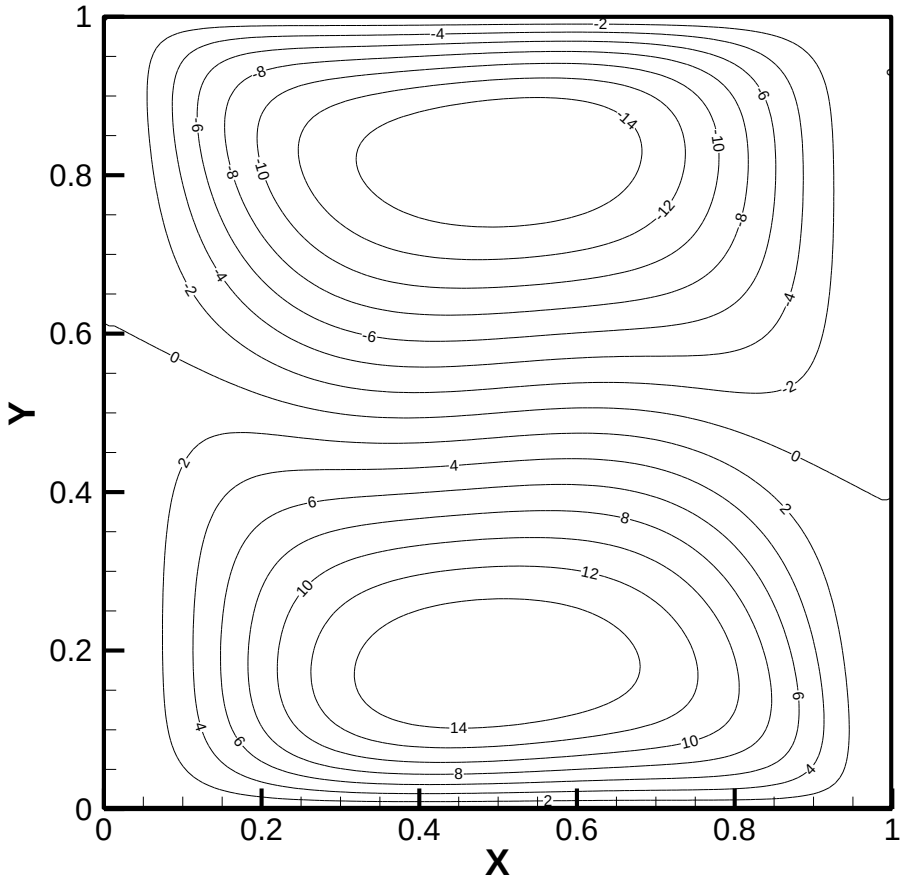

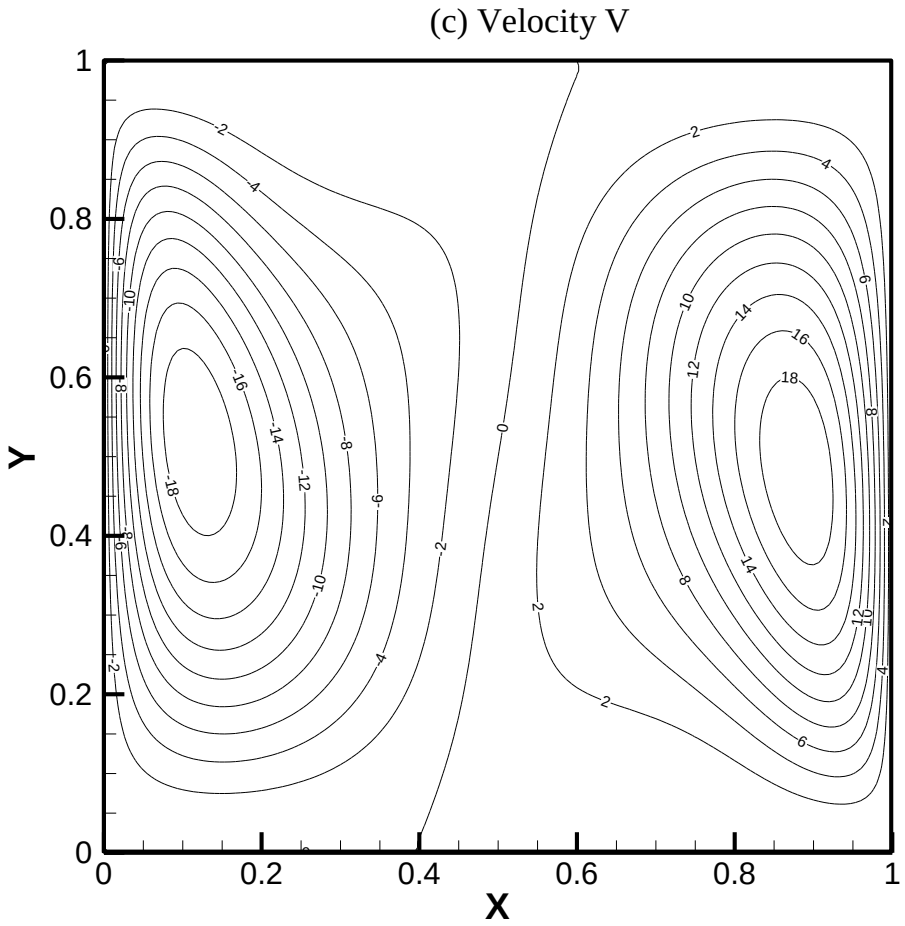


Figure 2.3 Natural convection in a square cavity with $Ra = 10^4$: (a) temperature contour; (b) velocity U contour; (c) velocity V contour;

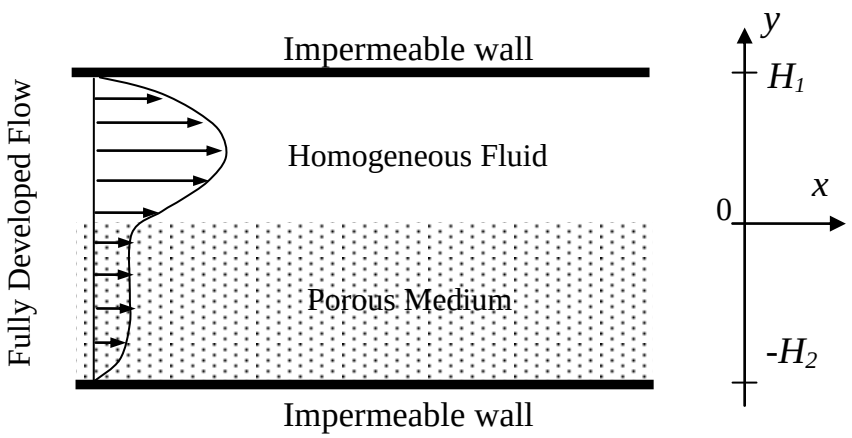


Figure 2.4 Schematic of flow in a channel partially filled with saturated porous medium

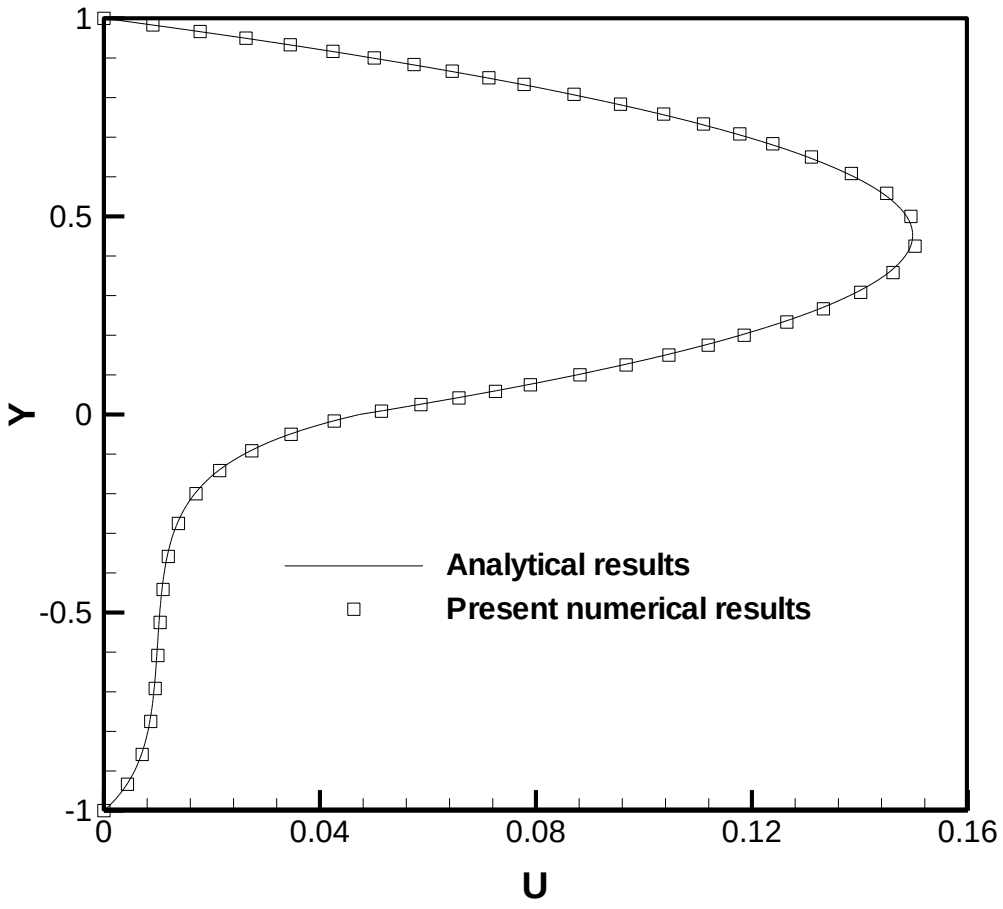


Figure 2.5 Validation of numerical method by comparison of velocity profiles between numerical and analytical results with $\beta = 0$, $\beta_1 = 0$, $\varepsilon = 0.7$, $Da = 10^{-2}$.

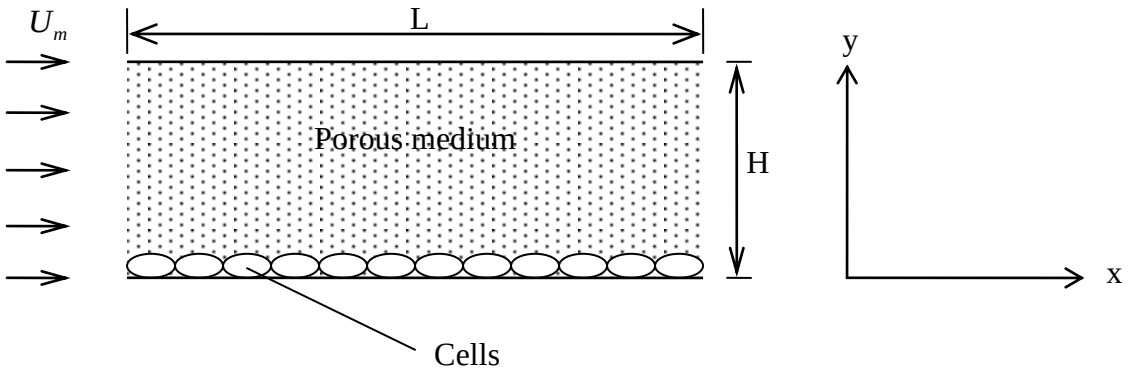


Figure 2.6 Scheme of the microchannel bioreactor (not to scale)

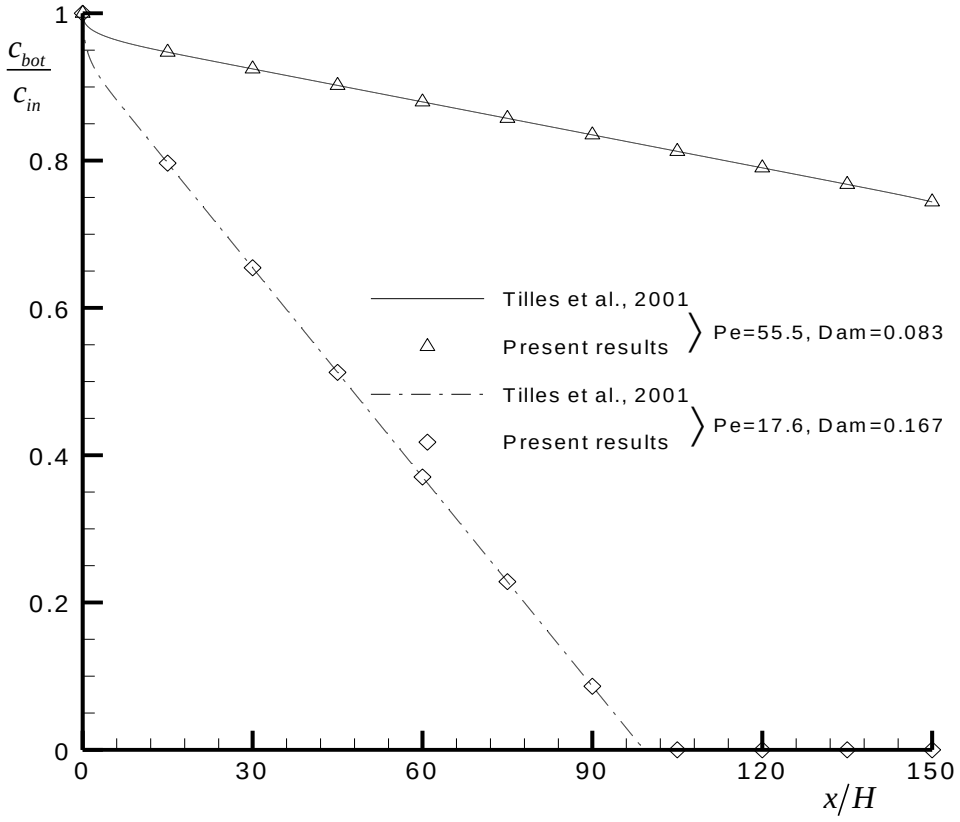


Figure 2.7 Axial distribution of substrate concentration at base plane (y=0) in 2D microchannel bioreactor

# Chapter 3 Simplified Analysis

In this chapter, the flow and mass transfer in a microchannel with a porous wall are analytically studied with a view to correlate the numerical results of Chapter 6. The reaction kinetics is based on zeroth-order type, Michaelis-Menten type and first-order type. The mathematical models are simplified to deduce the analytical solutions. Several non-dimensional parameters, such as combined interface concentration parameter, effective channel length/distance, reaction effectiveness factor, reactor efficiency and utilization efficiency are defined for the purpose of presenting generalized results (as presented in Chapter 6) which can find applications in the design analysis of such micro-channel reactors with a porous wall.

## 3.1 Problem Statement

### 3.1.1 Modeling of microchannel reactor with a porous wall

The reactor modeled in this chapter was a channel with dimensions typically of length 300 mm, 150 $\mu m$ in depth and width 2.5cm as shown in Figure 3.1. In practice due to its larger value, the width effect is small as shown by Zeng et al. (2006). Thus the numerical model considered here is simplified into a two-dimensional one like that of Zhao et al. (2005). The porous wall has a depth of $150\,\mu m$. A list of parameter values compiled from previous literature, giving their practical ranges, is given in Table 3.1.

The culture medium flows through the channel along the x direction, and there is a porous medium scaffold in the bottom region (see Figure 3.1) where the two cell types are uniformly distributed. The absorption cells and release cells adherent to the porous medium scaffold consume and secrete the species, respectively, forming the reactions in the porous scaffold. The incoming flow is steady, laminar and incompressible with substrate concentration $c_{in}$ . The inlet velocity is specified as that of a fully-developed flow.

The governing equations for the plain flow and porous flow are the same as described in Equations (2.9) to (2.10) and Equations (2.11) to (2.12). For the mass transfer equation in the porous part, the consumption reaction is assumed to follow the Michaelis-Menten model (Michael and Fikret, 1992; Chow et al., 2001a and 2001b):

$$u\frac{\partial c}{\partial x}+v\frac{\partial c}{\partial y}=D_{eff}\left(\frac{\partial^2 c}{\partial x^2}+\frac{\partial^2 c}{\partial y^2}\right)-\frac{\gamma_a V_{ma} c}{c+k_m} \tag{3.1}$$

where $c$ is volume-averaged concentration, $\gamma_a$ is the volume density of the absorb cells or enzymes, $V_{ma}$ is the maximal substrate uptake rate (SUR), $k_m$ is Michaelis-Menten constant or substrate concentration at which the SUR is half-maximal, $D_{eff}$ is the effective mass diffusivity in porous medium. The Michaelis-Menten model under certain conditions may be simplified to the zero order and first order reactions as given later.

As for the secretion reaction, the release rate is set as constant (Zeng et al. 2007). By including the secretion reaction in the previous equation, the mass transfer equation for the porous region is:

$$u\frac{\partial c}{\partial x}+v\frac{\partial c}{\partial y}=D_{eff}\left(\frac{\partial^2 c}{\partial x^2}+\frac{\partial^2 c}{\partial y^2}\right)+\gamma_r V_{mr}-\frac{\gamma_a V_{ma} c}{c+k_m} \tag{3.2}$$

where $\gamma_r$ is the volume density of the release cell or enzyme, $V_{mr}$ is the maximal substrate release rate (SRR) for release cell. $\gamma_a$ is the absorb cell or enzyme volume density, $V_{ma}$ is the maximal substrate uptake rate (SUR) for absorb cell. The above equation can be rearranged to obtain,

$$u\frac{\partial c}{\partial x}+v\frac{\partial c}{\partial y}=D_{eff}\left(\frac{\partial^2 c}{\partial x^2}+\frac{\partial^2 c}{\partial y^2}\right)-\gamma_a V_{ma}\left(\frac{c}{c+k_m}-a\right) \tag{3.3}$$

where $a$ is the ratio of release rate over absorb rate and is defined as:

$$a=\frac{V_{mr}\gamma_r}{V_{ma}\gamma_a} \tag{3.4}$$

The porous medium consists of a matrix structure with either cells or enzymes attached on it. The volume fraction occupied by the matrix and cells/ enzymes are $\varepsilon_s$ and $\varepsilon_c$ respectively. The porosity of the porous medium can be defined as:

$$\varepsilon=1-\varepsilon_s-\varepsilon_c \tag{3.5}$$

Generally, for the matrix without cells, the porosity may vary from 0.6 to 0.95 (Cooper et al., 2005) and the permeability of the porous medium is in the range of $10^{-12}$ to $10^{-9}$ $m^2$ (Wang and Tarbell, 2000). The results in Chapter 5 show that porosity makes relatively little effect on flow and heat transfer, compared with permeability; thus for simplicity the porosity $\varepsilon$ is set to be $\varepsilon$=0.8 in the simulations.

As for the permeability, it determines the velocity (under a driving pressure), which is characterized by the Peclet numbers of the fluid and porous flows.

The mass transfer equation in fluid part is:

$$u\frac{\partial c}{\partial x}+v\frac{\partial c}{\partial y}=D(\frac{\partial^2 c}{\partial x^2}+\frac{\partial^2 c}{\partial y^2}) \tag{3.6}$$

where $D$ is the mass diffusivity in plain fluid region.

### 3.1.2 Boundary conditions

For the concentration boundary conditions, zero mass flux condition was imposed on the upper and bottom solid-walls. Uniform concentration of $c_{in}$ was set at the inlet. As for the outlet, $\partial^2 c/\partial x^2=0$ was imposed so that the concentration flux is stable. At the interface between the homogeneous fluid region and porous media scaffold, continuities of mass and mass flux (Equations 2.18 and 2.19) were imposed.

For the velocity boundary conditions, the non-slip condition was imposed on the solid upper and bottom walls. As this is a steady laminar channel flow, to save computation cost, a fully-developed axial velocity was imposed for the channel inlet and outlet. At the interface between the homogeneous fluid region and porous media scaffold, the stress-jump interfacial conditions (Equation 2.15) together with continuities of velocity and normal stress (Equations 2.16 and 2.17) were imposed.

## 3.2 Analysis

### 3.2.1 Non-dimensional parameters

The non-dimensional substrate concentration and x, y coordinate are defined as:

$$C = \frac{c}{c_{in}} \tag{3.7}$$

$$X = \frac{x}{L} \tag{3.8}$$

$$Y = \frac{y}{H} \quad \text{for plain fluid region} \tag{3.9}$$

$$Y = \frac{y}{h} \quad \text{for porous medium region} \tag{3.10}$$

where $c_{in}$ is inlet concentration, $L$ is channel length, $h$ is the porous medium height and $H$ is the plain fluid height.

The porous and fluid Peclet numbers represent the ratio of convection to diffusion in porous and fluid domains, respectively. They are defined as:

$$Pe_p = \frac{u_{p\_av} h}{D_{eff}} \tag{3.11}$$

$$Pe_f = \frac{u_{f\_av} H}{D} \tag{3.12}$$

where $u_{p\_av}$ and $u_{f\_av}$ are the average flow velocities in porous and fluid regions respectively.

The fluid and porous Damkohler numbers for absorption and release are defined as:

$$Dam_{fa} = \frac{V_{ma}\gamma_a h}{u_{f\_av} c_{in}} \tag{3.13}$$

$$Dam_{fr} = \frac{V_{mr}\gamma_r h}{u_{f\_av} c_{in}} \tag{3.14}$$

$$Dam_{pa} = \frac{V_{ma}\gamma_a h^2}{D_{eff} c_{in}} \tag{3.15}$$

$$Dam_{pr} = \frac{V_{mr}\gamma_r h^2}{D_{eff} c_{in}} \tag{3.16}$$

$Dam_{fa}$ and $Dam_{fr}$ characterize the ratio of the time scales of substrate absorb and release reactions, respectively, to substrate convection in the fluid domain. $Dam_{pa}$ and $Dam_{pr}$ characterize the ratio of the time scales of substrate absorb and release reactions, respectively, to substrate diffusion in the porous medium.

The non-dimensional Michaelis-Menten constant, which is the non-dimensional concentration at which specific uptake rate is half maximal, is defined as:

$$K_m = \frac{k_m}{c_{in}} \tag{3.17}$$

## 3.2.2 Simple analysis for porous region

### 3.2.2.1 Zeroth order reaction type

Due to the relatively higher flow resistance provided by the porous medium, the axial velocity there is much smaller than that in the fluid part. Since the reactor

length is relatively larger than the porous medium depth, the mass transfer by diffusion is dominant in the Y-direction, that is $\frac{\partial c}{\partial y} >> \frac{\partial c}{\partial x}$ . When $k_m$ =0**,** the reaction rate in the whole porous scaffold is constant at the maximal value. It becomes the zeroth-order reaction type and Equation (3.3) can be simplified to:

$$\frac{\partial^2 c}{\partial y^2} = \frac{\gamma_a V_{ma} - \gamma_r V_{mr}}{D_{eff}} = \frac{\gamma_a V_{ma}(1-a)}{D_{eff}} \tag{3.18}$$

By normalizing the concentration and y-coordinate by $c_{in}$ and *h* respectively, the above equation is expressed in non-dimensional form as:

$$\frac{\partial^2 C}{\partial Y^2} = \frac{\gamma_a V_{ma}(1-\alpha)h^2}{D_{eff} c_{in}} = Dam_{pa}(1-a) \tag{3.19}$$

The boundary conditions at the interface and bottom wall are:

$$\text{Y=1, } C = C_{\text{int}} \tag{3.20}$$

$$\text{Y=0, } \frac{\partial C}{\partial Y} = 0 \tag{3.21}$$

Using the boundary conditions, the solution of Equation (3.19) is:

$$C = \frac{1}{2} Dam_{pa}(1-a)Y^2 + C_{\text{int}} - \frac{1}{2} Dam_{pa}(1-a) \tag{3.22}$$

At the bottom wall where Y=0,

$$C_{bot} = C_{\text{int}} - \frac{1}{2} Dam_{pa}(1-a) \tag{3.23}$$

$$\frac{C_{\text{int}} - C_{bot}}{Dam_{pa}(1-a)} = \frac{1}{2} \tag{3.24}$$

Equation (3.24) presents a simple relationship between the concentration difference and porous Damkohler number. It shows that, under one dimensional assumption, the

concentration difference normalized by the porous Damkohler number is a constant. This simplified analysis indicates the significance of a concentration difference parameter $\kappa$ express as:

$$\kappa = \frac{C_{\text{int}} - C_{bot}}{Dam_{pa}(1-a)} = \frac{\dfrac{D_{eff}\left(c_{\text{int}} - c_{bot}\right)}{h}}{V_{ma}\gamma_a h(1-a)} \tag{3.25}$$

The parameter $\kappa$ also gives an indication of the ratio of the concentration flux into the porous medium and the reaction rate.

### 3.2.2.2 Michaelis-Menten reaction type

For Michaelis-Menten reaction type, the substrate uptake rate (SUR) is a function of local concentration. When the concentration is zero, SUR is also zero. When the local concentration equals to Michaelis-Menten constant, SUR equals to its half maximal value. The SUR approaches a maximum value when the concentration is very large (zeroth order reaction). Using one dimensional assumptions similar to that for zeroth order reaction type, the mass transfer Equation (3.3) can be simplified as:

$$\frac{\partial^2 c}{\partial y^2} = \frac{\gamma_a V_{ma}}{D_{eff}}\frac{c}{c+k_m} - \frac{\gamma_r V_{mr}}{D_{eff}} = \frac{\gamma_a V_{ma}}{D_{eff}}\left(\frac{c}{c+k_m} - a\right) \tag{3.26}$$

As before, non-dimensionalize the equation by using $c_{in}$ and h. Assuming that the non-dimensional concentration in porous region varies from its value 1 at inlet to a critical value $K_m$ at outlet, the average concentration in porous region is assumed to be approximated as $C = \dfrac{1+K_m}{2}$.

Equation (3.26) can be expressed in a linear form as:

$$\frac{\partial^2 C}{\partial Y^2} = \frac{\gamma_a V_{ma} h^2}{D_{eff} c_{in}} \left( \frac{C}{C + K_m} - a \right) \approx Dam_{pa} \left( \frac{1 + K_m}{1 + 3K_m} - a \right) \tag{3.27}$$

With similar boundary conditions (3.20) and (3.21) as in the zeroth order model, the above equation can be solved as:

$$C = \frac{1}{2} Dam_{pa} \left( \frac{1 + K_m}{1 + 3K_m} - a \right) Y^2 - \frac{1}{2} Dam_{pa} \left( \frac{1 + K_m}{1 + 3K_m} - a \right) + C_{\text{int}} \tag{3.28}$$

When Y=0,

$$C_{bot} = C_{\text{int}} - \frac{1}{2} Dam_{pa} \left( \frac{1 + K_m}{1 + 3K_m} - a \right) \tag{3.29}$$

Rearrange to obtain:

$$C_{\text{int}} - C_{bot} = \frac{1}{2} Dam_{pa} \left( \frac{1 + K_m}{1 + 3K_m} - a \right) \tag{3.30}$$

$$\frac{C_{\text{int}} - C_{bot}}{Dam_{pa} \left( \frac{1 + K_m}{1 + 3K_m} - a \right)} = \frac{1}{2} \tag{3.31}$$

Equation (3.31) presents a simple relationship between the concentration difference and porous Damkohler number. It indicates the significance of a concentration difference parameter $\kappa$ expressed as:

$$\kappa = \frac{C_{\text{int}} - C_{bot}}{Dam_{pa} \left( \frac{1 + K_m}{1 + 3K_m} - a \right)} = \frac{\frac{D_{eff} (c_{\text{int}} - c_{bot})}{h}}{V_{ma} \gamma_a h \left( \frac{1 + K_m}{1 + 3K_m} - a \right)} \tag{3.32}$$

This expression is similar in form to that for the zeroth order model except that it includes additional terms of the Michaelis-Menten constant $K_m$.

### 3.2.2.3 First order reaction type

Similar one dimensional assumption, as in the previous two sections, is used for the first-order reaction type. It is for small concentration, or large $k_m$, and hence small reaction. The mass transfer Equation (3.3) can be simplified as:

$$\frac{\partial^2 c}{\partial y^2} = \frac{\gamma_a V_{ma}}{D_{eff} k_m} c \tag{3.33}$$

As before, non-dimensionalize the equation by using $c_{in}$ and h:

$$\frac{\partial^2 C}{\partial Y^2} = \frac{\gamma_a V_{ma} h^2}{D_{eff} c_{in} K_m} C = \frac{Dam_{pa}}{K_m} C \tag{3.34}$$

With boundary conditions similar to the previous two sections for the interface and bottom wall, as given by Equations (3.20) and (3.21), the above linear equation can be solved as:

$$C = \frac{C_{\text{int}}}{e^{\sqrt{\frac{Dam_{pa}}{K_m}}} + e^{-\sqrt{\frac{Dam_{pa}}{K_m}}}} \left( e^{\sqrt{\frac{Dam_{pa}}{K_m}} Y} + e^{-\sqrt{\frac{Dam_{pa}}{K_m}} Y} \right) \tag{3.35}$$

At Y=0,

$$C_{bot} = \frac{2C_{\text{int}}}{e^{\sqrt{\frac{Dam_{pa}}{K_m}}} + e^{-\sqrt{\frac{Dam_{pa}}{K_m}}}} \tag{3.36}$$

where $\frac{e^{\sqrt{\frac{Dam_p}{K_m}}} + e^{-\sqrt{\frac{Dam_p}{K_m}}}}{2} \approx 1 + \frac{1}{2}\frac{Dam_p}{K_m}$ by using series expansion for the exponential terms and neglecting higher order terms (small $Dam_p / K_m$).

Hence the above Equation (3.36 ) is expressed as:

$$(\frac{C_{\text{int}} - C_{bot}}{C_{\text{int}}}) / \frac{Dam_p}{K_m} \approx \frac{0.5}{1 + 0.5\frac{Dam_p}{K_m}} \tag{3.37}$$

Equation (3.37) gives a simple relationship between the concentration difference and porous Damkohler number. For first-order reaction, the concentration along the interface $C_{\text{int}}$ is close to 1.0. Thus, as in the previous two sections, the above equation indicates the significance of a concentration difference parameter $\kappa$:

$$\kappa = \frac{C_{\text{int}} - C_{bot}}{\frac{Dam_{pa}}{K_m}} = \frac{\frac{D_{eff}(c_{\text{int}} - c_{bot})}{h}}{\frac{V_{ma}\gamma_a h}{K_m}} \tag{3.38}$$

## 3.2.3 Simple analysis for fluid region

### 3.2.3.1 Zeroth order reaction type

A simple analysis is carried out to combine the non-dimensional parameters for the purpose of correlating the numerical data. It is assumed that the flow is uniform and the diffusion is in y-direction. The mass transfer equation in fluid part (Equation 3.6) is simplified to:

$$\frac{\partial C}{\partial X} = \frac{L}{H}\frac{1}{Pe_f}\frac{\partial^2 C}{\partial Y^2} \tag{3.39}$$

The flux at the interface may be approximated by a first order discretisation using concentration difference. Then, using Equation (3.24) the flux may be expressed as:

$$\left.\frac{\partial C}{\partial Y}\right|_{\text{int}} = \frac{(C_{\text{int}} - C_{bot})H}{h} = \frac{1}{2}\frac{H}{h} Dam_{pa}(1-a) = \frac{1}{2} Dam_{pa}\lambda \tag{3.40}$$

where $\lambda$ is a reaction rate parameter:

$$\lambda = \frac{H}{h}(1-a) \tag{3.41}$$

Using separation of variables techniques, with the above boundary condition and zero flux at the top wall, the mass transfer equation can be solved to give the concentration distribution along the interface:

$$\begin{aligned} C_{\text{int}} - 1 = & -\frac{1}{2}\frac{x}{H}\frac{1}{Pe_f} Dam_{pa}\lambda - \frac{1}{6} Dam_{pa}\lambda \\ & + \frac{1}{\pi^2} Dam_{pa}\lambda \sum_{n=1}^{\infty} \frac{(-1)^n}{n^2} \cos(n\pi) \exp(-n^2\pi^2 \frac{x}{H}\frac{1}{Pe_f}) \end{aligned} \tag{3.42}$$

The above equation may be re-arranged to give:

$$\frac{C_{\text{int}} - 1}{Dam_{pa}\lambda} = -\frac{1}{2}\frac{x}{H}\frac{1}{Pe_f} - \frac{1}{6} + \frac{1}{\pi^2}\sum_{n=1}^{\infty}\frac{(-1)^n}{n^2}\cos(n\pi)\exp(-n^2\pi^2\frac{x}{H}\frac{1}{Pe_f}) \tag{3.43}$$

Note that for this simplified analyses, the diffusivity $D_{eff}$ in the porous region was assumed to be the same as the diffusivity $D$ in the fluid region. The above equation shows that the interface concentration parameter $\frac{C_{\text{int}} - 1}{Dam_{pa}\lambda}$ is a function of the parameters $\frac{x}{H}\frac{1}{Pe_f}$ only.

The above simplified analysis indicates the two combined parameters which may be useful for correlating the interface concentration at various $Pe_f$ , $Dam_{pa}$ and $K_m$:

Effective distance parameter:

$$\zeta = \frac{x}{H}\frac{1}{Pe_f} \tag{3.44}$$

Interface concentration reaction parameter:

$$\xi_k = \frac{C_{\text{int}} - 1}{Dam_{pa}\lambda} \tag{3.45}$$

### 3.2.3.2 Michaelis-Menten reaction type

Similar to the zeroth order model, the flux at the interface may be approximated by a first order discretisation using concentration difference. Then, using Equation (3.31), the flux may be expressed as:

$$\left.\frac{\partial C}{\partial Y}\right|_{\text{int}} = \frac{(C_{\text{int}} - C_{bot})H}{h} = \frac{1}{2}\frac{H}{h}Dam_{pa}\left(\frac{1+K_m}{1+3K_m} - a\right) = \frac{1}{2}Dam_{pa}\lambda \tag{3.46}$$

where $\lambda$ is reaction rate parameter:

$$\lambda = \frac{H}{h}\left(\frac{1+K_m}{1+3K_m} - a\right) \tag{3.47}$$

Using similar techniques as that for the zeroth-order reaction, the mass transfer equation can be solved to give the concentration distribution along the interface:

$$C_{\text{int}} - 1 = -\frac{1}{2}\frac{x}{H}\frac{1}{Pe_f} Dam_{pa}\lambda - \frac{1}{6} Dam_{pa}\lambda + \frac{1}{\pi^2} Dam_{pa}\lambda \sum_{n=1}^{\infty} \frac{(-1)^n}{n^2} \cos(n\pi) \exp(-n^2\pi^2 \frac{x}{H}\frac{1}{Pe_f}) \tag{3.48}$$

The equation may be re-arranged to give:

$$\frac{C_{\text{int}} - 1}{Dam_{pa}\lambda} = -\frac{1}{2}\frac{x}{H}\frac{1}{Pe_f} - \frac{1}{6} + \frac{1}{\pi^2} \sum_{n=1}^{\infty} \frac{(-1)^n}{n^2} \cos(n\pi) \exp(-n^2\pi^2 \frac{x}{H}\frac{1}{Pe_f}) \tag{3.49}$$

The above equation shows that the interface concentration parameter is a function of the parameters $\frac{x}{H}\frac{1}{Pe_f}$ only. The above simplified analysis proposes two combined parameters which may be useful for correlating the interface concentration at various $Pe_f$ , $Dam_{pa}$ and $K_m$ :

Effective distance parameter:

$$\zeta = \frac{x}{H}\frac{1}{Pe_f} \tag{3.50}$$

Interface concentration reaction parameter:

$$\xi_k = \frac{C_{\text{int}} - 1}{Dam_{pa}\lambda} \tag{3.51}$$

### 3.2.3.3 First order reaction type

Similar to the previous two models, the flux at the interface may be approximated by a first order discretisation using concentration difference. Then, using Equation (3.37), the flux may be expressed as:

$$\left.\frac{\partial C}{\partial Y}\right|_{\text{int}} = \frac{(C_{\text{int}} - C_{bot})H}{h} = \frac{1}{2}\frac{H}{h} Dam_{pa} / K_m = \frac{1}{2} Dam_{pa}\lambda \tag{3.52}$$

where $\lambda$ is reaction rate parameter:

$$\lambda = \frac{H}{h}\frac{1}{K_m} \tag{3.53}$$

Using similar techniques as that for the previous two models, the mass transfer equation can be solved to give the concentration distribution along the interface:

$$\begin{aligned} C_{\text{int}} - 1 &= -\frac{1}{2}\frac{x}{H}\frac{1}{Pe_f} Dam_{pa}\lambda - \frac{1}{6} Dam_{pa}\lambda \\ &+ \frac{1}{\pi^2} Dam_{pa}\lambda \sum_{n=1}^{\infty} \frac{(-1)^n}{n^2} \cos(n\pi) \exp(-n^2\pi^2 \frac{x}{H}\frac{1}{Pe_f}) \end{aligned} \tag{3.54}$$

The Equation may be re-arranged to obtain:

$$\frac{C_{\text{int}} - 1}{Dam_{pa}\lambda} = -\frac{1}{2}\frac{x}{H}\frac{1}{Pe_f} - \frac{1}{6} + \frac{1}{\pi^2}\sum_{n=1}^{\infty}\frac{(-1)^n}{n^2}\cos(n\pi)\exp(-n^2\pi^2\frac{x}{H}\frac{1}{Pe_f}) \tag{3.55}$$

Equation (3.55) shows that the interface concentration parameter is a function of the parameters $\frac{x}{H}\frac{1}{Pe_f}$ only. The above simplified analysis proposes two combined parameters which may be useful for correlating the interface concentration at various $Pe_f$ , $Dam_{pa}$ and $K_m$ :

Effective distance parameter:

$$\zeta = \frac{x}{H}\frac{1}{Pe_f} \tag{3.56}$$

Interface concentration reaction parameter:

$$\xi_k = \frac{C_{\text{int}} - 1}{Dam_{pa}\lambda} \tag{3.57}$$

### 3.2.4 Definition of effectiveness and efficiency

The effectiveness factor was expressed by E. Gomez et al. (2006) as the ratio of observed reaction rate to reaction rate without mass transfer resistance. Based on this idea, Al-Muftah and Abu-Reesh (2005) defined the effectiveness factor as the ratio of actual reaction rate to that which would be obtained if the enzyme or cells were at the interface (that is without the porous medium diffusion resistance).

Based on the above definition, and assuming that the flux equals the reaction, the local effectiveness factor can be expressed as:

$$\begin{aligned}\xi &= \frac{\left.\frac{dC}{dY}\right|_{\text{int}}}{Dam_{pa}\left(\frac{C_{\text{int}}}{C_{\text{int}}+K_m}-a\right)} = \frac{\left.\frac{dC}{dY}\right|_{\text{int}}}{\frac{V_{ma}\gamma_a h^2}{D_{eff}c_{\text{in}}}\left(\frac{C_{\text{int}}}{C_{\text{int}}+K_m}-a\right)} \\ &= \frac{D_{eff}\left.\frac{dc}{dy}\right|_{\text{int}}}{V_{ma}\gamma_a h\left(\frac{c_{\text{int}}}{c_{\text{int}}+k_m}-a\right)}\end{aligned} \tag{3.58}$$

where $c_{int}$ is the local interface concentration. The critical reaction parameter may be introduced from the above equation:

$$R_c = \frac{c_{\text{int}}}{c_{\text{int}} + k_m} - a \tag{3.59}$$

The critical reaction parameter presents the relationship between the consumption rate and release rate. When $R_c$>0, the concentration flux at the interface is positive into the porous scaffold. When $R_c$<0, the release rate is higher than consumption rate and thus the concentration flux becomes negative. When $R_c$<0, the concentration in the porous scaffold keeps on increasing, and such a study is not useful for application purposes. The present study only considers the cases of $R_c$>0.

The reactor efficiency is the ratio of actual reaction rate over the maximum reaction rate based on concentration at the inlet. For present study, considering the Darcy velocity is at least one order smaller than plain fluid velocity, the convective mass transfer in porous wall may be negligible compared with convective mass transfer in plain fluid region. Thus the reactor efficiency may be expressed based on inlet and outlet flux difference in the plain fluid region:

$$\begin{aligned}\eta &= \frac{1-\bar{C}_{out}}{Dam_{fa}\left(\frac{1}{1+K_m}-a\right)\frac{L}{H}} = \frac{\frac{c_{\text{in}}-\bar{c}_{out}}{c_{\text{in}}}}{\frac{V_{ma}\gamma_a h}{u_{f\_av}c_{\text{in}}}\left(\frac{c_{\text{in}}}{c_{\text{in}}+k_m}-a\right)\frac{L}{H}} \\ &= \frac{u_{f\_av}H\left(c_{\text{in}}-\bar{c}_{out}\right)}{hL\left(V_{ma}\gamma_a\frac{c_{\text{in}}}{c_{\text{in}}+k_m}-V_{mr}\gamma_r\right)}\end{aligned} \tag{3.60}$$

where $\bar{c}_{out}$ is the average outlet concentration in plain fluid region and $c_{in}$ is inlet concentration.

To evaluate the wastage of substrate in reactors, the utilization efficiency (or conversion rate) is defined as the ratio of actual utilized mass rate over the inlet mass rate:

$$\eta_u = \frac{u_{f\_av} H \left( c_{\text{in}} - \bar{c}_{out} \right)}{u_{f\_av} H c_{\text{in}}} = 1 - \bar{C}_{out} \tag{3.61}$$

Combining the above two equations, the utilization efficiency may be expressed as:

$$\eta_u = \eta \cdot Dam_{fa} \left( \frac{1}{1 + K_m} - a \right) \frac{L}{H} \tag{3.62}$$

## 3.3 Conclusions

It should be noted that the above analyses in Section 3.2 are meant only for the purpose of developing the combined dimensionless parameters and defining the effectiveness or efficiencies of the reactor. It is based on simplified reaction models and assumes no convection but only diffusion in the Y-direction in the porous medium. It is necessary to evaluate from the numerical results whether the use of the combined parameters is able to give good collapse of data. It is interesting to find that the simplified analytical solution of concentration parameters along the interface is function of effective channel distance only. It will be discussed later in Chapter 6 whether the use of the combined parameters is able to give good collapse of numerical data.

Table 3.1 List of parameter values for model predictions.

| Type of Applications | Parameters | | References |
|---|---|---|---|
| Perfusion Bioreactor (oxygen) | | Assumed Values | |
| | L | 100 *mm* | Chou et al., 2001, Zhao et al., 2005 and 2007; Pathi et al., 2005. |
| | H | 6 *mm* | |
| | h | 0.6 *mm* | |
| | $C_{in}$ | $2.2 \times 10^{-7}\ mol/ml$ | |
| | $k_m$ | $1.1 \times 10^{-8}\ mol/ml$ | |
| | $D_{eff}$ | $1.59 \times 10^{-9}\ m^2/s$ | |
| | $D$ | $3.29 \times 10^{-9}\ m^2/s$ | |
| | $V_m$ | $1.25 \times 10^{-17}\ mol/cell/s$ | |
| | $\gamma$ | $5.40 \times 10^{5} \sim 3.60 \times 10^{7}\ cells/ml$ | Zhao et al., 2005; Pathi et al., 2005. |
| | | Computed Values | |
| | $K_m$ | $5.0 \times 10^{-2}$ | |
| | $Pe_f$ | 15 ~225 | |
| | $Pe_p$ | $5.60 \times 10^{-7} \sim 8.40 \times 10^{-6}$ | |
| | $Dam_p$ | $6.94 \times 10^{-3} \sim 0.463$ | |
| | $Dam_f$ | $1.66 \times 10^{-4} \sim 0.111$ | |
| Micro-Enzyme Reactor (glucose) | | Assumed Values | |
| | L | 11 *mm* | Drott et al., 1997 and 1999. |
| | H | $32.5\ \mu m$ | |
| | h | $\leq 15\ \mu m$ | |
| | $c_{in}$ | $0.5, 1.2, 5\ mol/m^3$ | |
| | $k_m$ | $3 \sim 10\ mol/m^3$ | |
| | $D_{eff}$ | $5.4 \times 10^{-10}\ m^2/s$ | Ye et al., 2006. |
| | $D$ | $5.4 \times 10^{-10}\ m^2/s$ | |
| | $V_m\ \gamma$ h | $\leq 3.05 \times 10^{-5}\ mol/m^2/s$ | Drott et al., 1997 and 1999. |
| | | Computed Values | |
| | $K_m$ | 0.6~20 | |
| | $Pe_f$ | $3.24 \times 10^{3}$ | |
| | $Pe_p$ | $3.53 \times 10^{-9}$ | Lysenko et al., 2004. |
| | $Dam_p$ | $\leq 1.60$ | |
| | $Dam_f$ | $\leq 6.1 \times 10^{-4}$ | |

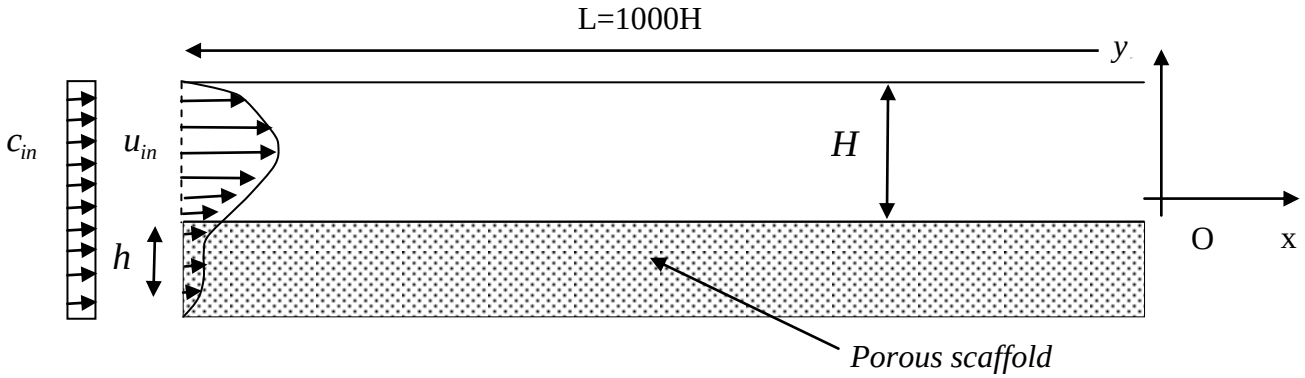


Figure 3.1 Schematic of the bioreactor model (not to scale)

# Chapter 4 Flow Through a Channel Partially Filled with a Fibrous Medium*

In this chapter, incompressible steady slow viscous flow through a channel partially filled with fibrous porous media will be studied. The fibrous porous media are modeled as periodic array of circular cylinders, where the aspect ratio of cylinder is 1. The porosity is adjusted by changing the cylinder diameter. The permeability of the fibrous medium could be readily changed by variation of the cylinder diameter or its spacing. One of the main objectives was to investigate the boundary conditions at the interface between fluid layer and fibrous porous medium. The slip coefficient, interfacial velocity, effective viscosity, and stress jump coefficients are determined and analyzed.

## 4.1 Problem Statement

The physical configuration and the coordinate systems are shown in Figure 4.1. The interface is at $y = 0$, and the top and bottom walls are at $y = \pm H$. The porous medium is simulated as hexagonal arrays of circular cylinders, which is bounded at the top by free fluid and at the bottom by solid wall. In the present study, the flow is transverse or perpendicular to the axis of cylinders. The periodic boundary condition is applied at the inlet and outlet of the channel. The channel flow is driven by a constant pressure gradient. The porosity was changed by changing the cylinder

*Parts of this chapter have been published in Bai et al., *International Journal for Numerical Methods in Fluids 60, 809-825, 2009*

diameter. The interface position was chosen to be the plane which is tangent to the outer edges of cylinders in the first row (Beavers and Joseph 1967, Sahraoui and M. Kaviany 1992, James and Davis 2001).

## 4.2 Results and Discussion

### 4.2.1 Non-dimensional parameters

The velocity, distance and permeability are non-dimensionalized as (Sadiq et at. 1995):

$$U = \frac{u}{u_D} \tag{4.1}$$

$$Y = \frac{y}{H} \tag{4.2}$$

$$Da = \frac{K}{H^2} \tag{4.3}$$

where $H$ is the channel semi-width of flow region as shown in Figure 4.1. $Da$ is Darcy number. The velocity gradients on either sides of the interface were obtained from the slope of the volume averaged velocity near the interface in the fluid and porous media. The selected calculation domain and the volume averaged velocity profile are shown in Figure 4.3.

### 4.2.2 Permeability of fibrous porous medium

There have been analytical studies of unbounded flow through infinite and semi-infinite lattices of infinitely long cylinders (Larson and Higdon 1987, Kaviany 1991, Sahraoui and M. Kaviany 1992 and Barrere et al. 1992). A numerical study on bounded flow has been given by James and Davies (2001). The present numerical results of permeability are compared with the previous studies.

Figure 4.2a and 4.2b shows the non-dimensional permeability $\frac{K}{d^2}$. It increases exponentially with increasing porosity, tending to infinitely large value when the porosity is close to unity. With the fixed cylinder center positions, a large porosity is associated with small cylinder diameter $d$ and large permeability K, so that $\frac{K}{d^2}$ becomes large.

The cell, lubrication and asymptotic models are shown in Figure 4.2a for comparison with the present result. It is seen that the present results tend towards the cell model at high porosity and towards the lubrication model at low porosity. The present result is consistent with the assumptions of both models. The present results show good agreement with the asymptotic model.

The results are compared with Carman-Kozeny model in Figure 4.2b, which has a Carman-Kozeny constant $k$. It is seen that with $k$ from 0.2 to 17.9, the Carman-Kozeny model bounds the present numerical results. The present results may be approximately fitted by the Carman-Kozeny model with a constant $k$ =1.5. However, note that the Carman-Kozeny constant varies with porosity, though not so obvious in the present results.

Figure 4.2c shows the permeability $K/A$ as a function of solid volume fraction $c=1-\varepsilon$ for hexagonal array of circular cylinders, where *A* is the area of the unit cell as defined by Larson and Higdon (1987). The comparison shows that the present results are in good agreement with those of Larson and Higdon (1987). The agreement is better at high solid fraction. Note that Larson and Higdon's (1987) model is for infinite array, but the present array is bounded by free fluid at the top and solid wall at the bottom.

### 4.2.3 Velocity profiles in cross section and grid convergence check

Figure 4.3a and 4.3b show the velocity profiles at two permeabilities. In Figure 4.3a, different element numbers are used to check the convergence. It is seen that 64 elements per cylinder are sufficient. Also presented in Figure 4.3b is an enlarged figure of the domain used for calculations of the velocity gradient near the interface.

The velocities are non-dimensionalized by the average Darcy velocity $u_D$. Thus the non-dimensional velocity in the porous medium is near to unity. At larger permeability, the Darcy velocity is larger, though not depicted by the non-dimensional plot. The maximum velocity in the fluid layer is much larger than those in the porous medium, well above an order of magnitude larger (see Figure 4.3a and 4.3b). In the domain scale results of Alazmi and Vafai (2001) their maximum velocities are 130–1300 times of the Darcy velocity. However their Darcy numbers are smaller, which varies from $10^{-3}-10^{-4}$ compared with the present Darcy number ranges from $7.3\times10^{-3}-10.1\times10^{-3}$. In the present velocity profiles (see Figure 4.3a

and 4.3b), the maximum velocity is greater at smaller permeability, which is consistent with the velocity results of Alazmi and Vafai (2001). It can be explained that, with constant pressure gradient, there is much more flow at the fluid side compared with that at the porous medium; the porous flow is lower at smaller permeability.

## 4.2.4 Interfacial boundary conditions

### 4.2.4.1 Slip boundary condition

The slip boundary condition has been used in the homogeneous modeling of interface between fluid and porous media. The interfacial shear is related to the interface velocity $u_{y=0}$ at the interface by a slip-coefficient $\alpha$:

$$\left.\frac{du}{dy}\right|_{y=0^+} = \frac{\alpha}{\sqrt{K}}\left(u_{y=0} - u_D\right) \tag{4.4}$$

Using the slip boundary condition, together with the no-slip boundary condition at the impermeable wall, the velocity distribution in the fluid side may be found. The uniform Darcy velocity in the fibrous medium is obtained from Darcy law. The interfacial velocity and slip coefficient may be related by analysis:

$$\frac{u_{y=0}}{u_D} = \frac{1}{2}\frac{1+2\alpha\sqrt{Da}}{Da+\alpha\sqrt{Da}} \tag{4.5}$$

Figure 4.4 shows the slip-coefficient $\alpha$ (calculated using Equation 4.4) at various Darcy number. The slip-coefficient varies between 0.4 and 8.4 and the average value is 5 over the present range of *Da*.

In Beavers and Joseph (1967) experiments, the slip-coefficient varies from 0.1 to 4, as permeability increases. It is difficult to make detailed comparison as Beavers and Joseph (1967) specified pore size and not Darcy number. It is interesting that their experimental slip-coefficients and the present results are of the same order even though the structures of the porous media were very different. A numerical study on array of cylinders has been carried out by Sahraoui and Kaviany (1992), and the slip-coefficient increases from 1.3 to 4.2 as porosity increases from 0.4 to 0.8. As compared with their numerical results, the present results are of the same order.

The interfacial velocity at the top of the fibrous medium is presented in Figure 4.5. Also presented is the prediction of interfacial velocity using Equation (4.5), based on Darcy law with the slip boundary condition, the slip coefficient (from Figure 4.4) was used. It is seen that, at large Darcy number 0.05, the interfacial velocity is around two times less when compared with the present results. The differences increase to around five times at low Darcy number $10^{-4}$. In the analytical work of Vafai and Thiyagaraja (1987), for Darcy number from $10^{-4}$ to 0.063, their interfacial velocity results agreed with the hypothesis proposed by Beavers and Joseph (1967) that the fluid side velocity gradient at the interface is proportional to the slip velocity. The Beavers-Joseph model only showed flow effect on slip coefficients. But actual slip coefficients will depend on both local geometry and outer flow conditions, as found in studies of Larson and Higdon (1987), Sahraoui and M. Kaviany (1992) and Wang C.Y. (2009). Present numerical simulation includes effects of both local geometry and outer flow conditions. Hence some discrepancies are found in Figure 4.5 when fitting the present numerical data to Beavers-Joseph model. In study of flow through strips

array, Wang C.Y. (2009) analytically deduced slip coefficients and found slip coefficients increase with both the fin distance and the clear fluid width. He concluded that Beavers-Joseph model is not valid. This supports the finding in present study.

#### 4.2.4.2 No shear jump boundary condition

In the no shear jump boundary condition, a shear term is added to the Darcy law to account for velocity gradient at the interface. The velocity there is assumed continuous and so is the shear stress through the use of an effective viscosity $\mu_{eff}$ .

Assumed effective viscosity $\mu_{eff}$ is uniform in the porous medium, where:

$$\mu_{eff} \left.\frac{du}{dy}\right|_{-} = \mu \left.\frac{du}{dy}\right|_{+} \tag{4.6}$$

The velocity gradients at the fluid and porous sides are shown in Figure 4.6; the gradients are non-continuous at the interface as expected. When Darcy number varies from $4\times10^{-6}$ to $3\times10^{-3}$, the velocity gradient on the fluid side decreases very slightly, but that on the porous side increases slightly. When Darcy number is larger than $3\times10^{-3}$, both the fluid side and the porous side velocity gradients decrease significantly. From the ratio of velocity gradients at the fluid and porous media sides of the interface, the effective viscosity was found and presented in Figure 4.7 as a function of Darcy number. The dimensionless effective viscosity $\mu_{eff} / \mu_f$ varies from around 3.1 to 5 for the present range of Darcy number.

In the experiments of Gilver and Altobelli (1994), $\mu_{eff} / \mu_f$ was found to be between 5 and 9 at low Reynolds number for large porosity $\varepsilon$ = 0.972. The present result is of the same order compared with the experiment results. However note that the experimental result is for flow normal to a porous plug, which is different from the present parallel flow past the interface.

Sahraoui and Kaviany (1992) have carried out numerical study on flow near the interface of a square array of cylinders and $\mu_{eff} / \mu_f$ was estimated to vary from 0.7 to 2 when porosity increases from about 0.5 to 0.8. In the numerical study of shear flow past a hexagonal cylindrical array by Larson and Higdon (1987) $\mu_{eff} / \mu_f$ varies from 0.9 to 3 when porosity increases from 0.1 to 1.0. As compared with the previous numerical studies, the present dimensionless effective viscosity is of the same order.

#### 4.2.4.3 Shear stress jump boundary condition

Like the above no-shear jump boundary condition, the porous medium is modeled by the Darcy-Brinkman equation. The velocity at the interface is continuous. However, there is a shear stress jump at the interface given by:

$$\frac{\mu}{\varepsilon}\frac{du}{dy}\bigg|_{-} - \mu\frac{du}{dy}\bigg|_{+} = \beta_O \frac{\mu}{\sqrt{K}} u_{y=0} \tag{4.7}$$

where $\beta_O$ is the shear jump coefficient. The above stress jump boundary condition was derived by Ochoa-Tapia and Whitaker (1995) based on the non-local form of the volume averaged momentum equation. Note that this stress jump equation has an effective viscosity term $\frac{\mu}{\varepsilon}$ for the porous medium.

The above equation is applied to the present numerical data of porosity, velocity gradients, permeability and interfacial velocity to determine the shear jump coefficient. The shear jump coefficient $\beta_O$ is presented in Figure 4.8a as a function of Darcy number. The shear jump coefficient is seen to vary from around 0 to -4.8 for the present range of Darcy number.

In the study of Ochoa-Tapia and Whitaker (1995), $\beta_O$ was estimated to range from 1.5 to -1.0. This range of $\beta_O$ was obtained by adjusting it so that their fractional excess flow-rate due to porous medium showed a good fit with the experimental data of Beavers and Joseph (1967). The present results of $\beta_O$ are of the same order as Ochoa-Tapia and Whitaker (1995). However it is difficult to make further comparison as their porosity was arbitrarily specified as 0.4. The porous media of Beavers and Joseph (1967) are made of foam metal (lattice type) and aloxite (granular type) whose pore sizes ranged from 0.013 to 0.045 in. Though the present porous medium structure is very different from that of Beavers and Joseph (1967), it is interesting the shear jump coefficients are of the same order.

Another model of shear stress jump at the interface is that of Chandesris and Jamet (2006), given by:

$$\mu \frac{du}{dy}\bigg|_{-} - \mu \frac{du}{dy}\bigg|_{+} = \beta_C \frac{\mu}{\sqrt{K}} u_{y=0} \tag{4.8}$$

where $\beta_C$ is the shear jump coefficient. Note that this stress jump equation has fluid viscosity term $\mu$ for the porous medium unlike Equation (4.7). The above equation was applied to the present numerical data of porosity, velocity gradients, permeability and interfacial velocity to determine the shear jump coefficient $\beta_C$.

The shear jump coefficient is presented in Fig 4.8b. The jump coefficient varies from around -0.5 to -4.8 for the present range of Darcy number. In the study of Chandesris and Jamet's (2006), $\beta_C$ was found to be between 4.28 to -0.637 in order to obtain good fit with Beavers and Joseph (1967) experimental data of the fractional increase in flow rate. The present coefficient shows similar trend as that of Chandesris and Jamet's (2006) in which the coefficient decreases with porosity increasing. However, the present $\beta_C$ is always of negative value, which is plausible if the velocity gradient of the porous side is always smaller than that of the fluid side.

## 4.3 Conclusions

A numerical study, using the boundary element method, was carried out on the flow through a channel partially filled with fibrous porous-medium, which was modeled as a periodic, hexagonal array of cylinders. The flow is transverse to the cylinders and the interfacial boundary conditions were analyzed. The slip-coefficient varies from around 0.4 to 8.4 for the present range of permeability. Using the slip coefficients, the slip boundary model gives an interfacial velocity which is less than the present results by around 2 to 5 times. The effective viscosity varies from around 3.1 to 5 for the present permeability. The stress jump coefficient is of order one, which is consistent with previous literature. However, it is interesting that the present jump coefficients are negative in value. Note that Beavers-Joseph model has inherent defect of not having local geometry effects on slip coefficients. Hence it is difficult to compare present numerical results with those results deduced or matched from

Beavers-Joseph model. The present results may give some indication of the range of values of the coefficients which are needed as empirical inputs to the various models of interfacial boundary conditions. The interfacial conditions obtained from the present pore scale modeling and REV scale averaging may be of interest to domain scale modeling of flow and heat transfer condition at the interface between fluid and porous media.

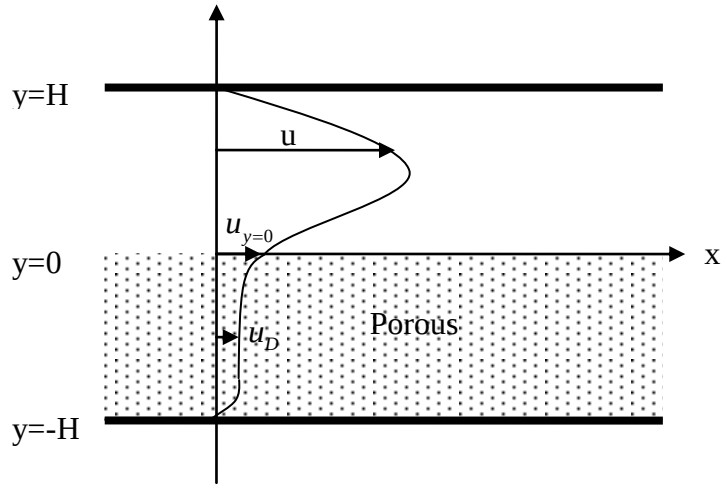


(a)

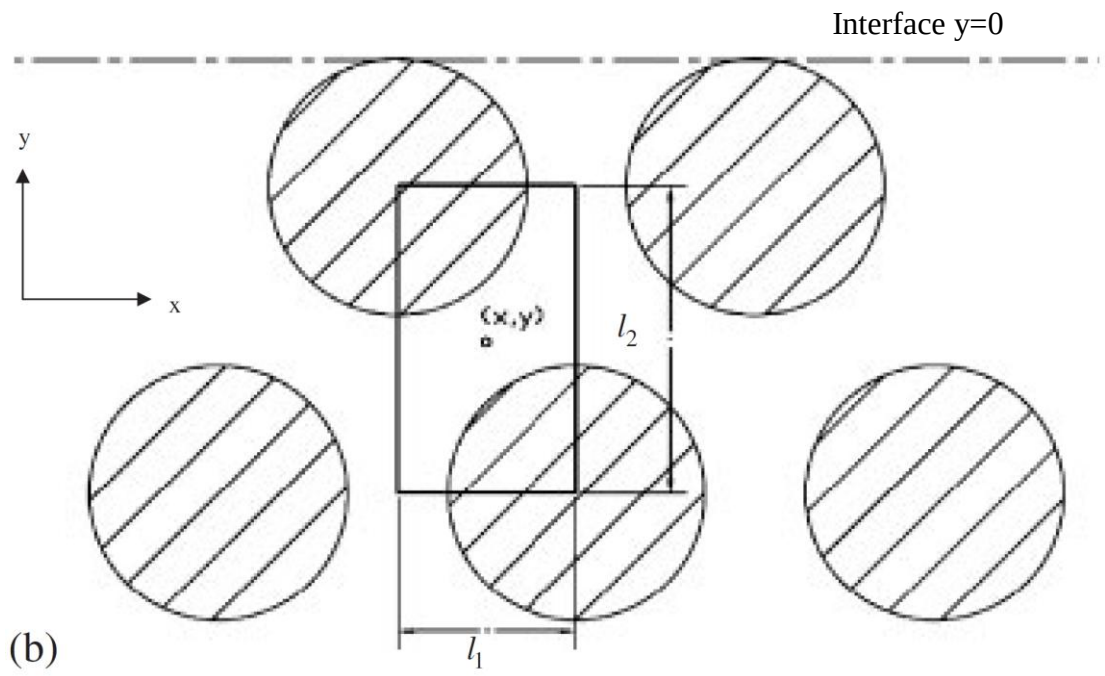
Interface y=0
y
x
(x,y)
$l_2$
$l_1$
(b)

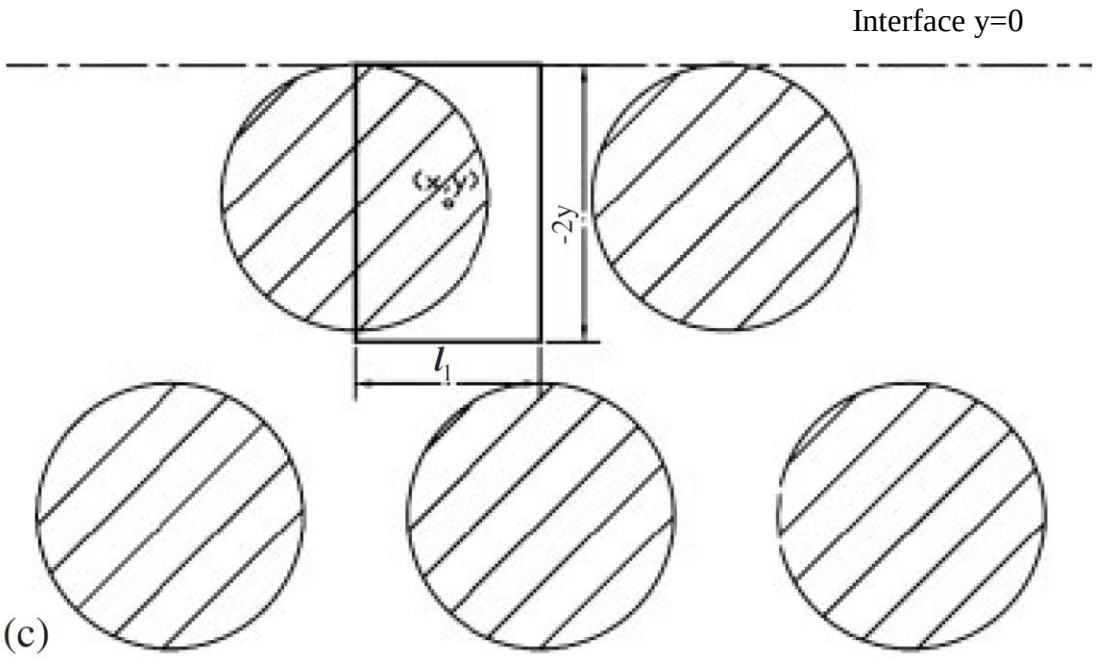


Figure 4.1 (a) Channel partially filled with fibrous porous-medium; (b) a unit cell showing the representative elementary volume; and (c) an averaging volume near the interface

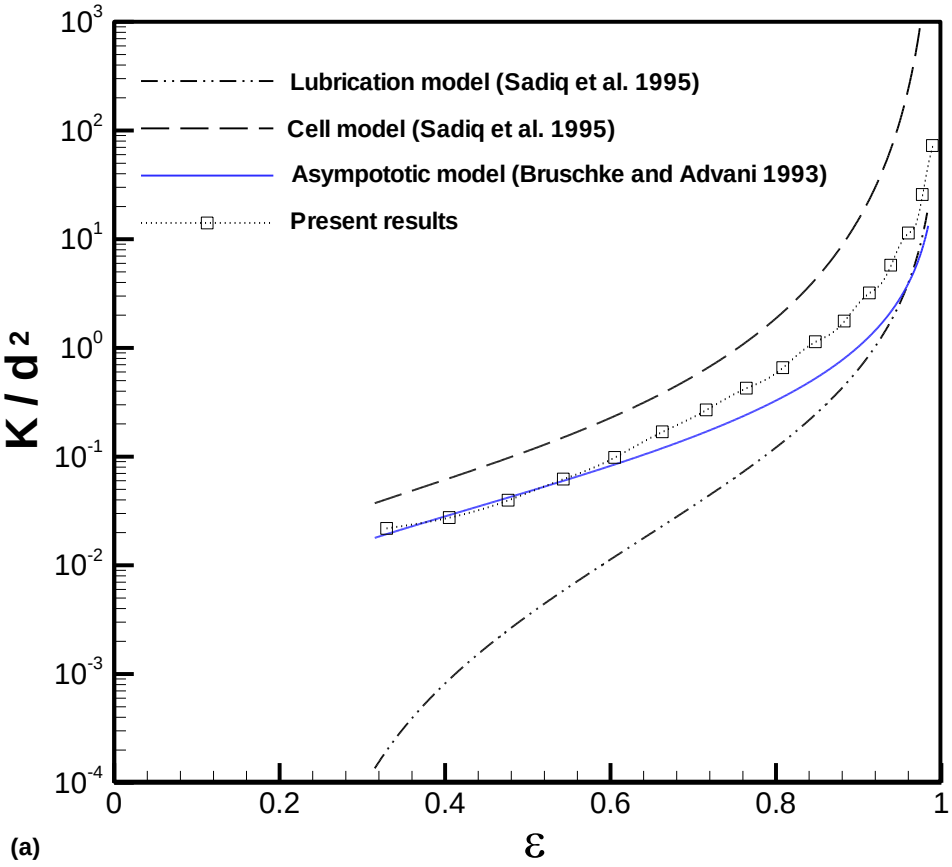
Lubrication model (Sadiq et al. 1995)
Cell model (Sadiq et al. 1995)
Asympototic model (Bruschke and Advani 1993)
Present results
K / d²
ε
(a)

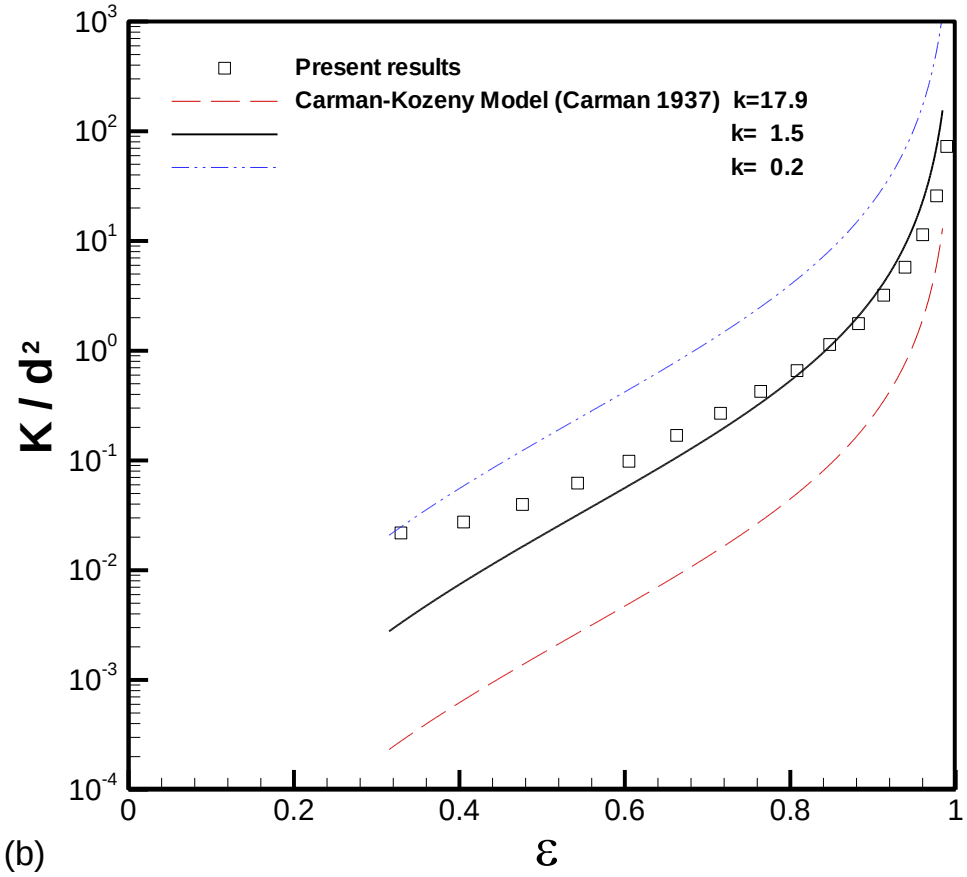
Present results
Carman-Kozeny Model (Carman 1937) k=17.9
k= 1.5
k= 0.2
K / d²
ε
10³
10²
10¹
10⁰
10⁻¹
10⁻²
10⁻³
10⁻⁴
0
0.2
0.4
0.6
0.8
1

(b)

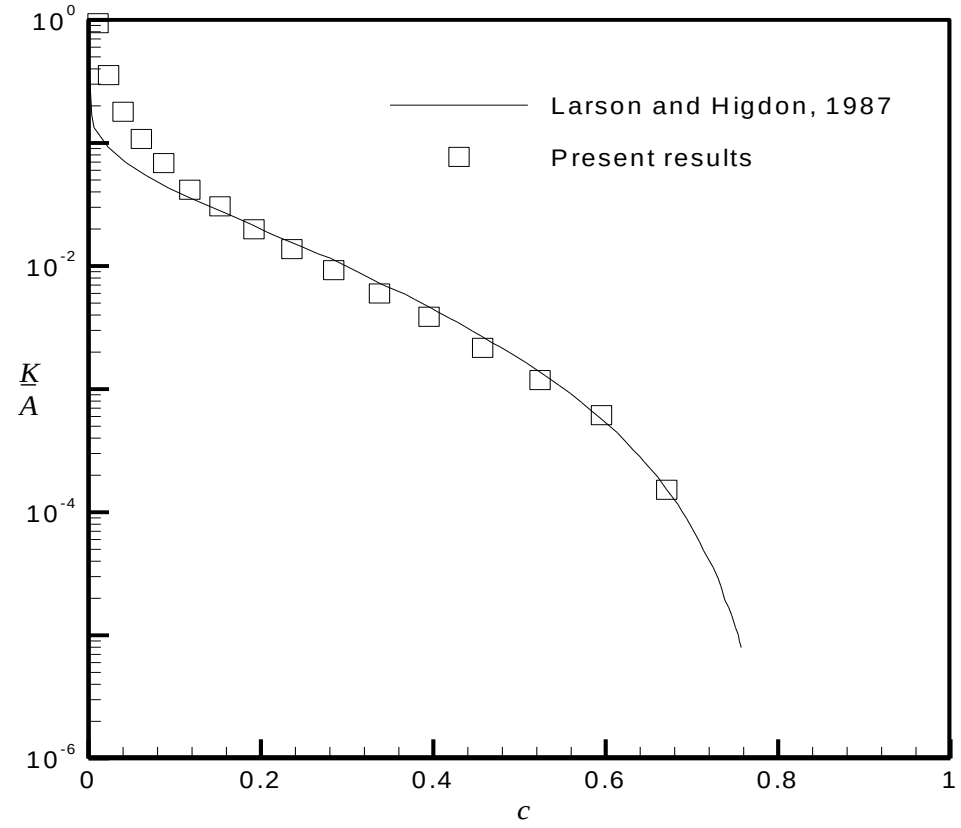


(c)

Figure 4.2 Permeability of fibrous porous-media modeled by cylinder arrays: (a) comparison with cell, lubrication and asymptotic models; (b) comparison with Carman-Konzeny model; and (c) comparison with the Larson and Higdon study, $c$ is solid volume fraction.

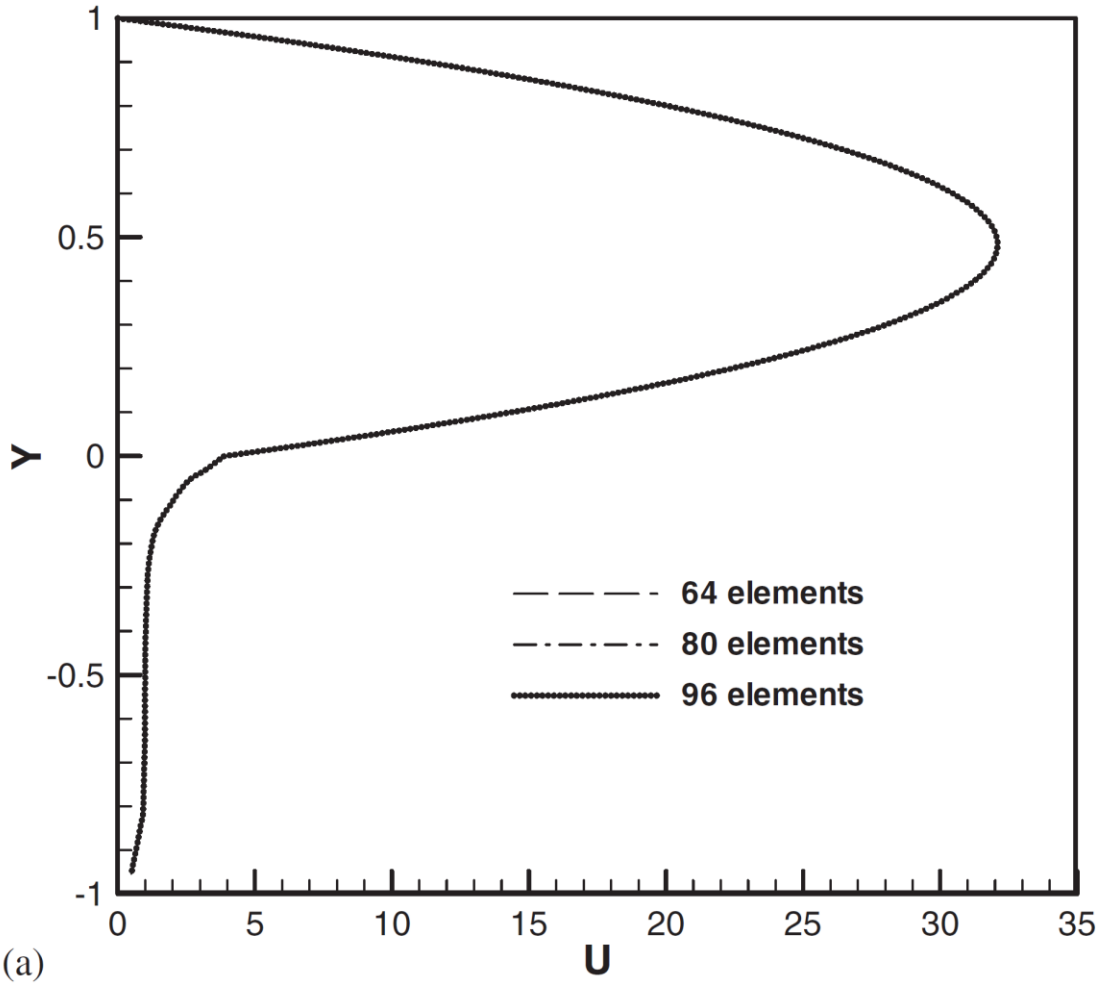
1
0.5
0
-0.5
-1
Y
0
5
10
15
20
25
30
35
U
64 elements
80 elements
96 elements

(a)

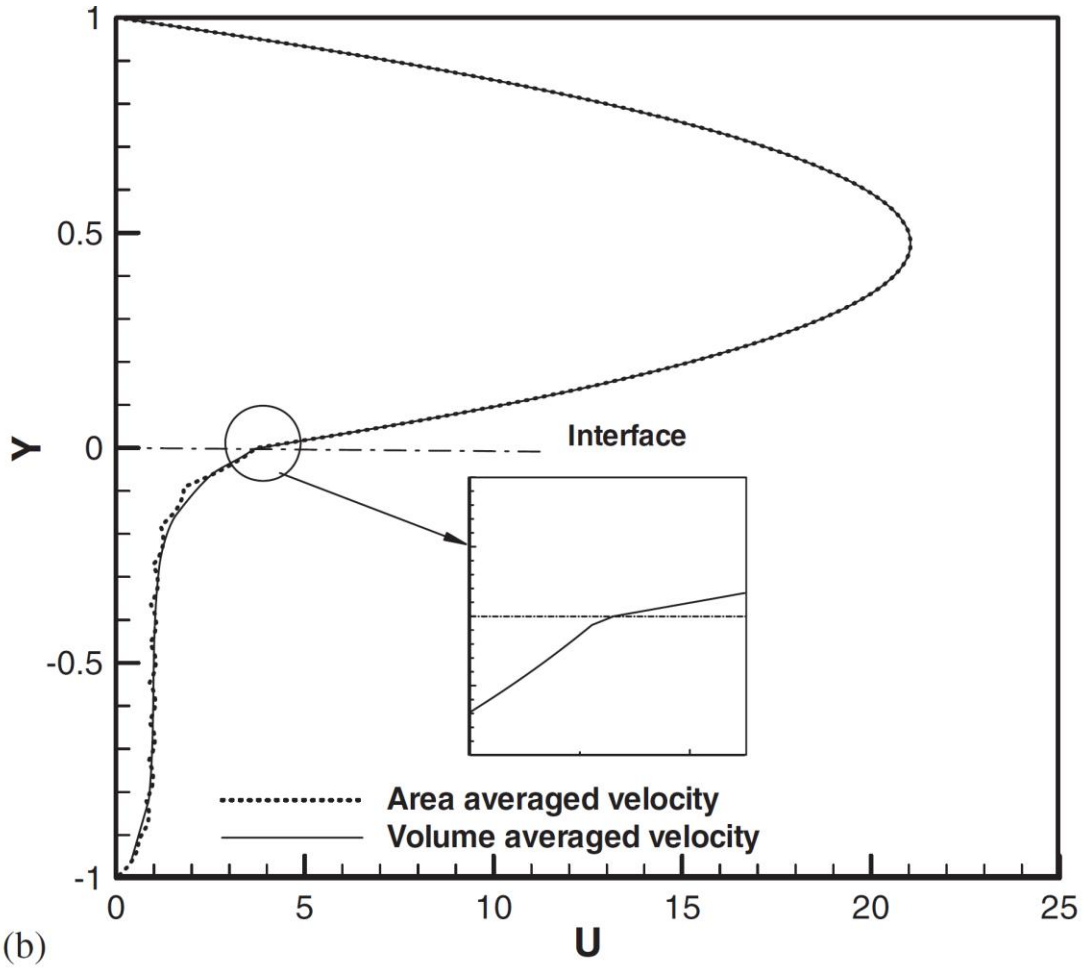


Figure 4.3 Non-dimensional averaged velocity profile: (a) convergence study with different element numbers; at $K = 2.93\times10^{-2}$ or $Da = 7.3\times10^{-3}$; (b) an enlarged velocity profile near interface; at $K = 4.3\times10^{-2}$ or $Da = 10.1\times10^{-3}$.

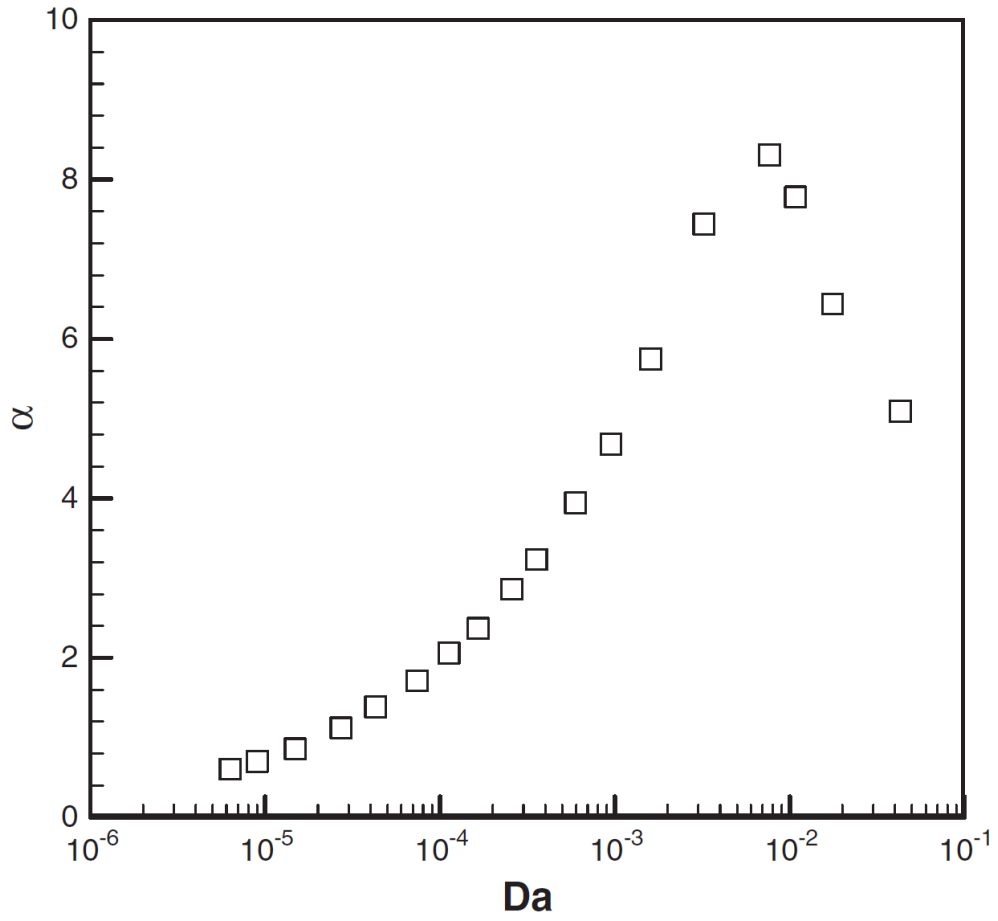


Figure 4.4 Slip-coefficient versus Darcy number

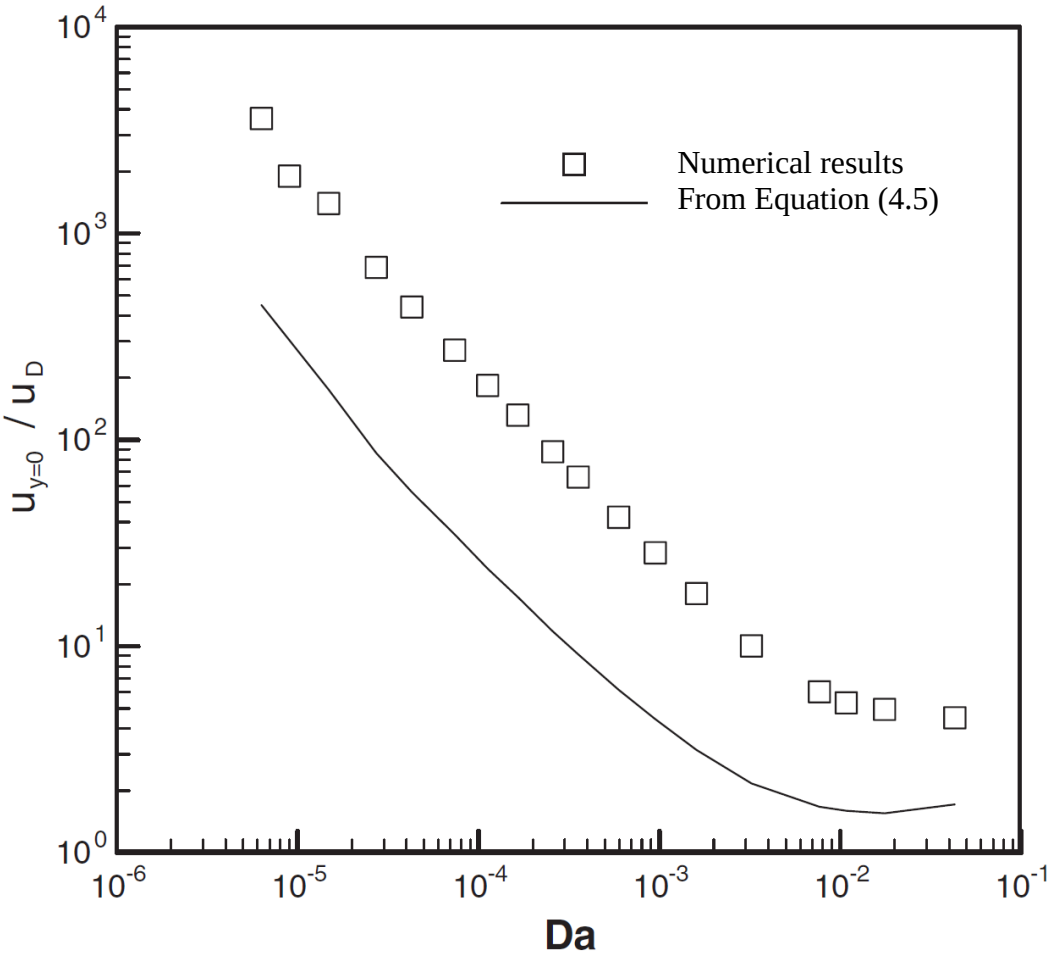


Figure 4.5 Dimensionless interface-velocity versus Darcy number

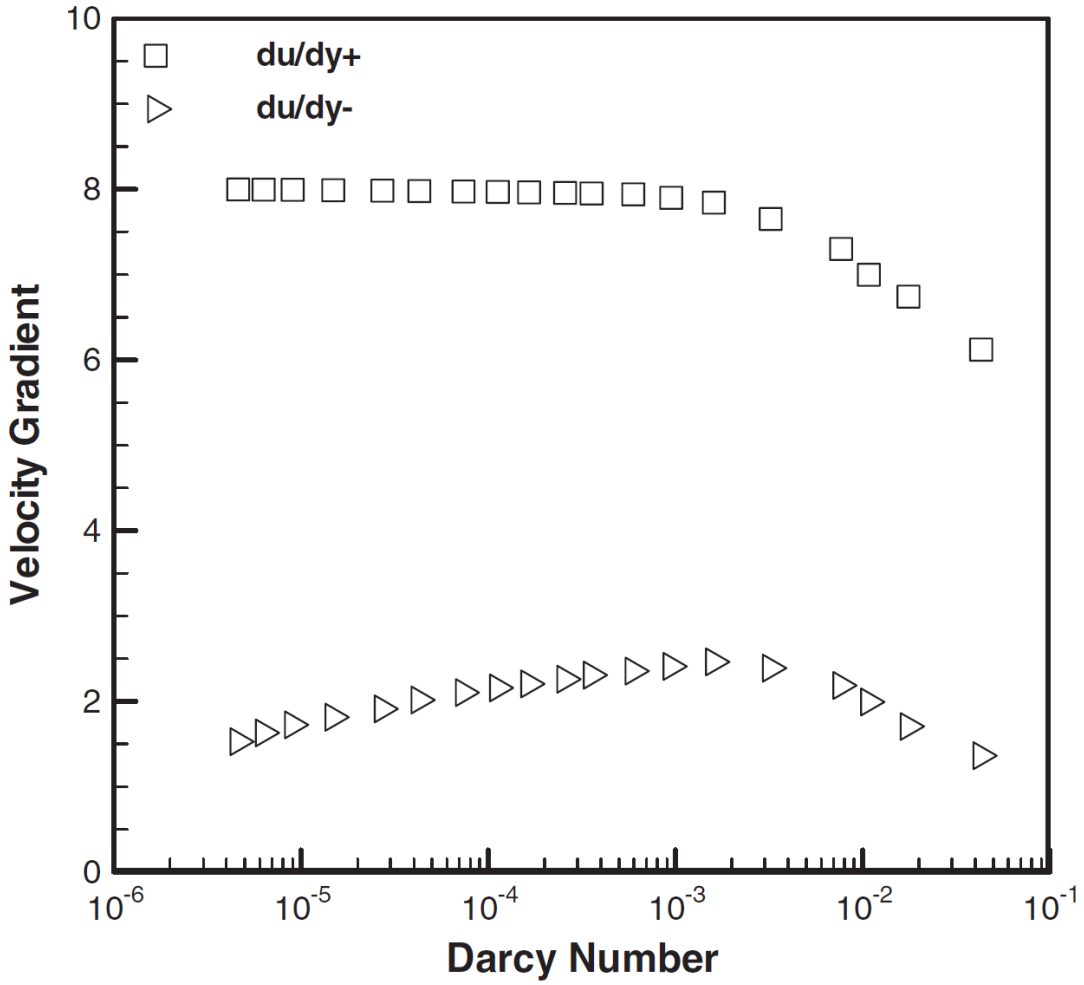


Figure 4.6 Velocity gradients at interface versus Darcy number

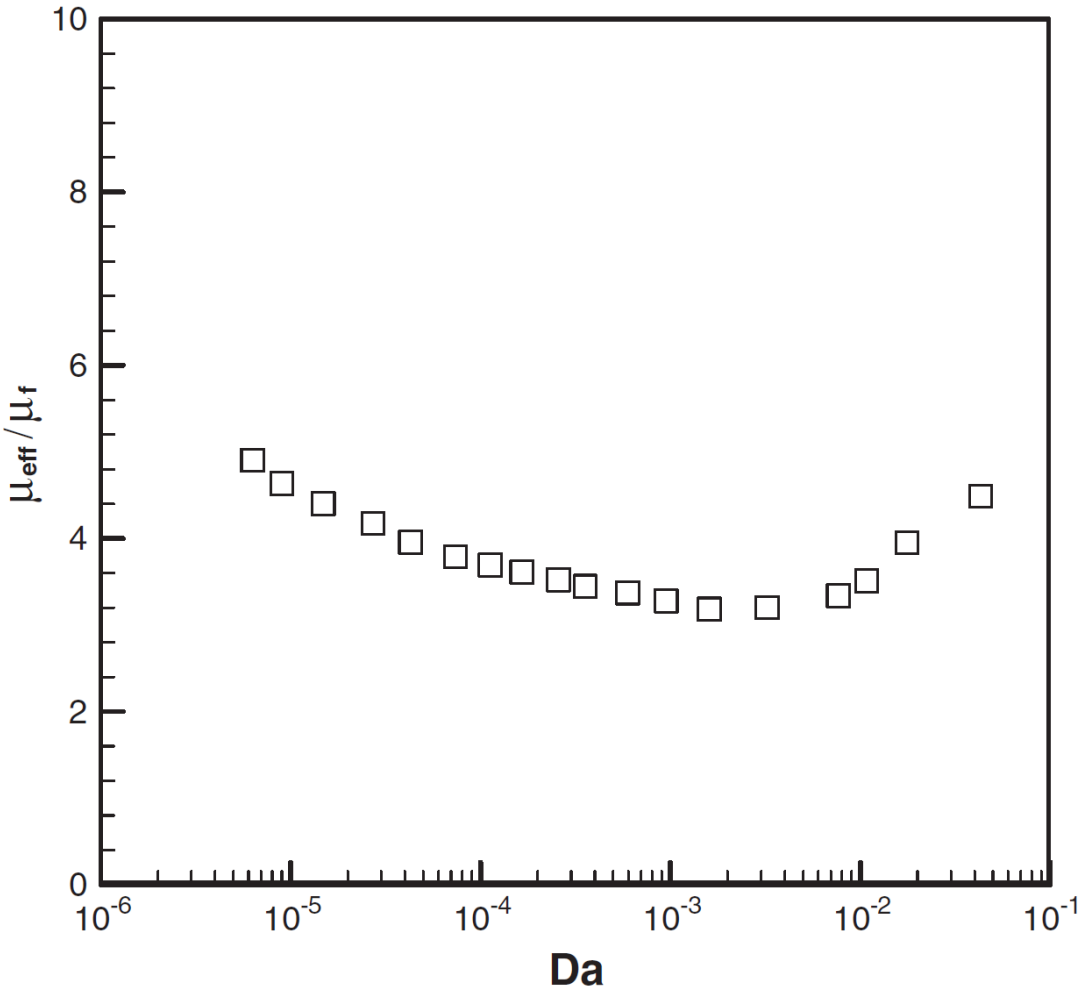


Figure 4.7 Dimensionless effective-viscosity versus Darcy number

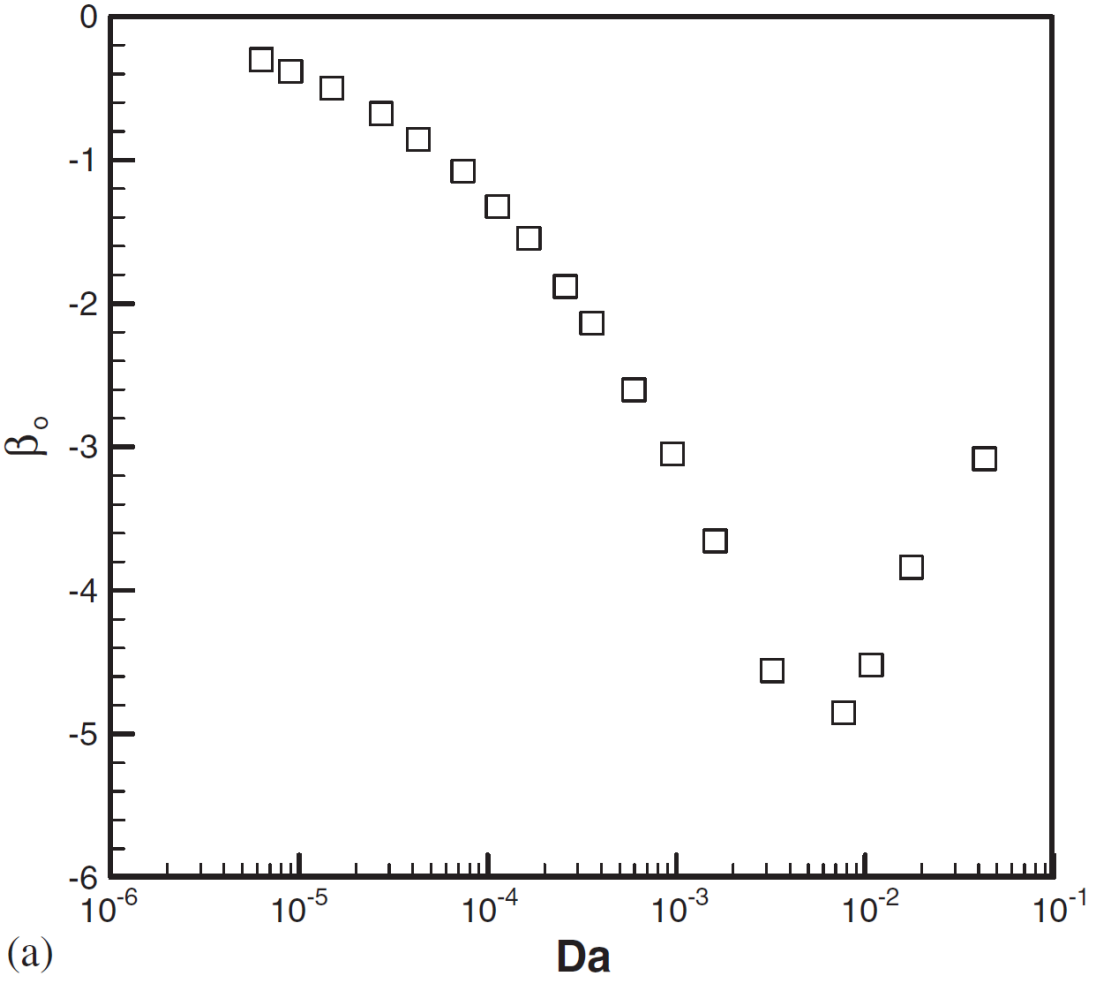


(a)

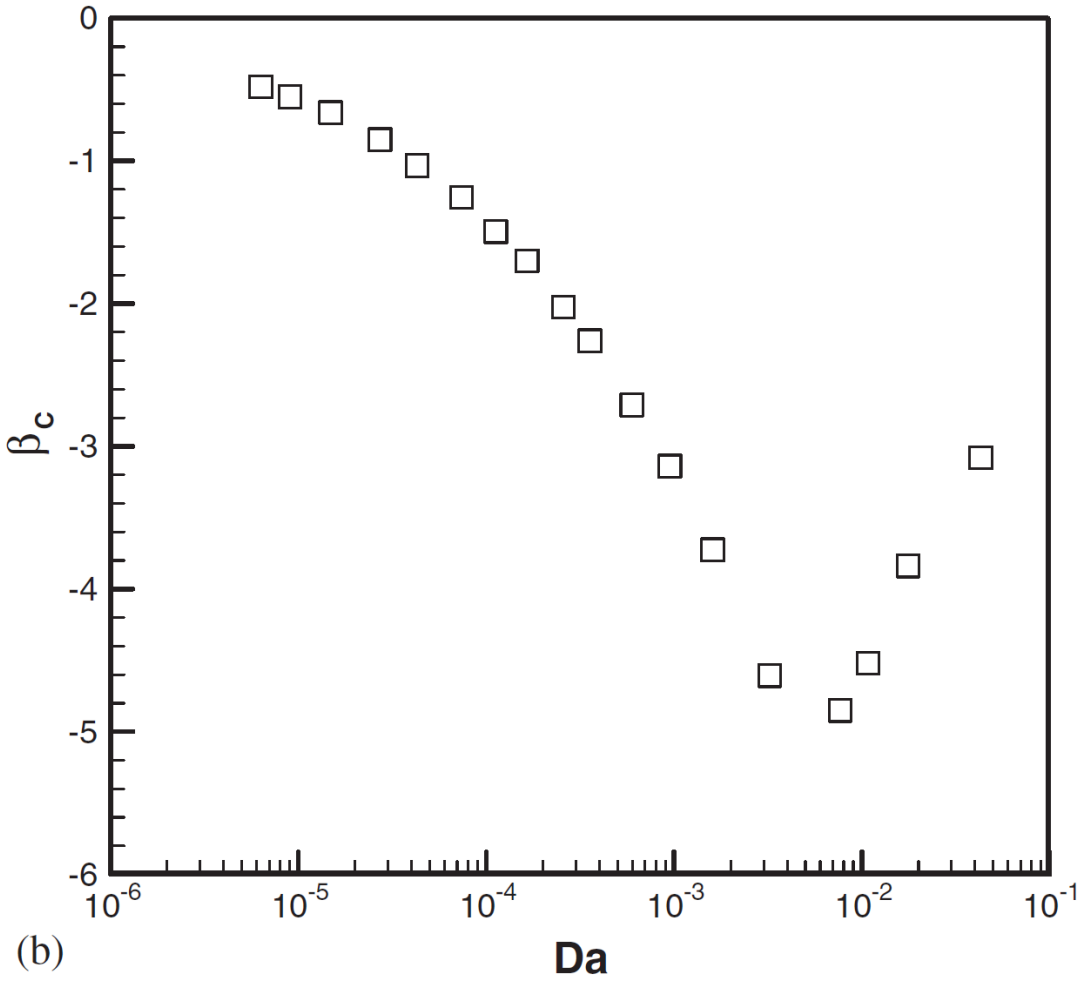


Figure 4.8 Shear jump coefficient versus Darcy number; (a) $\beta_O$ in Ochoa-Tapia & Whitaker's model; (b) $\beta_C$ in Chandesris & Jamet's model

# Chapter 5 Flow in Fluid-Porous Domains Coupled by Interfacial Stress Jump*

The purpose of this chapter is to extend the LBM to coupled problems of a fluid layer and porous medium layer, by using the stress jump interfacial boundary conditions. The treatments of both the velocity and distribution functions at the interface are described. To study the viscous and inertial effects, the lattice Boltzmann models (Guo and Zhao 2002) for Navier-Stokes equation and Darcy-Brinkmann Forchheimer equation, with incompressibility assumption, are used in this chapter.

## 5.1 Problem Statement

A numerical method is to be developed for flows involving an interface between a homogenous fluid and a porous medium. The numerical method is based on the lattice Boltzmann method (LBM) for incompressible flow. A generalized model, which includes Brinkman term, Forcheimmer term and non-linear convective term, is used to govern the flow in the porous medium region. At the interface, a shear stress jump that includes the inertial effect is imposed for the lattice Boltzmann equation, together with a continuity of normal stress.

*Parts of this chapter have been published in Bai et al., *International Journal for Numerical Methods in Fluids 60, 691-708, 2009*

The present method is implemented on three classic applications each of which has a porous medium partially occupying the flow region: channel flow (Figure 5.1), plug flow (Figure 5.4) and lid-driven cavity flow (Figure 5.7).

*Channel flow partially filled with porous medium*

The physical domain of channel flow is shown schematically in Figure 5.1. It consists of a planar channel whose upper region of height $H_1$ is filled with homogenous fluid and lower region of height $H_2$ is filled with a fluid-saturated porous medium region. A case of height ratio $H_2 / H_1 = 1$ is considered. The flow is assumed laminar and the driving force is a constant pressure gradient.

*Channel flow with a porous medium plug*

The physical domain of the flow through a channel with a porous plug is shown schematically in Figure 5.4, which is the same as that by Gartling *et al*. (1996), Betchen *et al*. (2006) and Yu *et al.* (2007). In this problem the dominating flow is perpendicular to the interface. The Poiseuille flow velocity profile is set in the inlet based on the mean velocity.

*Square cavity partially filled with porous medium*

Figure 5.7 is the schematic diagram of flow in a lid driven square cavity, which is three-quarter filled with porous medium. The fluid kinematic viscosity $\nu$ is set to be $2\times10^{-3}$.

## 5.2 Results and Discussion

### 5.2.1 Grid independence study

To guarantee grid-independent solution, a sufficiently fine mesh should be used. The grid independence study was implemented for channel flow partially filled with porous medium. Figure 5.2 shows the present results are in good agreement with the analytical results and also a mesh of 121 grids in the *y* direction is sufficient for numerical simulation. For all of the channel flow cases in this chapter, the driving force $G$ is set to be $10^{-4}$, and fluid kinematic viscosity $\nu$ is set to be $2\times10^{-3}$.

### 5.2.2 Channel flow with partially filled porous medium

There are several different ways to implement the driving force. In present study, the driving force $G=-\frac{dp_f}{dx}$ is included in the lattice Boltzmann model by adding a first order Hermite polynomials to the distribution functions (Martys 2001, Shi et al. 2006):

$$\tilde{f}_i(\vec{x}_t,t) = f_i(\vec{x},t) + \frac{\omega_i G e_{ix}}{c_s^2} \quad \text{for homogeneous fluid flow} \qquad (5.1)$$

$$\tilde{f}_i(\vec{x}_t,t) = f_i(\vec{x},t) + \frac{\varepsilon\omega_i G e_{ix}}{c_s^2} \quad \text{for porous medium flow} \qquad (5.2)$$

where $\tilde{f}_i(\vec{x}_t,t)$ represents the distribution function after including the driving force. The main dimensionless parameters are: $U = \frac{\mu u}{G H_1^2}$, Darcy number $Da = \frac{K}{H_1^2}$ and $Y = \frac{y}{H_1}$.

Fig. 5.3a, 5.3b and 5.3c show the velocity profiles at different *Da*, porosity and stress jump coefficient, respectively. The comparison shows that the present numerical results are in good agreement with the analytical solutions (Yu et al. 2007) at various Da, porosities and stress jump coefficients. It is found that Da has much effect on the velocity profiles. The velocity increases significantly with increasing Da and proportionately more so for the porous side. The stress jump coefficient $\beta$ has slight effect on the velocity profiles. The effect of the stress jump coefficient $\beta_1$ is negligible. This is attributed to the small Reynolds number and Darcy number. Thus the inertial effect is negligible, especially since the flow is parallel. The porosity has very little effect on the velocity profiles.

### 5.2.3 Channel flow with a porous plug

Different from the first problem, the main dimensionless parameters are: $U = \frac{u}{u_a}$, $X = \frac{x}{H}$, Reynolds number $Re = \frac{\rho u_a H}{\mu}$ and Darcy number $Da = \frac{K}{H^2}$, where $u_a$ is the mean velocity. The numerical results for the case of $Da = 10^{-2}$ and $10^{-3}$ are shown in Figure 5.5, where the centerline $U$ velocity along *x* direction are presented. The other parameters for the flows illustrated in Figure 5.5 are *Re* = 1, $\varepsilon = 0.7$, $\beta = 0$ and $\beta_1 = 0$. The lengths are set to be $\Delta x_1 = \Delta x_3 = 3H$ and $\Delta x_2 = 2H$. In the present study, 121 grids in the *y* direction are used and the preliminary numerical tests confirmed that the solutions are grid-independent.

Figure 5.5 shows that the velocity drops rapidly in the porous plug, especially for the case with the low Darcy number. The flow field is predominantly axial over most of the homogenous fluid and porous medium regions, but it is two-dimensional in the region near the interface between the homogenous fluid and the porous medium. The present results are in good agreement with those of Gartling *et al*. (1996), Betchen *et al*. (2006) and Yu *et al.* (2007).

The centerline velocity distributions at the different stress jump coefficients $\beta$ and $\beta_1$ are shown in Figure 5.6. It is seen that the two coefficients have negligible effects as the dominant flow direction is perpendicular to the interface. The present results agree well with those of previous studies (Gartling *et al*. 1996, Betchen *et al*. 2006 and Yu *et al.* 2007).

### 5.2.4 Cavity flow with partially filled porous medium

The governing dimensionless parameters are: Reynolds number based on lid velocity $u_0$, $\mathrm{Re} = u_0 H / \nu$ and is given as a constant, Darcy number $Da = K/H^2$, $U = u/u_0$, $V = v/u_0$, $X = x/H$ and $Y = y/H$, where $H$ is the square cavity height. The lid velocity $u_0$ can be calculated from the definition of Reynolds number. The mesh size of 121x121 is used, based on the previous grid independence studies. The stress jump conditions are implemented for x-component velocity $U$ as given in Equation (2.15) of Chapter 2. And the stress continuity conditions are used for y-component velocity $V$ as given in Equation (2.17) of Chapter 2.

Figure 5.8a and 5.8b show the velocity profiles at different Da. It can be seen that there is more flow passing through the porous medium region with larger Darcy number. The interfacial velocity $V$ increases with increasing Da. It shows that Darcy number has much effect on velocity profiles. The comparison shows that the present results are in good agreement with the finite volume results.

The velocity profiles at different porosity are shown in Figure 5.9a and 5.9b. It shows that porosity has very slight effects on velocity profiles. Figure 5.10a and 5.10b shows the velocity profiles at different stress jump coefficients. It can be seen that jump coefficient $\beta$ has slight effect on the x-component velocity $U$. However, it has negligible effect on the y-component velocity $V$. The effect of the jump coefficient $\beta_1$ is negligible for both $U$ and $V$. This may due to the reason that for small Reynolds number and Darcy number used in present study, the inertial effects are negligible.

## 5.3 Conclusions

In this chapter the lattice Boltzmann method was extended to flow systems with regions of homogeneous fluid and porous medium coupled by the stress jump interfacial boundary condition of Ochoa-Tapia and Whitaker (1995a, 1995b, 1998). A treatment of the velocity and distribution functions at the interface was described. The interfacial velocity was calculated with the difference approximation of the velocity gradient derivatives in the stress jump condition. Then the updated interfacial velocity was used to update the distribution functions at the interface.

This interfacial treatment was applied to simulate coupled flow problems such as channel flow, porous plug and cavity flow. These cases cover a variety of situations where the major flow is parallel, perpendicular and oblique to the interface. The stress jump parameter $\beta$ has more effect when the velocity is parallel to the interface. The results are in consistent with the analytical and/or finite volume results.

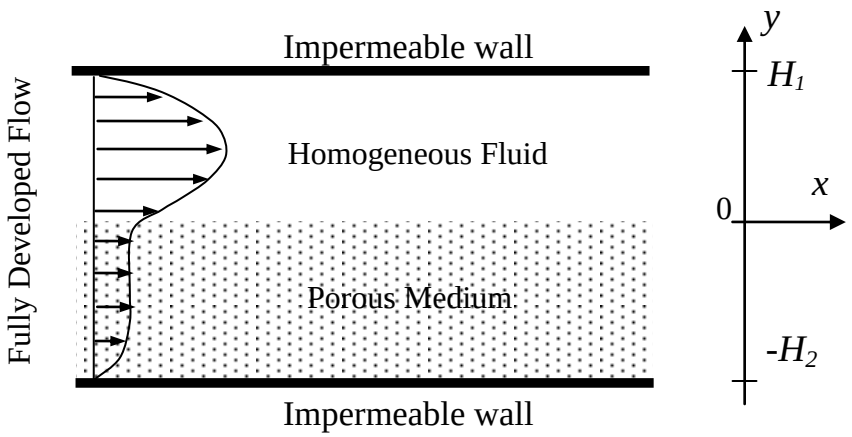


Figure 5.1 Schematic of flow in a channel partially filled with saturated porous medium

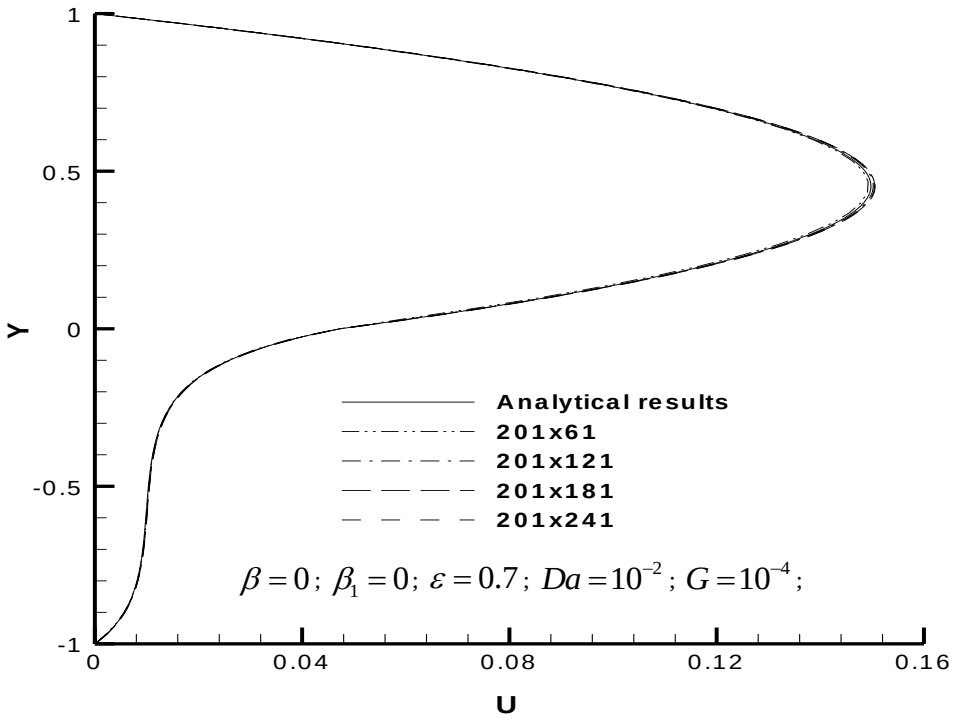


Figure 5.2 Effects of grid size on velocity profile

(a)

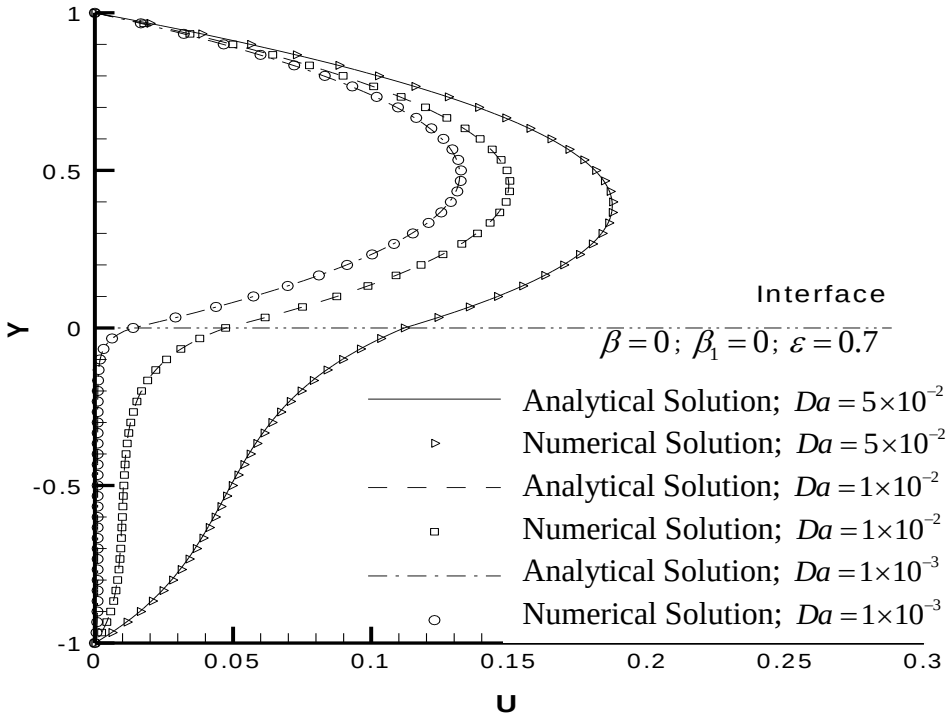
1
0.5
0
-0.5
-1
Y
0
0.05
0.1
0.15
0.2
0.25
0.3
U
Interface
$\beta = 0;\ \beta_1 = 0;\ \varepsilon = 0.7$
Analytical Solution; $Da = 5\times10^{-2}$
Numerical Solution; $Da = 5\times10^{-2}$
Analytical Solution; $Da = 1\times10^{-2}$
Numerical Solution; $Da = 1\times10^{-2}$
Analytical Solution; $Da = 1\times10^{-3}$
Numerical Solution; $Da = 1\times10^{-3}$

(b)

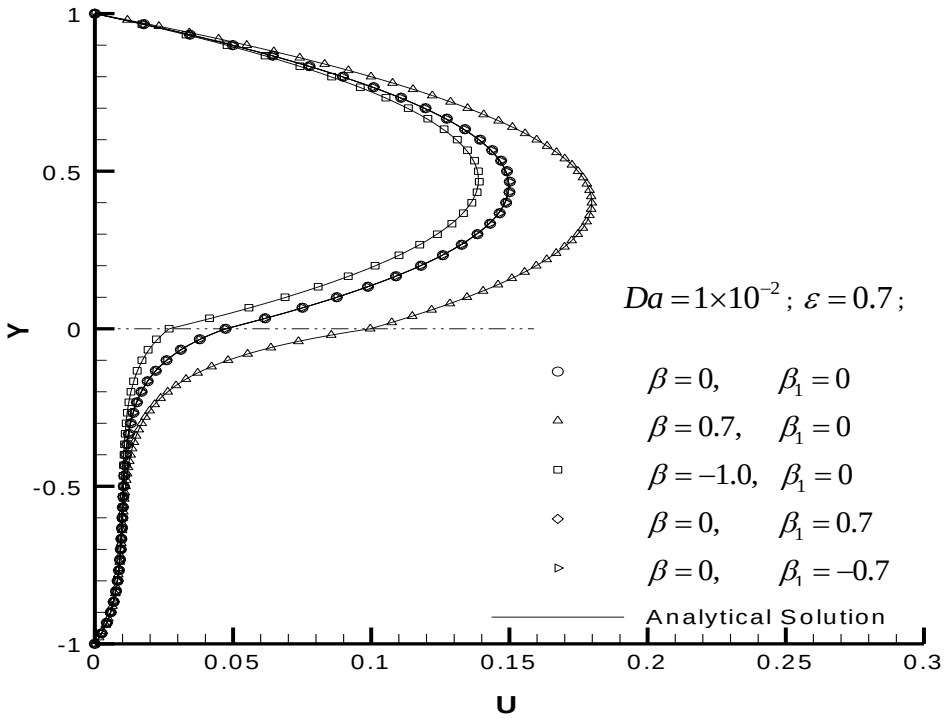
1
0.5
0
-0.5
-1
Y
0
0.05
0.1
0.15
0.2
0.25
0.3
U
$Da = 1\times10^{-2}$; $\varepsilon = 0.7$;
$\beta = 0,\quad \beta_1 = 0$
$\beta = 0.7,\quad \beta_1 = 0$
$\beta = -1.0,\quad \beta_1 = 0$
$\beta = 0,\quad \beta_1 = 0.7$
$\beta = 0,\quad \beta_1 = -0.7$
Analytical Solution

(c)

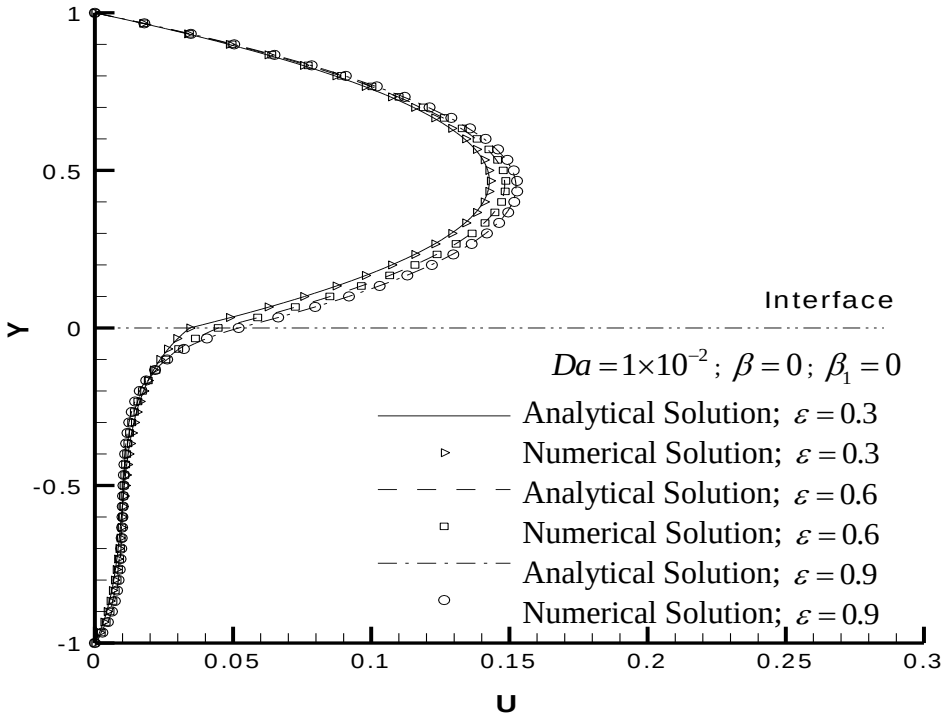


Figure 5.3 The *U* velocity profile under different flow conditions: (a) Darcy number effect; (b) stress jump coefficients $\beta$ and $\beta_1$ effect; (c) porosity effect.

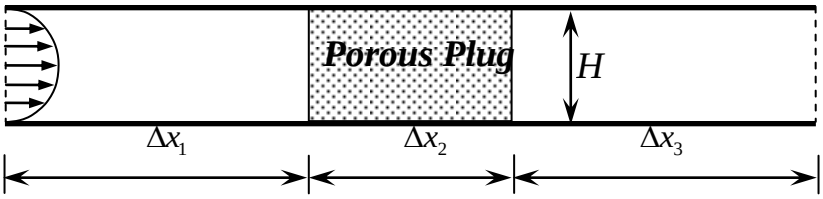


Figure 5.4 Schematic of flow in a channel with a porous plug

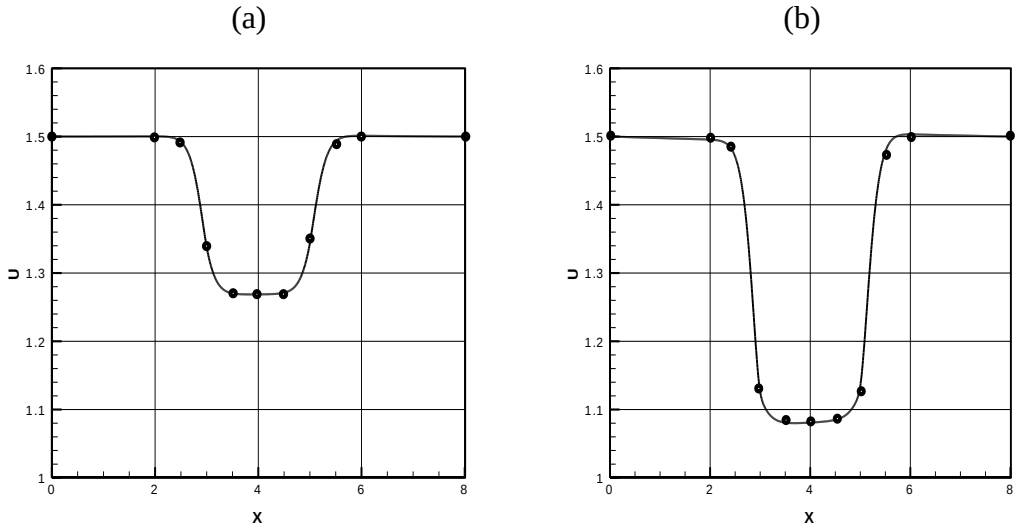


Figure 5.5 The velocity distributions along the centerline at: (a) $Da = 10^{-2}$ and (b) $Da = 10^{-3}$; other parameters are $\mathrm{Re} = 1, \varepsilon = 0.7, \beta = 0, \beta_1 = 0, \Delta x_1 = \Delta x_3 = 3H$ and $\Delta x_2 = 2H$.

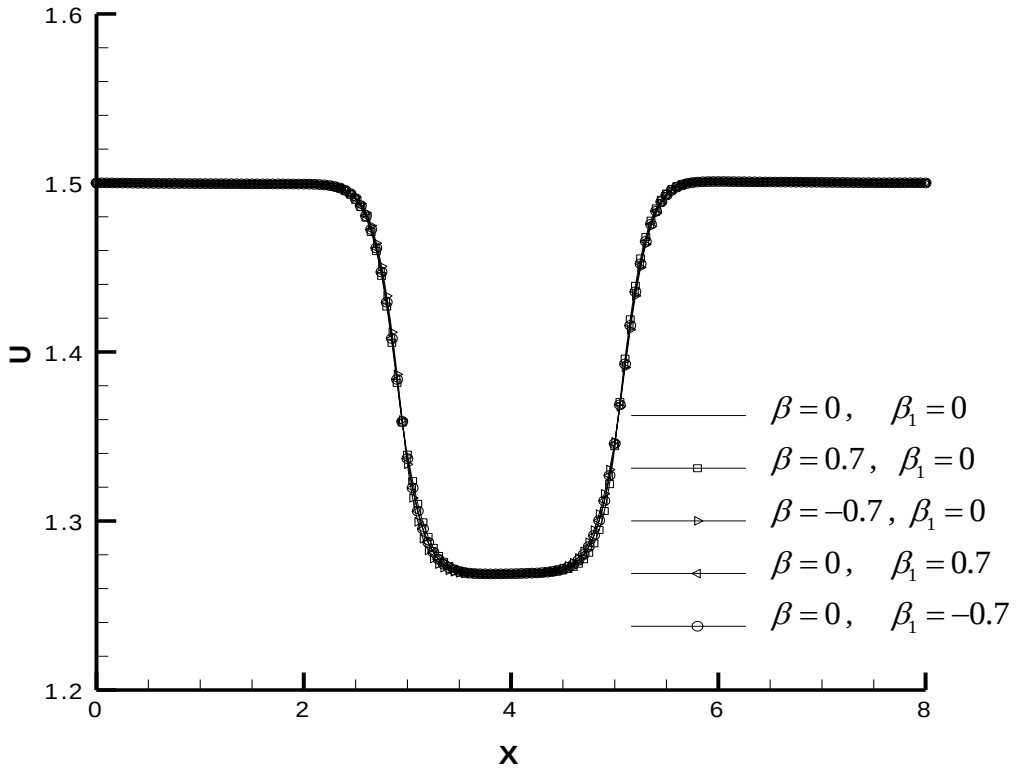


Figure 5.6 The velocity distribution along the centerline at different stress jump coefficients with $Da = 10^{-2}$, $\mathrm{Re} = 1$, $\varepsilon = 0.7$, $\Delta x_1 = \Delta x_3 = 3H$ and $\Delta x_2 = 2H$

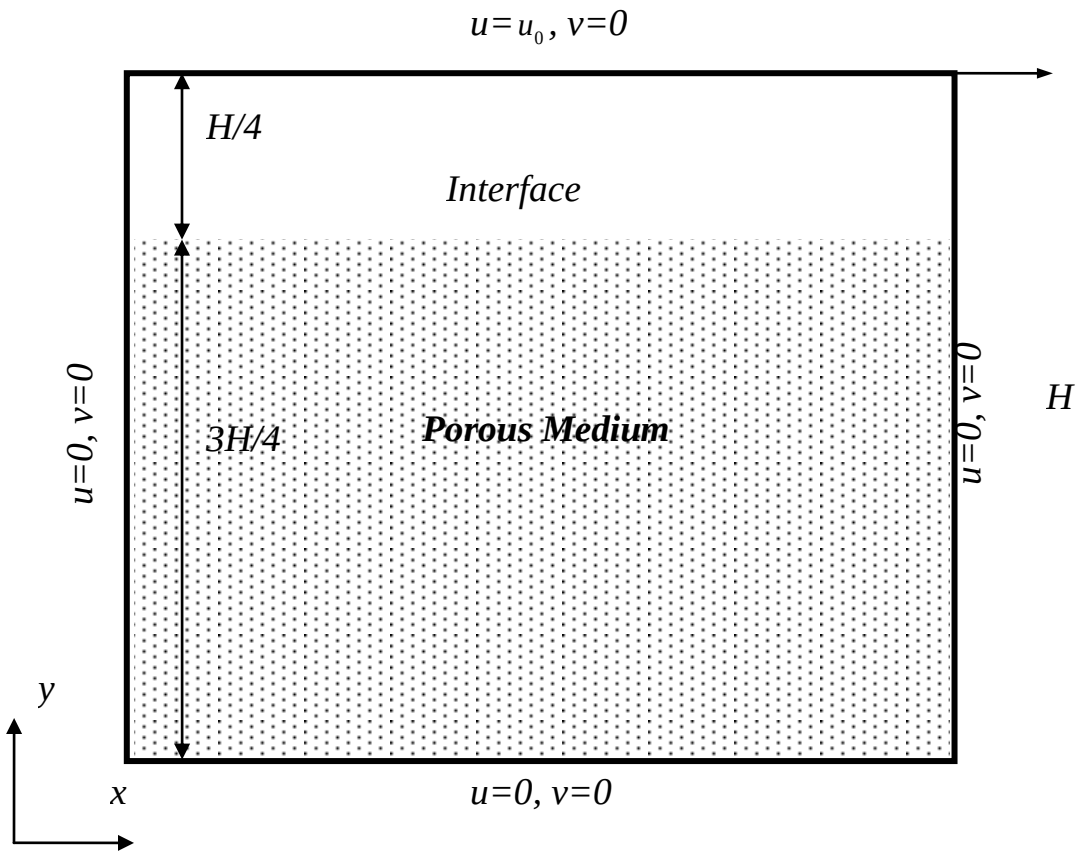


Figure 5.7 Schematic of flow in a square cavity partially filled with porous medium

(a)

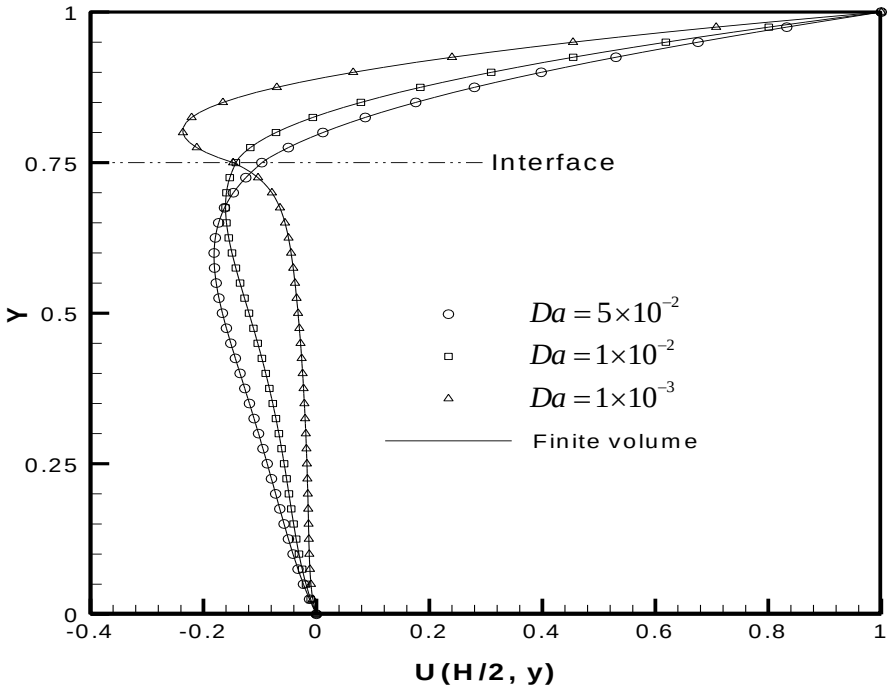
1
0.75
0.5
0.25
0
Y
Interface
$Da = 5\times10^{-2}$
$Da = 1\times10^{-2}$
$Da = 1\times10^{-3}$
Finite volume
-0.4
-0.2
0
0.2
0.4
0.6
0.8
1
U(H/2, y)

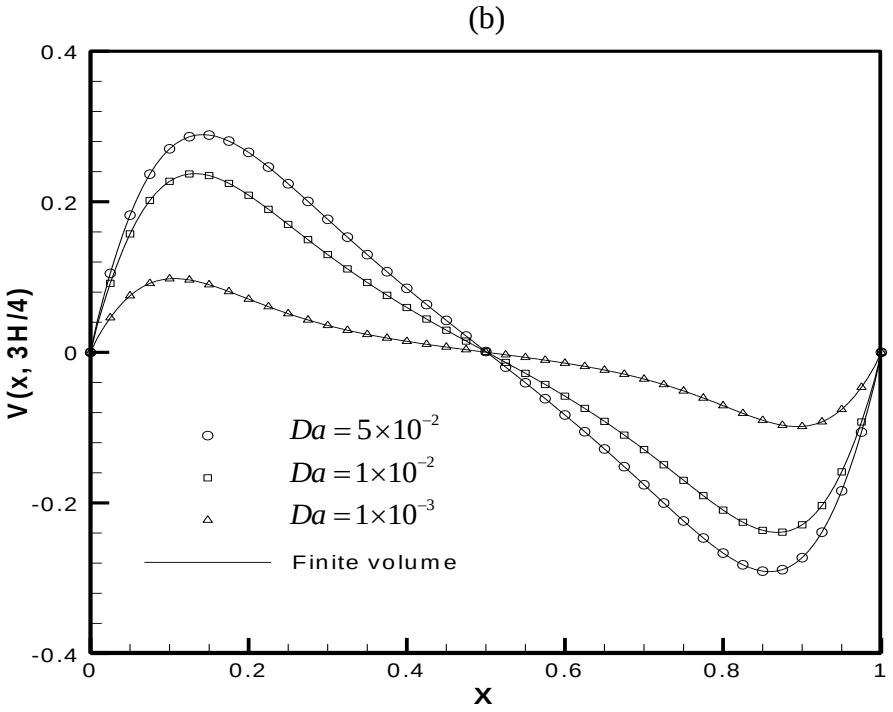


Figure 5.8 Velocity profiles at different Darcy number; symbols represent LBM solutions and solid lines represent finite-volume solutions: (a) centerline velocity $U$ along y direction and (b) interfacial velocity $V$ along x direction; other parameters are $\mathrm{Re} = 1$, $\varepsilon = 0.7$, $\beta = 0$ and $\beta_1 = 0$.

(a)

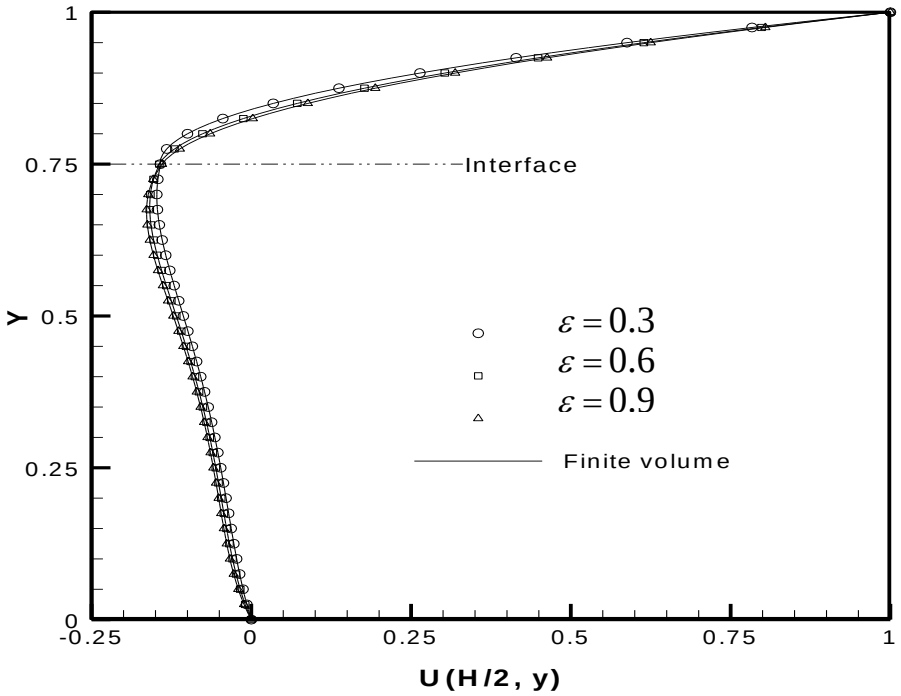
1
0.75
0.5
0.25
0
Y
-0.25
0
0.25
0.5
0.75
1
U(H/2, y)
Interface
$\varepsilon = 0.3$
$\varepsilon = 0.6$
$\varepsilon = 0.9$
Finite volume

(b)

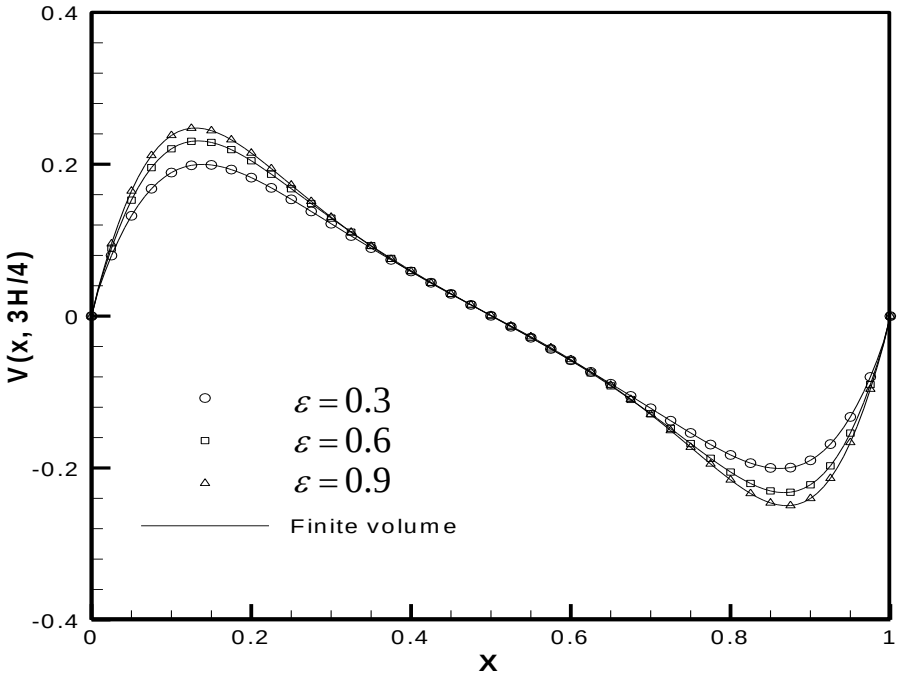


Figure 5.9 Velocity profiles at different porosity; symbols represent LBM solutions and solid lines represent finite-volume solutions: (a) centerline velocity $U$ along y direction and (b) interfacial velocity $V$ along x direction; other parameters are $\mathrm{Re} = 1$, $Da = 10^{-2}$, $\beta = 0$ and $\beta_1 = 0$.

(a)

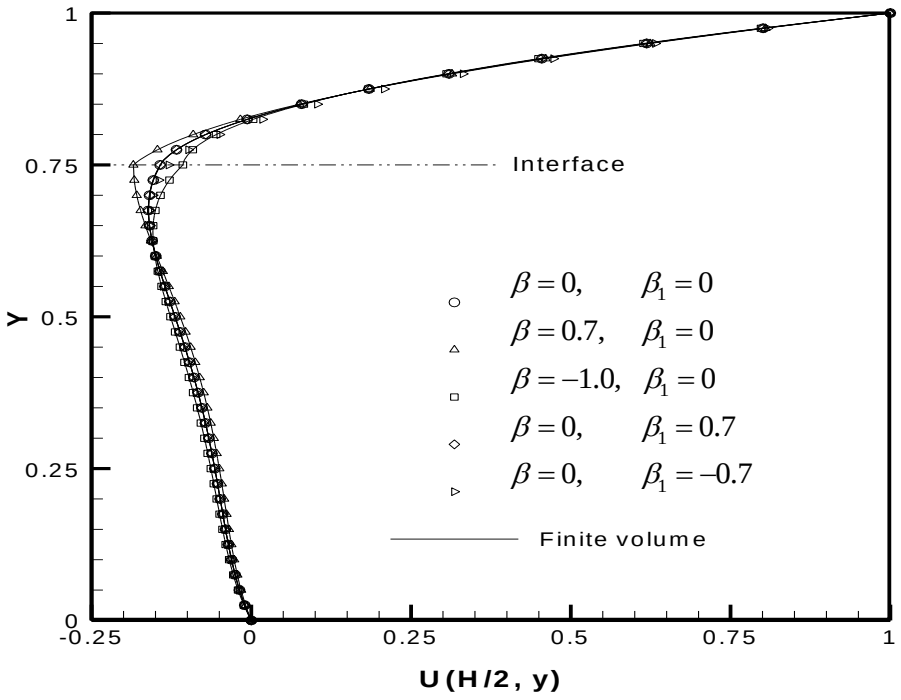
1
0.75
0.5
0.25
0
Y
-0.25
0
0.25
0.5
0.75
1
U(H/2, y)
Interface
β = 0, β1 = 0
β = 0.7, β1 = 0
β = –1.0, β1 = 0
β = 0, β1 = 0.7
β = 0, β1 = –0.7
Finite volume

(b)

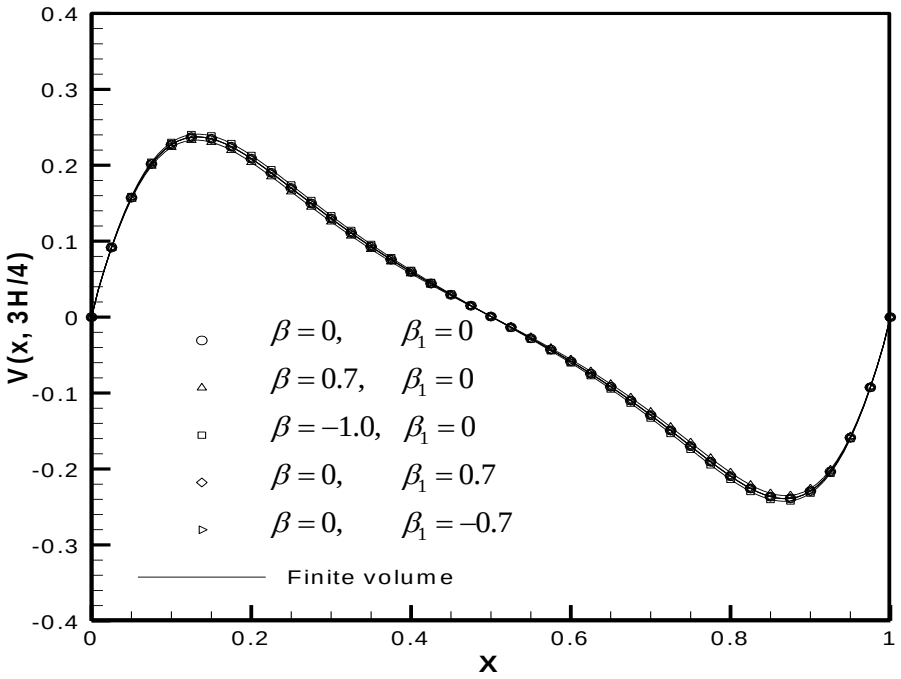


Figure 5.10 Velocity profiles at different stress jump coefficients; symbols represent LBM solutions and solid lines represent finite-volume solutions: (a) centerline velocity $U$ along y direction and (b) interfacial velocity $V$ along x direction; other parameters are $\mathrm{Re} = 1$, $\varepsilon = 0.7$ and $Da = 10^{-2}$.

# Chapter 6 Mass Transfer in a Microchannel Reactor With a Porous Wall

In this chapter, the flow and mass transfer in a microchannel reactor with a porous wall are studied with a view to applications in enzyme reactors and cell bioreactors. The Navier-Stokes equation in the fluid domain and the Darcy-Brinkman-Forcheimmer extended model in the porous medium domain are coupled and numerically solved. For porous-fluid interface, the Ochoa-Tapia and Whitaker's stress jump interfacial condition (1998b) is used to investigate its effects on flow and mass transfer. The reaction kinetics is based on first-order, zeroth-order, and Michaelis-Menten types. The numerical results are correlated by non-dimensional parameters for the purpose of presenting generalized results which can find applications in the design analysis of such micro-channel reactors with a porous wall.

## 6.1 Problem Statement

The reactor modeled in this chapter was a channel with dimensions typically of length 300 mm, 150 $\mu m$ in depth of fluid region and width 2.5cm as shown previously in Figure 3.1. In practice due to its larger value, the width effect is small as shown by Zeng et al. (2006). Thus the numerical model considered here is simplified into a two-dimensional one like Zhao et al. (2005).

The culture medium flows through the channel along the x direction, and there is a porous medium scaffold of typical depth 150 $\mu m$ in the below region (see Figure 3.1) where two cell types are uniformly distributed. The absorption cells and release cells adherent to the porous medium scaffold consume and secrete the species, respectively, forming the reactions in the porous scaffold. The incoming flow is steady, laminar and incompressible with substrate concentration $c_{in}$ . The inlet velocity is specified as that of a fully-developed flow.

The governing equations for flow and mass transfer in plain fluid and porous medium are presented in Section 3.1. As for the boundary conditions and normalization parameters, please refer to the Section 3.1 and 3.2.

## 6.2 Results and Discussion

### 6.2.1 Uncorrelated results for flow and concentration

*Grid independence study*

In chapter 5, a grid independency study had been implemented for channel flow partially filled with a porous medium. Thus in this chapter, a grid independency study was investigated for mass transfer only. Considering the computational cost and accuracy, a total number of 201x81 meshes for the channel, were found to be adequate as showed in Figure 6.1.

*Concentration and velocity fields*

As defined previously in Equation (3.59), the critical reaction parameter presents the relationship between the consumption rate and release rate. For present study, only the reaction type of $R_c > 0$ is studied. The reason is because when $R_c < 0$, release rate is larger than consumption rate, which means mass concentration in bioreactor porous region keeps on increasing and such cases are not meaningful to study.

Figure 6.2a, b and c show the typical concentration contour field for the fluid and porous regions with different reaction rate. There is relatively higher substrate concentration in the fluid region than in the porous scaffold. The substrate in the fluid is transported to the interface by convection and diffusion; there the concentration is higher than that in the bottom due to the substrate consumption in the porous medium (for $R_c >0$, consumption rate is larger than release rate). It is clear that along the downstream direction, the concentrations at the interface and bottom are decreasing due to the consumption. When the ratio of release over consumption rates $a$ increases from 0 to 0.4, the concentration is also increasing. This is because for higher ratio $a$, more substrate will be released which makes the concentration higher as shown clearly in Figure 6.2a, b and c.

To study the stress jump coefficients effect, zero release rates are used with different combination of $\beta$ and $\beta_1$ varying from -0.7 to +0.7, respectively. Figures 6.3a, b and c show a typical interface concentration distribution, concentration profile normal to the interface, and velocity profile respectively. In these concentration and velocity plots, the effects of interfacial boundary conditions are explored by the

variation of stress jump coefficients. The velocity is normalized by the Darcy velocity in the porous scaffold. The Darcy velocity is mainly determined by permeability, which was kept constant for the present cases with different stress jump coefficients.

Figure 6.3c shows that the first stress jump coefficient $\beta$ has some effects especially on the interfacial velocity and the maximum velocity, but little effect on velocity deeper into the porous scaffold. However, the second stress jump coefficient $\beta_1$ has very slight effect and can almost be neglected. This is because in the interfacial boundary conditions, the term involving $\beta_1$ is associated with velocity square which is low in present study. But the term involving $\beta$, associated with inverse of the Darcy number, can become large if *Da* is low. However, the effects of $\beta$ and $\beta_1$ on the velocity profile are not large.

The effects of $\beta$ and $\beta_1$ on concentrations (Figures 6.3a and b) are even smaller than that on the velocity. Thus, to facilitate study of other parameters' effects in the following computations, the continuities of both stress and velocity are implemented to couple the plain fluid and porous flow governing equations. However if the Darcy number was large, which makes the porous flow large, then the effects of $\beta$ and $\beta_1$ may not be negligible.

*Effect of porous Damkohler number and fluid Damkohler number*

To study the effects of the reaction rate over mass transfer ( $Dam_{fa}$ for fluid region convection and $Dam_{pa}$ for porous region diffusion), the substrate concentration

in interface, bottom and their difference were investigated with reaction rate for Michaelis-Menten type.

It is seen that the interface and bottom concentration (Figure 6.4a and b) are larger when fluid Damkohler number $Dam_{fa}$ or porous Damkohler number $Dam_{pa}$ are lower, which is expected as these are associated with smaller consumptions. For the effect on concentration difference (Figure 6.4c) it is larger when $Dam_{pa}$ is larger or when $Dam_{fa}$ is smaller. A larger $Dam_{pa}$ is associated with larger consumption and hence larger flux (as reflected by larger concentration difference). The significance of parameter $Dam_{pa}$ in reaction and diffusion has been highlighted by Griffith and Swartz (2006) for porous tissue constructs. As for the smaller $Dam_{fa}$, it is associated with larger convection (in fluid) relative to consumption and hence larger flux into porous medium.

The present results, for both small to large reaction rates, show that the mass transfer is influenced by two consumption parameters: $Dam_{fa}$ and $Dam_{pa}$. These two parameters characterize the reaction rate over convection and diffusion. In a previous study, Zhao et al. (2007) suggested two parameters: Peclet number $Pe_f$ and Thiele modulus (related to $\frac{V_m \gamma H^2}{Dc_{in}}$). The Thiele modulus was also suggested by Griffith and Swartz (2006), but unlike Zhao et al (2007), the axial length of the porous tissue was used. The present parameter $Dam_{pa}$ uses the depth of the porous medium, which is used in a previous study (Chen et al. 2010).

### 6.2.2 Correlation of results by combined parameters

Figure 6.5a and 6.5b present concentration reaction parameter as a function of effective distance parameter, at different fluid Damkohler number $Dam_{fa}$ and Peclet number $Pe_f$, respectively. It shows that concentration reaction parameter is a function of effective distance $\frac{x}{H \cdot Pe_f}$ as explained in Section 3.2.3. Hence the parameters $Dam_{fa}$ and $Pe_f$ need not be duplicated if the results, normalized by $Dam_{pa}$, are presented as a function of effective distance $\frac{x}{H \cdot Pe_f}$. Note that in a previous study by Chen et al. (2010) different definitions of parameters for concentration and distance were used, so that their interface concentration results show a dependence on the fluid Damkohler number $Dam_{fa}$.

Figure 6.6a and 6.6b present concentration reaction parameter and concentration difference parameter as a function of effective distance parameter at different Michaelis-Menten constant $K_m$, respectively. It shows that the results at different $K_m$ have collapsed because $K_m$ has been incorporated in the definition of concentration reaction parameter (see Equations 3.57 and 3.47) and concentration difference parameter (see Equation 3.32). The parameter $K_m$ needs not be duplicated if the results are normalized by the reaction parameter $\lambda$.

#### 6.2.2.1 Interface concentration reaction parameter

*Reactions close to Michaelis-Menten type*

The interface concentration at different release, consumption, convection and distance is plotted as a correlated plot in Figure 6.7a with the use of effective distance parameter $\frac{x}{H \cdot Pe_f}$ and normalized by $Dam_{pa}\lambda$. The correlation is for Michaelis-Menten reaction type ( $K_m$ is not zero).

The results show that the concentration reaction parameter decreases with increasing effective distance parameter. The numerical results agree with the general trend of the analytical solution (Equation 3.49) except the gradient is steeper. The variations of $Dam_{pa}$ and $a$ do not significantly change the non-dimensional results, except for one case at large $Dam_{pa}$ of 0.5 and zero release ratio $a$. The normalization of the interface concentration by $Dam_{pa}\lambda$ and plotted against effective distance $\frac{x}{H \cdot Pe_f}$ is effective in collapsing the numerical data.

*Reactions close to first order type*

The interface concentration at different release, consumption, convection and distance is plotted as a correlated plot in Figure 6.7b with the use of effective distance

parameter $\frac{x}{H \cdot Pe_f}$ and normalized by $Dam_{pa}\lambda$ . The correlation is for first order reaction type ( $Dam_{pa}/K_m$ is very small).

The results show that the concentration reaction parameter decreases with increasing effective distance parameter. The numerical results agree with the general trend of the analytical solution (Equation 3.55) except the gradient is steeper. The variations of $Dam_{pa} / K_m$ do not significantly change the non-dimensional results, even at the largest $Dam_{pa} / K_m$ of 0.25. The normalization of the interface concentration by $Dam_{pa}\lambda$ and plotted against effective distance $\frac{x}{H \cdot Pe_f}$ is successful in collapsing the numerical data.

#### 6.2.2.2 Concentration difference parameter

*Reactions close to Michaelis-Menten type*

The concentration difference at different release, consumption, convection and distance is plotted as a correlated plot in Figure 6.8a. The concentration difference parameter $\kappa = \frac{C_{\text{int}} - C_{bot}}{Dam_{pa}\lambda}$ is plotted as a function of the effective distance parameter $\frac{x}{H \cdot Pe_f}$ . It is seen that Figure 6.8a has correlated the numerical data satisfactorily except for the case at large $Dam_{pa}$ of 0.5 and zero release ratio $a$ . The spread of data is less at smaller effective distance less than 2. The effects of

$Dam_{pa}$ and $a$ have been incorporated in the concentration difference parameter. It is noted that away from the inlet, the concentration difference parameter is around 0.5 which agrees with the analytical solution (Equation 3.31 and 3.32).

*Reactions close to first order type*

The concentration difference at different release, consumption, convection and distance is plotted as a correlated plot in Figure 6.8b. The concentration difference parameter $\kappa = \frac{C_{\text{int}} - C_{bot}}{Dam_{pa} / K_m}$ is plotted as a function of the effective distance parameter $\frac{x}{H \cdot Pe_f}$. It is seen that Figure 6.8b has correlated the numerical data satisfactorily even though the $Dam_{pa} / K_m$ changes by a factor of 5 times and the large $Dam_{pa} / K_m = 0.25$ may not be truly of the first order type. The spread of data arises because the effects of $Dam_{pa} / K_m$ have not been completely absorbed in the concentration difference parameter. It is noted that away from the inlet, the concentration difference parameter is around 0.4 which close to the analytical value of 0.5 (Equation 3.37).

### 6.2.2.3 Effectiveness factor

To quantify the mass transfer resistance of the porous medium, an effectiveness factor is defined. It is the ratio of actual reaction rate to that which would be obtained if the enzyme or cells are at the interface (that is without the porous medium

resistance). In present study, the actual reaction rate is expressed based on concentration flux normal to the interface.

*Reactions close to Michaelis-Menten type*

Figure 6.9a presents effectiveness factor as a function of effective distance when the reaction is close to Michaelis-Menten type. It shows that away from the inlet, the effectiveness factor vary from around 0.9 to 0.6. The effectiveness is lower at large $Dam_{pa}$ and small release ratio $a$ . With large $Dam_{pa}$ (relatively large consumption), the concentration in the porous medium is much lower than that at the interface. Thus the actual reaction in the porous medium compared to that at the interface is smaller; and hence the porous medium is less effective for mass transfer across the interface. The effectiveness factor is a local parameter and far away from the inlet, it becomes lower due to the lower concentration in the porous medium.

*Reactions close to first order type*

Figure 6.9b presents effectiveness factor as a function of effective distance when the reaction is close to first order type. It shows that away from the inlet, the effectiveness factor is around 0.85 and is slightly higher at smaller $Dam_{pa} / K_m$ . The effectiveness of the porous medium is good because the consumption is relatively small with the assumption of small $Dam_{pa} / K_m$ for first order reaction. The concentration in the porous medium is relatively close to that at the interface.

Although the effectiveness factor is a local parameter, it is relatively constant along the effective length.

#### 6.2.2.4 Reactor efficiency

The reactor efficiency is the ratio of actual reaction-rate over the maximum reaction rate (based on the inlet concentration). The actual reaction rate is averaged over the reactor length. The reactor efficiency incorporates the effects of the porous medium and reactor length on the transfer of substrates into the porous medium for reaction by the cells or enzymes.

*Reactions close to Michaelis-Menten type*

Figure 6.10a presents reactor efficiency as a function of effective channel length at different $Dam_{pa}$ and $a$ when the reaction is close to Michaelis-Menten type. The reactor efficiency varies from around 0.85 to 0.6. The efficiency is lower at larger $Dam_{pa}$ and smaller $a$ due to the smaller concentration in the porous medium. At longer reactor length the efficiency is smaller. This is because of the decreasing interface concentration with length, which gives a lower concentration in the porous medium and hence the average reaction is low.

*Reactions close to first order type*

Figure 6.10b presents reactor efficiency as a function of effective channel length at different $Dam_{pa}/K_m$ when the reaction is close to first order type. The reactor efficiency away from the inlet is around 0.7. The reactor efficiency is good because the consumption is relatively small with the assumption of small $Dam_{pa}/K_m$ for first order reaction. As expected the efficiency is larger for smaller $Dam_{pa}/K_m$. The concentration in the porous medium is relatively close to that at the interface. The efficiency is averaged over the length, and does not vary much for effective length larger than 0.5.

### 6.2.2.5 Utilization efficiency

The utilization efficiency (or conversion rate) is the ratio of actual utilized mass rate over the inlet mass rate. The utilized mass rate is the difference in mass rates at reactor inlet and outlet. The utilization efficiency incorporates the effects of the porous medium, reactor length and fluid convection on the transfer of substrates into the porous medium for reaction by the cells or enzymes.

*Reactions close to Michaelis-Menten type*

Figure 6.11a presents utilization efficiency as a function of effective channel length at different $Dam_{pa}$ and $a$ when the reaction is close to Michaelis-Menten type.

The utilization efficiency varies from around 0 to 0.8. The utilization efficiency is very low at small $\frac{\mathrm{L}}{\mathrm{H}\cdot\mathrm{Pe}_f}$, that is either small $L/H$ or large $\mathrm{Pe}_f$. This is because the convection time scale is relatively short compare to the diffusion time. Hence the substrates further away from the interface are not utilized. At larger $Dam_{pa}$ the consumption is larger and hence gives better utilization. At smaller release ratio $a$ there is a requirement for more flux and hence larger utilization. The utilization efficiency highlights the importance of effective length to achieve good utilization.

*Reactions close to first order type*

Figure 6.11b presents utilization (or conversion) efficiency as a function of effective channel length at different $Dam_{pa}/K_m$ when the reaction is close to first order type. The utilization efficiency varies from around 0 to 0.15. The utilization efficiency is generally low due to the small consumption rate. At small $\frac{\mathrm{L}}{\mathrm{H}\cdot\mathrm{Pe}_f}$, that is either small $L/H$ or large $\mathrm{Pe}_f$, the utilization efficiency is very low because the convection time scale is relatively short compare to the diffusion time. Hence the substrates further away from the interface are not utilized. At larger $Dam_{pa}/K_m$ the consumption is larger and hence gives better utilization.

### 6.2.3 Applications in design of bioreactors

The present generalized results can be used for design of microchannel bioreactors. Several bioreactor design criteria, such as critical channel length, critical inlet concentration, effectiveness factor, reactor efficiency and utilization efficiency can be checked and optimized.

To illustrate the application of present generalized results, the following perfusion bioreactor systems (Chow et al. 2001, Zhao et al. 2005, 2007 and Pathi et al. 2005) for growth of mesenchymal stem cells (MSC) and hematopoietic cells will be considered. These bioreactor systems consisted of a microchannel with a porous wall, like the present model. Both the geometry and mass transfer properties are listed previously in Table 3.1. One important parameter is the cell density and in this section it is taken to be the MSC density at day 20, given as $3.99\text{x}10^6 cells/ml$ (Zhao et al., 2005).

*Critical channel length*

The critical channel length is an important parameter which can be used to avoid species insufficiency for cell growth in bioreactor. From the consideration of effective length $\frac{L}{H}\frac{1}{Pe_f}$, a long microchannel bioreactor would not suffer from species inadequacy if proper $H$ or $Pe_f$ are selected, that is either large enough $H$ or $Pe_f$.

As listed previously in Table 3.1, the reactor parameters are typically: $Pe_f = 20.2$, $K_m = 0.05$, $Dam_{pa}$ =0.0513 and $Dam_{pa}\lambda = 0.468$. A simple iteration

procedure will be needed to find the critical channel length. Assume the bottom concentration at the outlet to be equal the critical concentration, $C_{bot} = K_m = 0.05$, so as to avoid hypoxia. With a trial value of initial channel length L = 100mm, the effective channel length is calculated as $\zeta = \frac{L}{H}\frac{1}{Pe_f} = 0.825$. Using Figure 6.8a, the concentration difference parameter $\kappa = \frac{C_{\text{int}} - C_{bot}}{Dam_{pa}\lambda} = 0.5$ ; hence the interface concentration at outlet $C_{\text{int}} = 0.284$. Then the interface concentration parameter at outlet is calculated: $\xi_k = \frac{C_{\text{int}} - 1}{Dam_{pa}\lambda} = -1.53$. Using Figure 6.7a, with $\xi_k = -1.53$, the critical effective channel length is determined as $\zeta = \frac{L}{H}\frac{1}{Pe_f} = 1.4$. Hence the critical channel length $L = 170mm$, which can be used for the next iteration. The critical value of channel length can be approximately determined within two iterations and found to be about 172 mm. In the bioreactors of Chow et al. (2001), Zhao et al. (2005, 2007) and Pathi et al. (2005), the channel length is 100mm which is within the present calculation of critical channel length.

*Critical inlet concentration*

Consider the example bioreactor system with $L = 100\ mm$ , $H = 6\ mm$ and $k_m = 1.1\times10^{-8} mol/ml$ . The effective channel length is calculated as $\zeta = \frac{L}{H}\frac{1}{Pe_f} = 0.825$. From Figure 6.7a, the interface concentration parameter is

determined as $\xi_k = \frac{C_{\text{int}} - 1}{Dam_{pa}\lambda} = -1.1$, and hence $C_{\text{int}} = 0.485$. From Figure 6.8a, and also using the effective length $\zeta = \frac{L}{H}\frac{1}{Pe_f} = 0.825$, the concentration difference parameter is determined as $\kappa = \frac{C_{\text{int}} - C_{bot}}{Dam_{pa}\lambda} = 0.5$. Hence, with the calculated $C_{\text{int}} = 0.485$, the bottom concentration is calculated as $C_{bot} = \frac{c_{bot}}{c_{in}} = 0.251$. If the outlet is assumed to be at the critical concentration $c_{bot} = k_m = 1.1\times10^{-8} mol/ml$, the critical inlet concentration can be calculated as $c_{\text{in\_critical}} = 4.38\times10^{-8} mol/ml$. In the bioreactor systems of Chow et al. (2001), Zhao et al. (2005, 2007) and Pathi et al. (2005), the inlet concentration is $c_{in} = 2.2\times10^{-7} mol/ml$ which is satisfactory as it is larger than the present calculation of critical inlet concentration.

## 6.3 Conclusions

The velocity and concentration fields have been calculated in a microchannel reactor with a porous wall. To characterize the mass transfer in the porous medium the porous Damkohler number $Dam_{pa}$ is defined as the ratio of consumption to diffusion of the substrates in the porous medium. The convective and diffusion time scales in the fluid region is characterized by an effective distance $\frac{x}{H}\frac{1}{Pe_f}$. The simplified analytical solutions indicate that the concentration should be normalized by the Damkohler number $Dam_{pa}$, Michaelis-Menten constant $K_m$ and release ratio $a$.

The normalized numerical data, of the interface concentration and concentration difference, show satisfactory correlation when presented as a function of the effective distance $\frac{x}{H}\frac{1}{Pe_f}$.

To quantify the local mass transfer resistance along the length of the porous medium, an effectiveness factor is defined. For reaction close to Michaelis-Menten type, the effectiveness factor varies from around 0.9 to 0.6. For reaction close to first order type, the effectiveness factor is around 0.85, because the mass flux into the porous medium is relatively small with the assumption of small $Dam_{pa} / K_m$.

The reactor efficiency is the ratio of actual reaction-rate over the maximum reaction rate (based on the inlet concentration). The actual reaction rate is averaged over the reactor length and incorporates the effects of the porous medium and reactor length. For reaction close to Michaelis-Menten type, the reactor efficiency varies from around 0.85 to 0.6. For reaction close to first order type, the reactor efficiency is around 0.7.

The utilization efficiency (or conversion rate) is the ratio of actual utilized mass rate over the inlet mass rate. The utilization efficiency incorporates the effects of the porous medium, reactor length and fluid convection on the transfer of substrates into the porous medium for reaction by the cells or enzymes. When the reaction is close to Michaelis-Menten type, the utilization efficiency varies from around 0 to 0.8. When the reaction is close to first order type, the utilization efficiency varies from around 0 to 0.15. For both Michaelis Menten and first order type reactions, the utilization efficiencies are very low at small $\frac{\mathrm{L}}{\mathrm{H}\cdot \mathrm{Pe}_f}$, that is either small $L/H$ or large $\mathrm{Pe}_f$.

This is because the convection time scale is relatively short compare to the diffusion time.

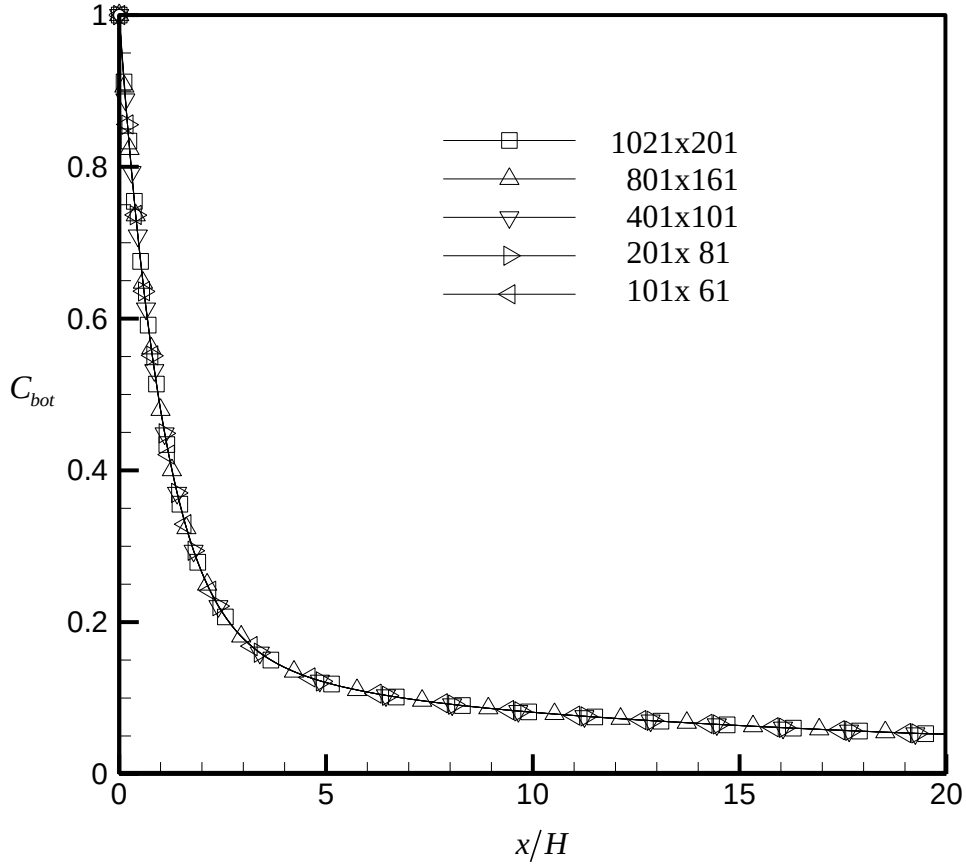


Figure 6.1 Grid independence study for concentration at the bottom with different grid size when $\varepsilon = 0.8$, $a = 0.0$, $K_m = 0.26$, $Dam_{pa}$=2.0, $Dam_{fa}$=0.05, $\beta = 0$ and $\beta_1 = 0$.

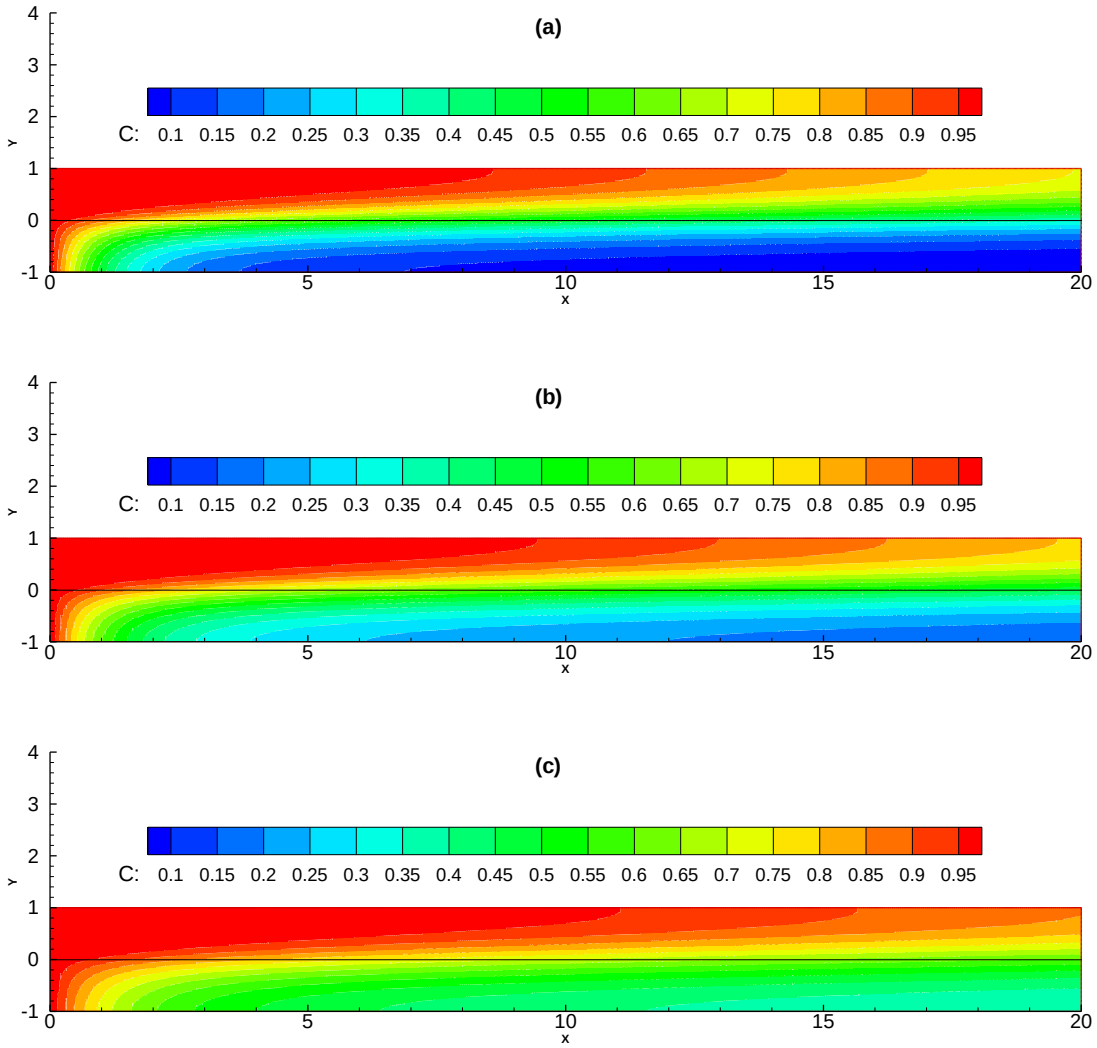


Figure 6.2 Contour of concentration field with effect of different release rate when $\varepsilon = 0.8$, $K_m = 0.26$, $Dam_{pa}$=2.0, $Dam_{fa}$=0.05, $\beta = 0$ and $\beta_1 = 0$: (a) $a = 0.0$; (b) $a = 0.2$; (c) $a = 0.4$.

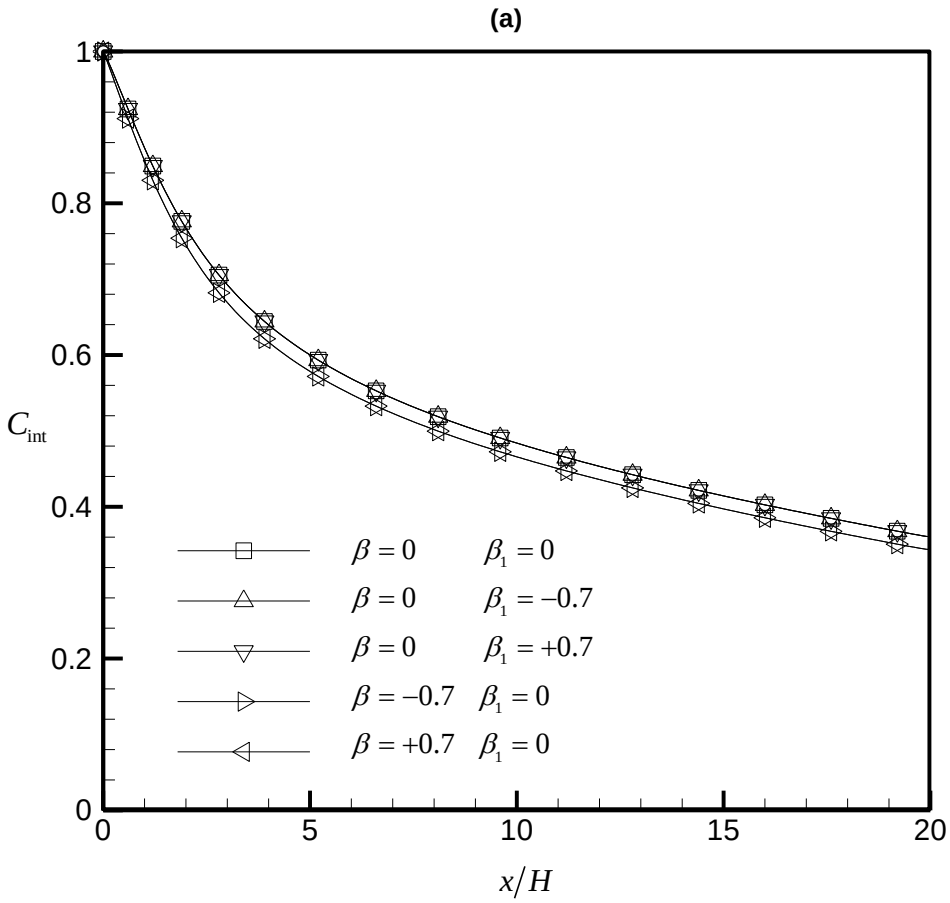
(a)
1
0.8
0.6
0.4
0.2
0
$C_{\text{int}}$
0
5
10
15
20
$x/H$
$\beta = 0$ $\beta_1 = 0$
$\beta = 0$ $\beta_1 = -0.7$
$\beta = 0$ $\beta_1 = +0.7$
$\beta = -0.7$ $\beta_1 = 0$
$\beta = +0.7$ $\beta_1 = 0$

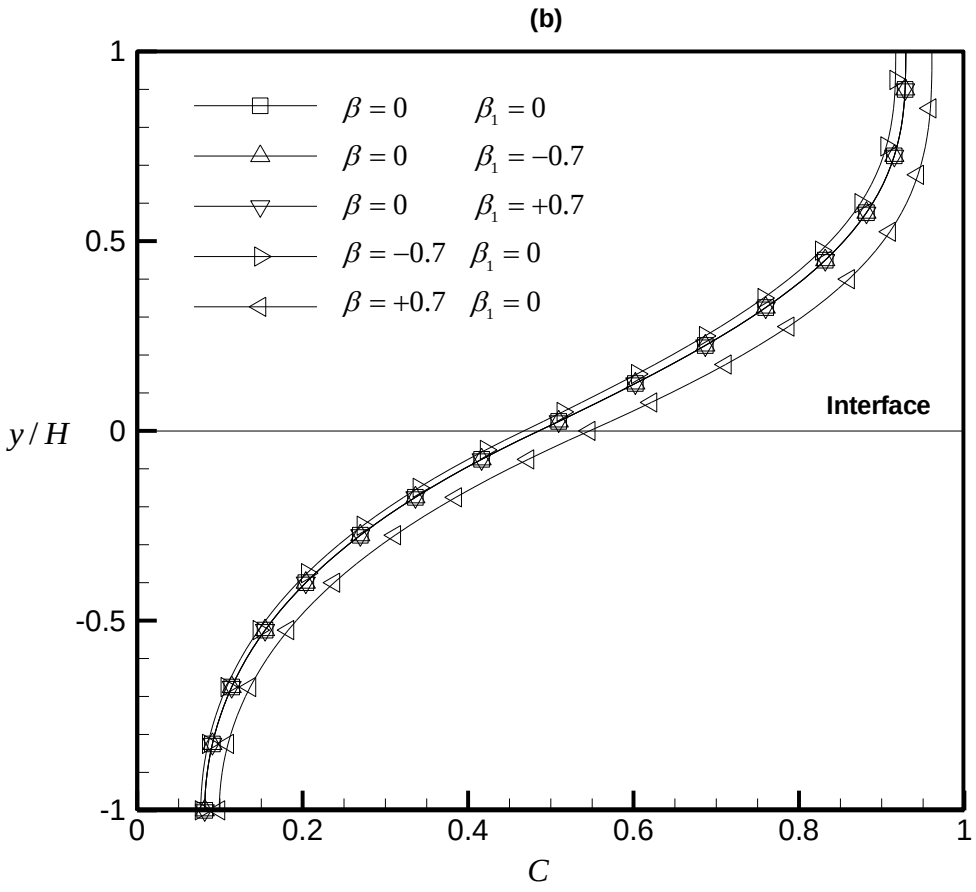
(b)
1
0.5
0
-0.5
-1
y / H
0
0.2
0.4
0.6
0.8
1
C
β = 0 β1 = 0
β = 0 β1 = −0.7
β = 0 β1 = +0.7
β = −0.7 β1 = 0
β = +0.7 β1 = 0
Interface

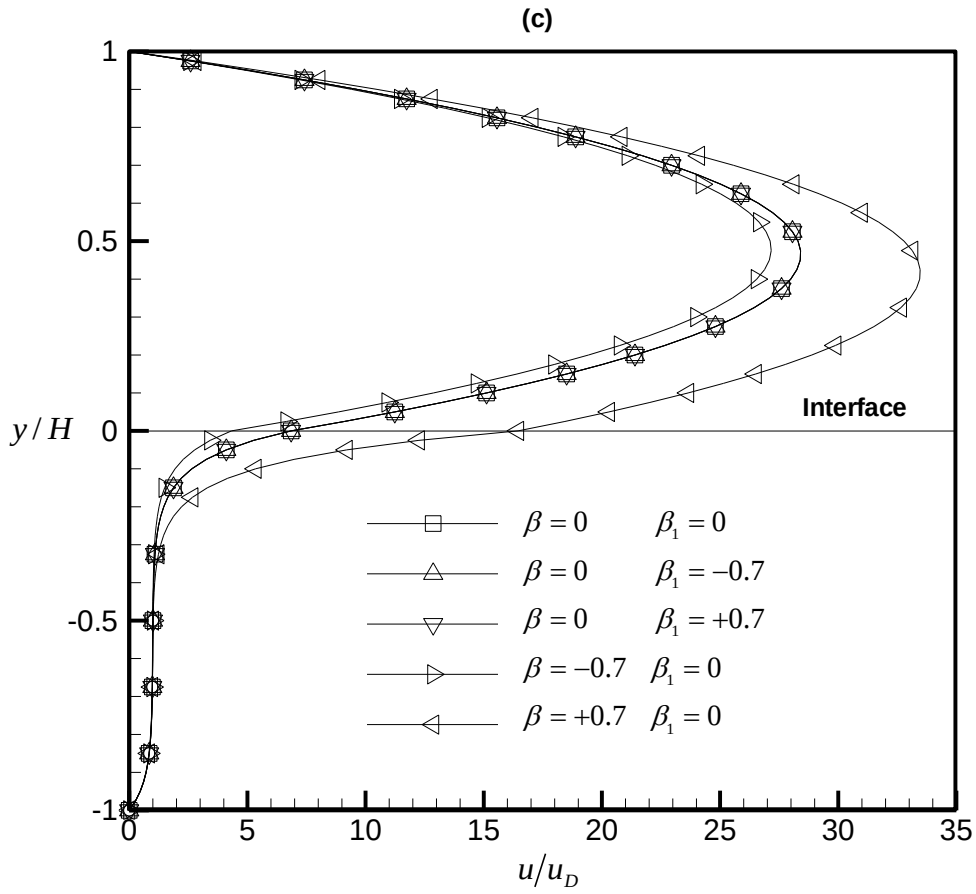


Figure 6.3 Effects of different stress jump coefficients when $\varepsilon = 0.8$, $a = 0.0$, $K_m = 0.26$, $Dam_{pa}$=2.0 and $Dam_{fa}$=0.05: (a) Concentration at interface; (b) Concentration profiles normal to interface at x/H=10.0; (c) Velocity profiles.

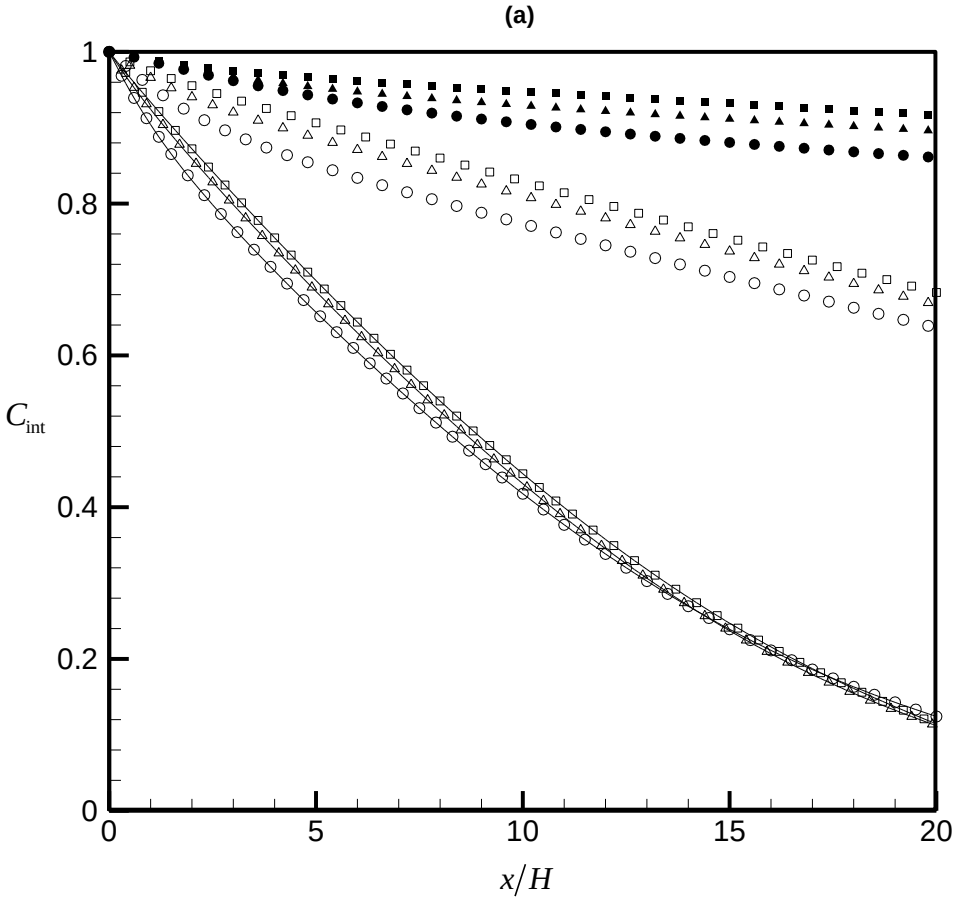
(a)
1
0.8
0.6
0.4
0.2
0
$C_{int}$
0
5
10
15
20
$x/H$

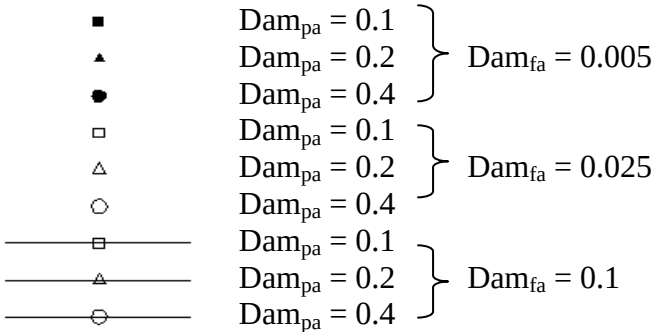
Dam$_{pa}$ = 0.1
Dam$_{pa}$ = 0.2
Dam$_{pa}$ = 0.4
Dam$_{fa}$ = 0.005
Dam$_{pa}$ = 0.1
Dam$_{pa}$ = 0.2
Dam$_{pa}$ = 0.4
Dam$_{fa}$ = 0.025
Dam$_{pa}$ = 0.1
Dam$_{pa}$ = 0.2
Dam$_{pa}$ = 0.4
Dam$_{fa}$ = 0.1

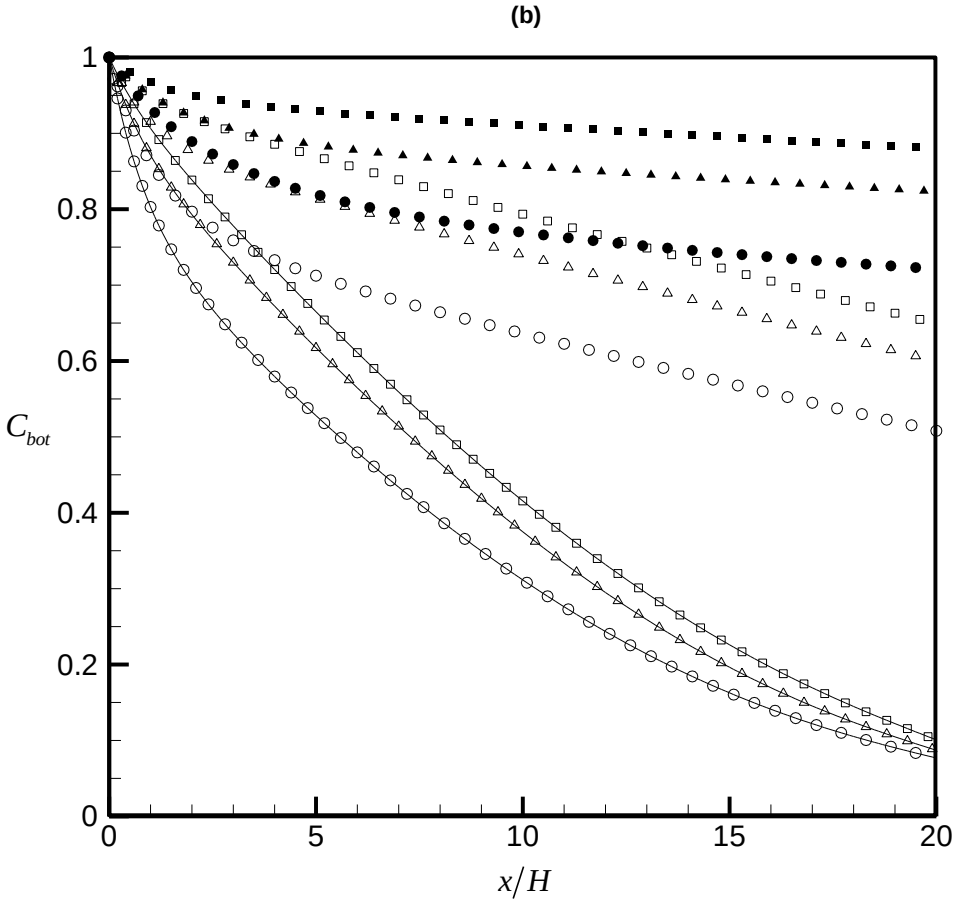
(b)
1
0.8
0.6
0.4
0.2
0
$C_{bot}$
0
5
10
15
20
$x/H$

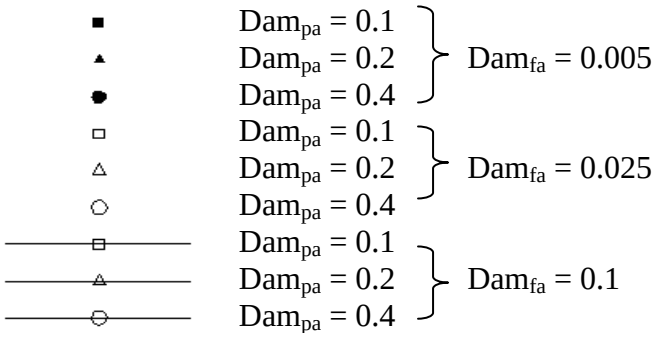
Dam$_{pa}$ = 0.1
Dam$_{pa}$ = 0.2
Dam$_{pa}$ = 0.4
Dam$_{fa}$ = 0.005
Dam$_{pa}$ = 0.1
Dam$_{pa}$ = 0.2
Dam$_{pa}$ = 0.4
Dam$_{fa}$ = 0.025
Dam$_{pa}$ = 0.1
Dam$_{pa}$ = 0.2
Dam$_{pa}$ = 0.4
Dam$_{fa}$ = 0.1

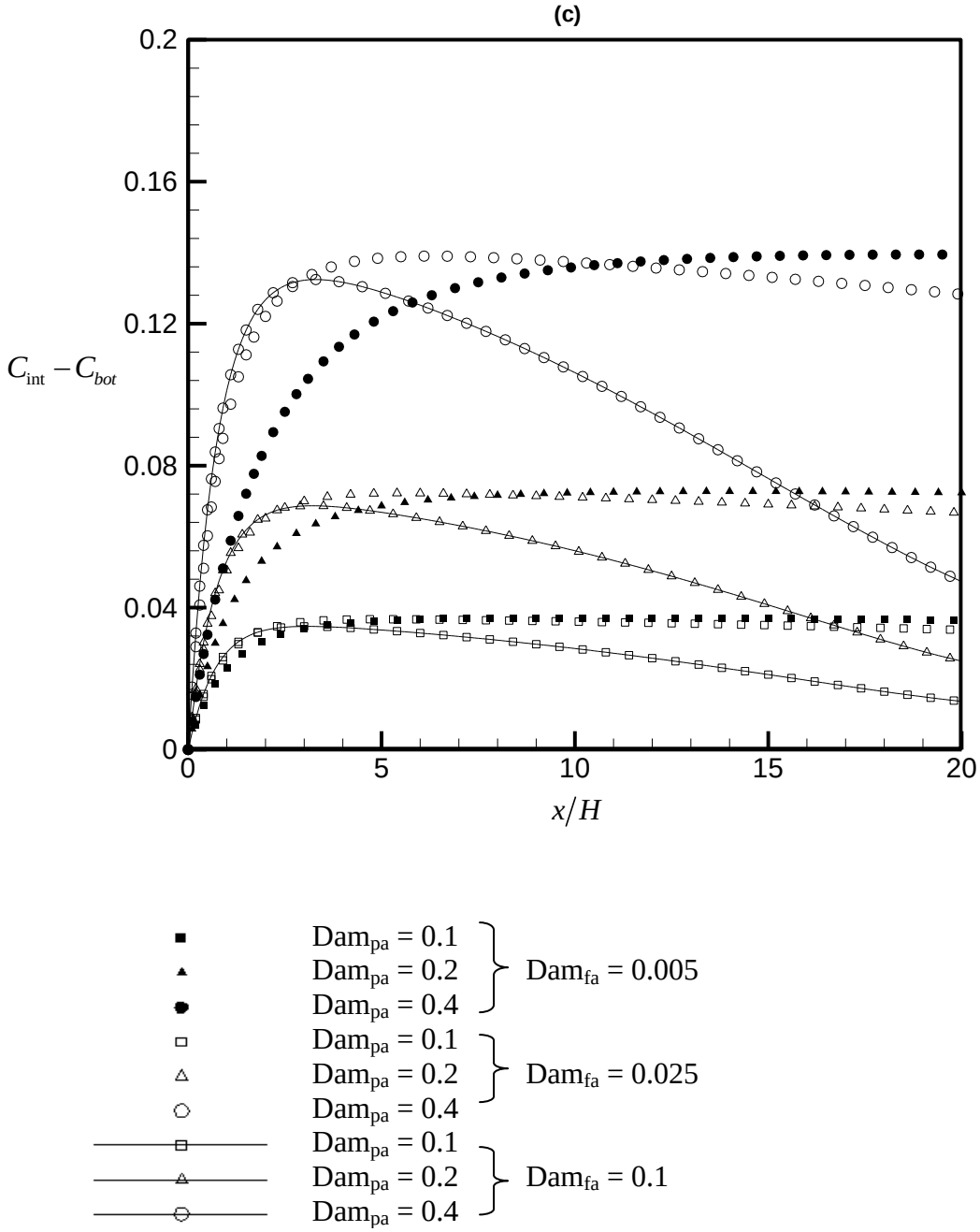


Figure 6.4 Concentration at different $\text{Dam}_{pa}$ and $\text{Dam}_{fa}$ for $\varepsilon = 0.8$, $K_m = 0.26$, $a$ = 0.0, $\beta = 0$ and $\beta_1 = 0$: (a) at interface; (b) at bottom; (c) Concentration difference.

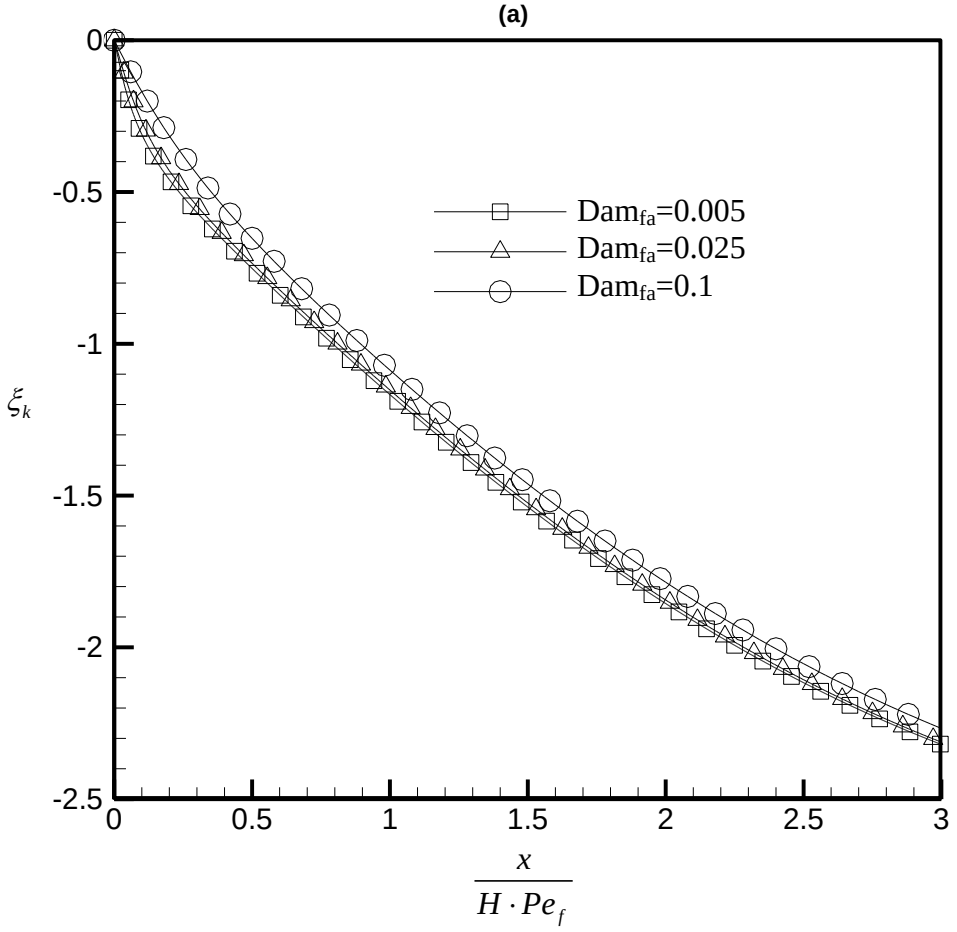
(a)
0
-0.5
-1
-1.5
-2
-2.5
0
0.5
1
1.5
2
2.5
3
$\xi_k$
$\frac{x}{H \cdot Pe_f}$
$Dam_{fa}$=0.005
$Dam_{fa}$=0.025
$Dam_{fa}$=0.1

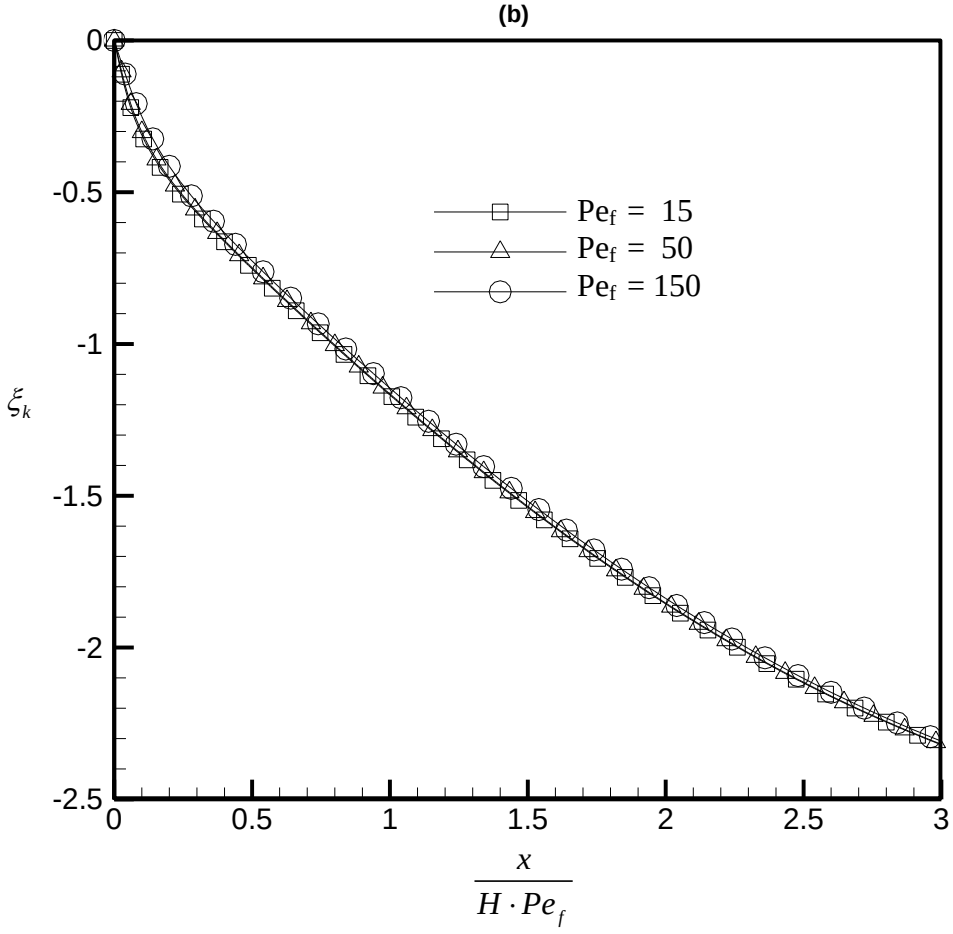


Figure 6.5 Concentration reaction parameter as function of effective distance parameter when $\varepsilon = 0.8$, $a = 0.0$, $Dam_{pa}$=0.5, $K_m$=0.26, $\beta = 0$ and $\beta_1 = 0$: (a) at different $Dam_{fa}$; (b) at different $Pe_f$

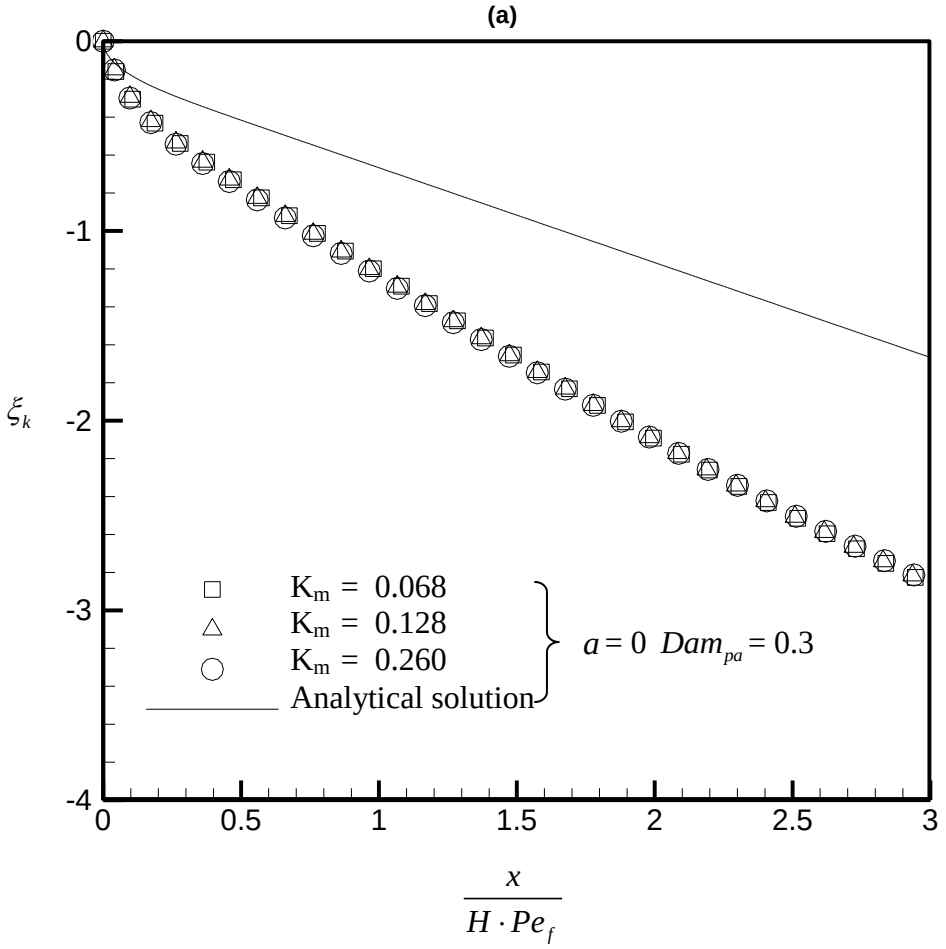
(a)
0
-1
-2
-3
-4
$\xi_k$
0
0.5
1
1.5
2
2.5
3
$\frac{x}{H \cdot Pe_f}$
$K_m$ = 0.068
$K_m$ = 0.128
$K_m$ = 0.260
Analytical solution
$a = 0$ $Dam_{pa} = 0.3$

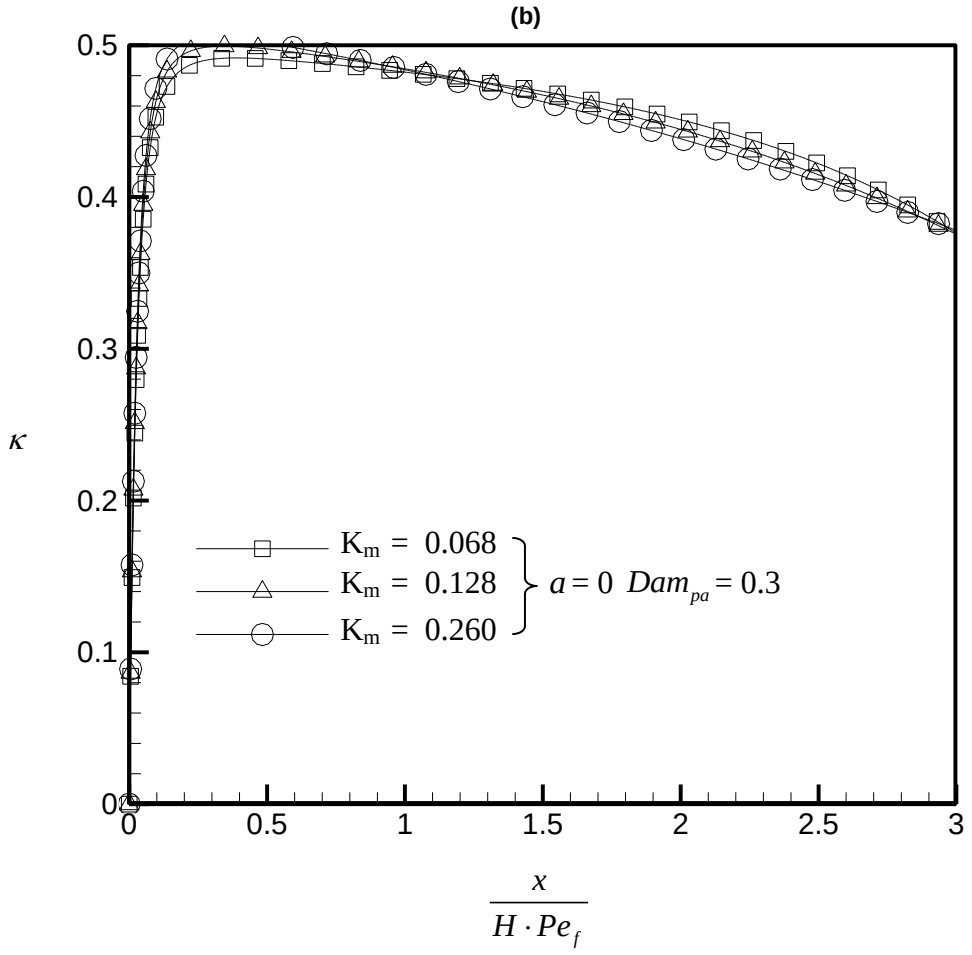


Figure 6.6 Concentration results on different $K_m$ when $\varepsilon = 0.8$, $\beta = 0$ and $\beta_1 = 0$ for: (a) concentration reaction parameter; (b) concentration difference parameter

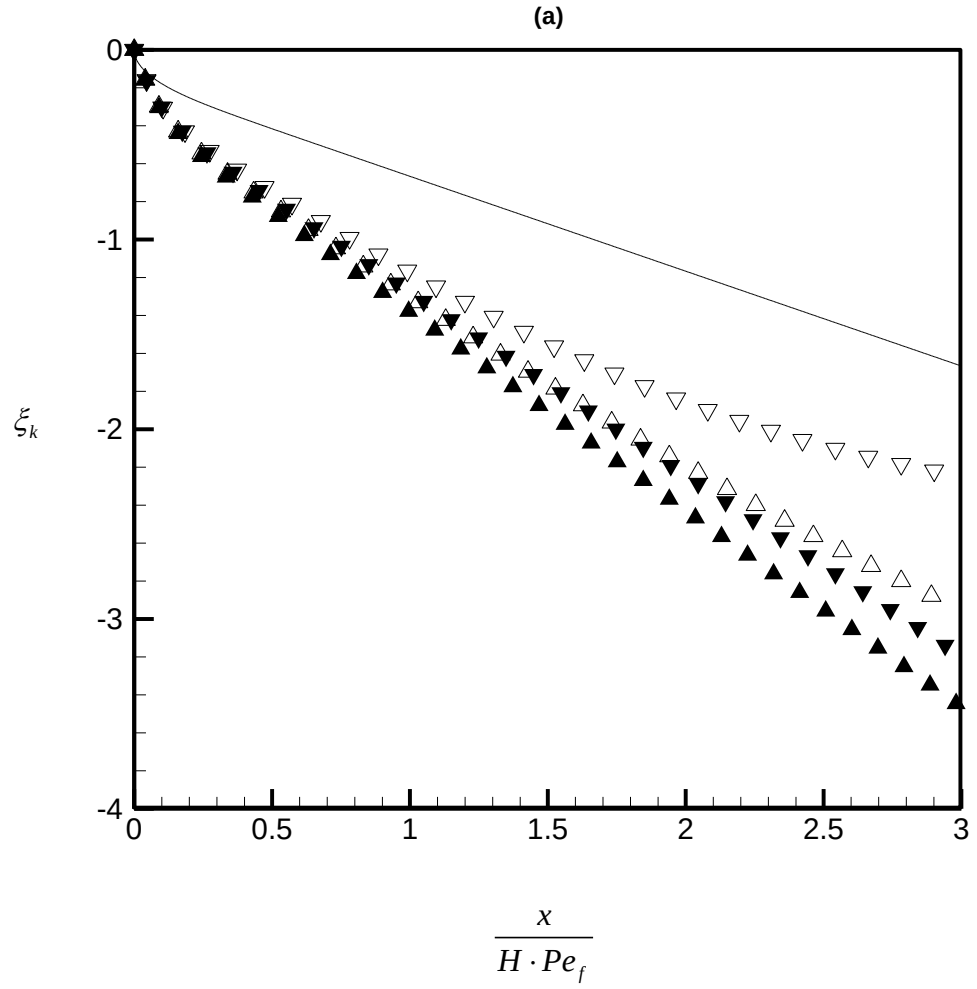
(a)
0
-1
-2
-3
-4
$\xi_k$
0
0.5
1
1.5
2
2.5
3
$\frac{x}{H \cdot Pe_f}$
$a$=0.0
$a$=0.4
Dam$_{pa}$=0.1
$a$=0.0
$a$=0.4
Dam$_{pa}$=0.5
Analytical solution for M-M Type

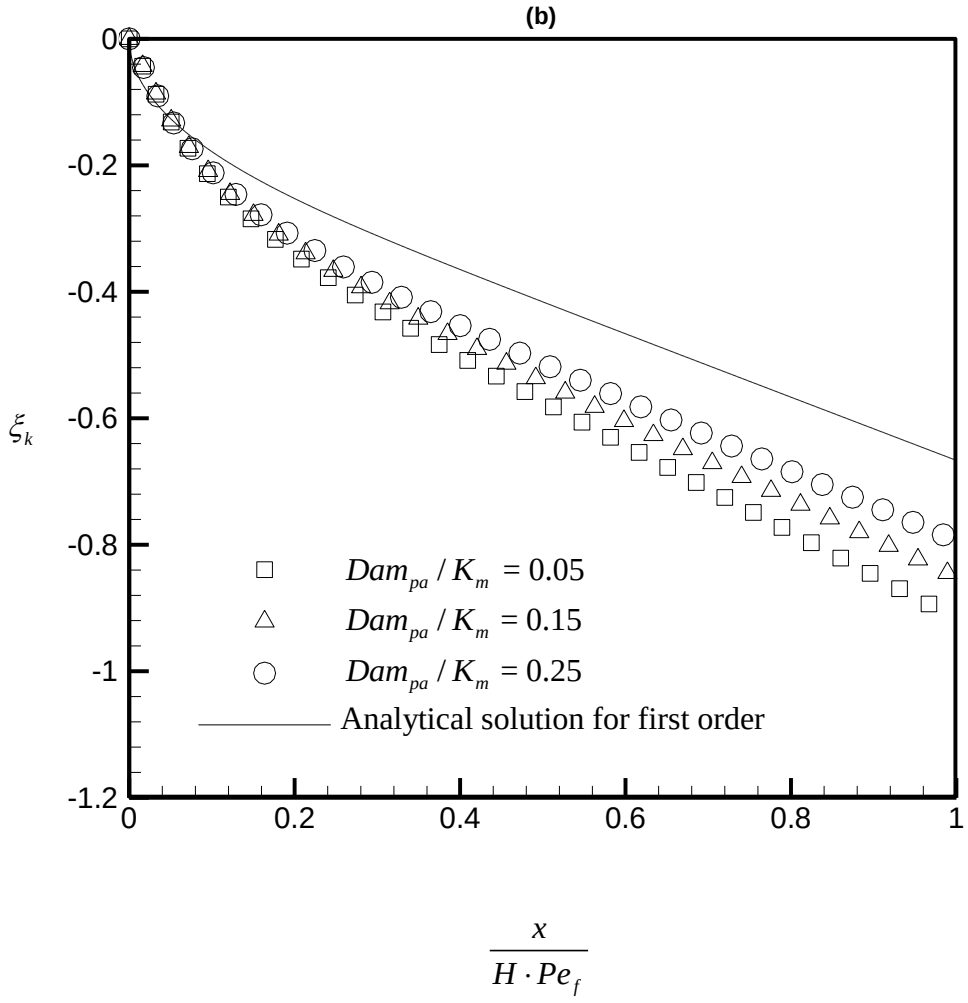


Figure 6.7 Concentration reaction parameter as function of effective distance parameter when $\varepsilon = 0.8$, $\beta = 0$ and $\beta_1 = 0$: (a) Michaelis-Menten reaction at different $a$ and $Dam_{pa}$ with $K_m$=0.128; (b) First order reaction at different $Dam_{pa} / K_m$.

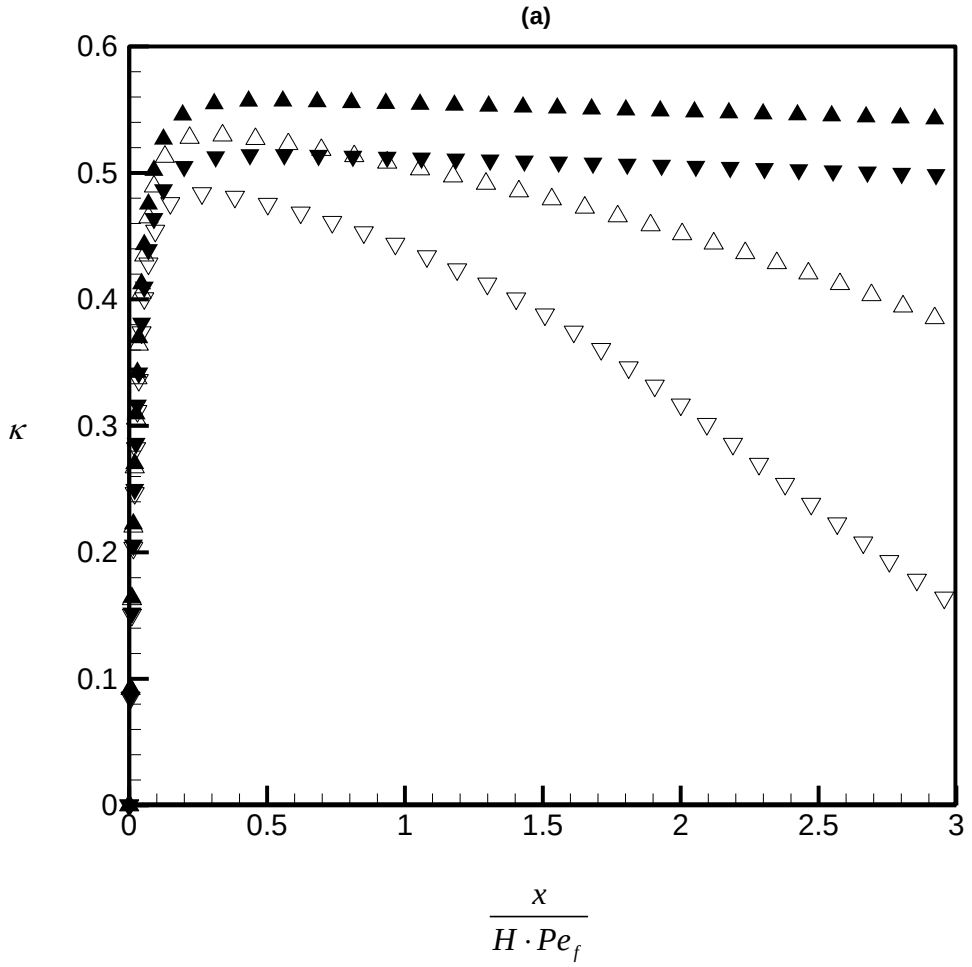
(a)
0.6
0.5
0.4
0.3
0.2
0.1
0
κ
0
0.5
1
1.5
2
2.5
3
x / (H · Pe_f)
a =0.0
a =0.4
Dam_pa=0.1
a =0.0
a =0.4
Dam_pa=0.5

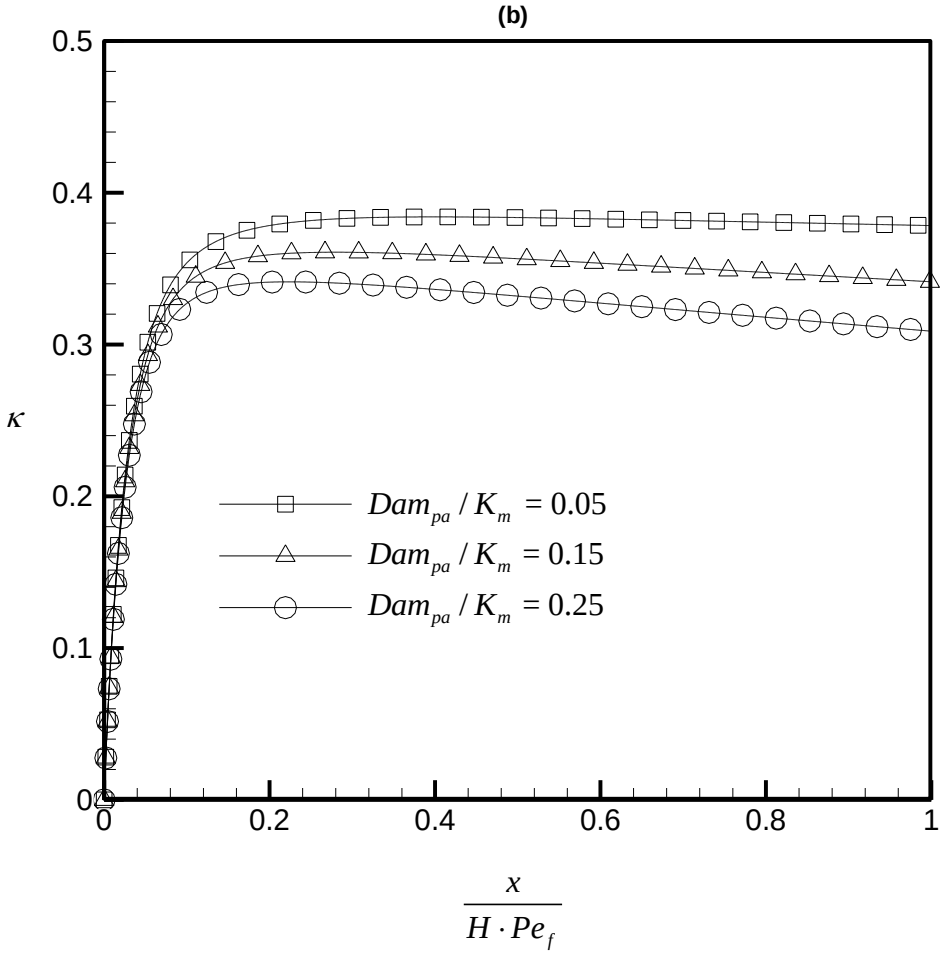


Figure 6.8 Concentration difference parameter as function of effective distance parameter when $\varepsilon = 0.8$, $\beta = 0$ and $\beta_1 = 0$: (a) Michaelis-Menten reaction at different $a$ and $Dam_{pa}$ with $K_m$=0.128; (b) First order reaction at different $Dam_{pa} / K_m$.

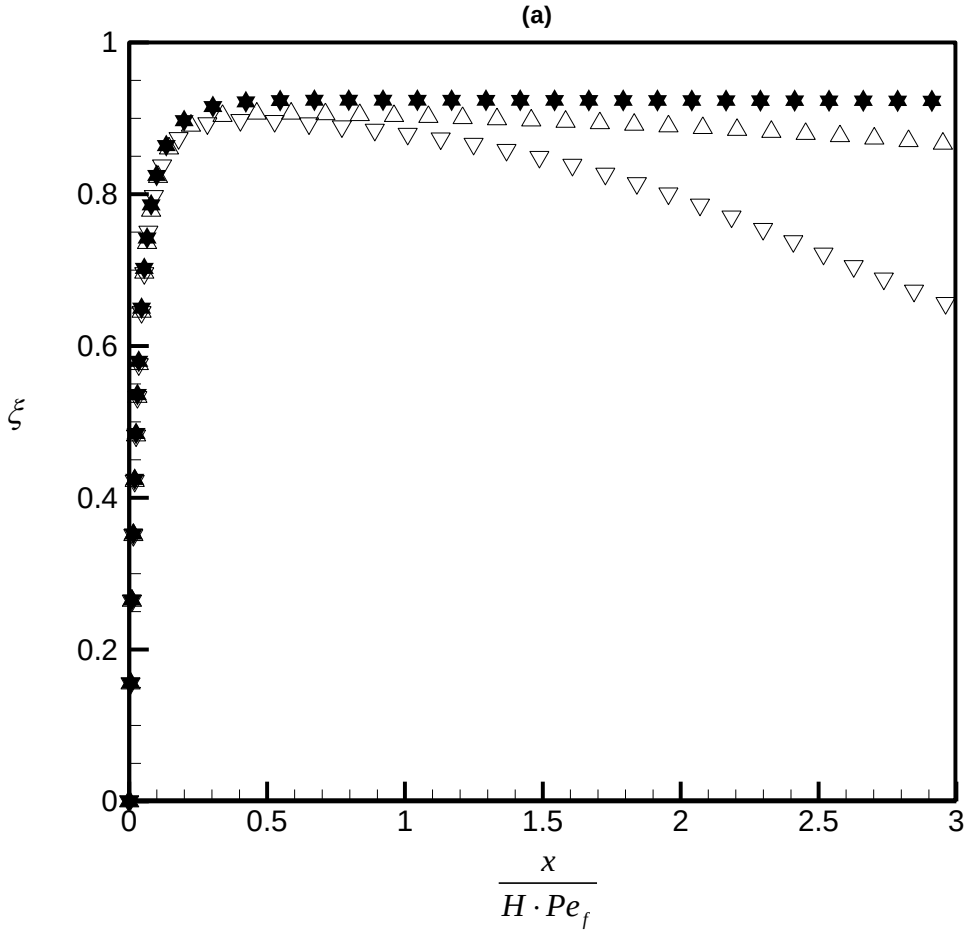


▼ $a$=0.0
▲ $a$=0.4
} $Dam_{pa}$=0.1

▽ $a$=0.0
△ $a$=0.4
} $Dam_{pa}$=0.5

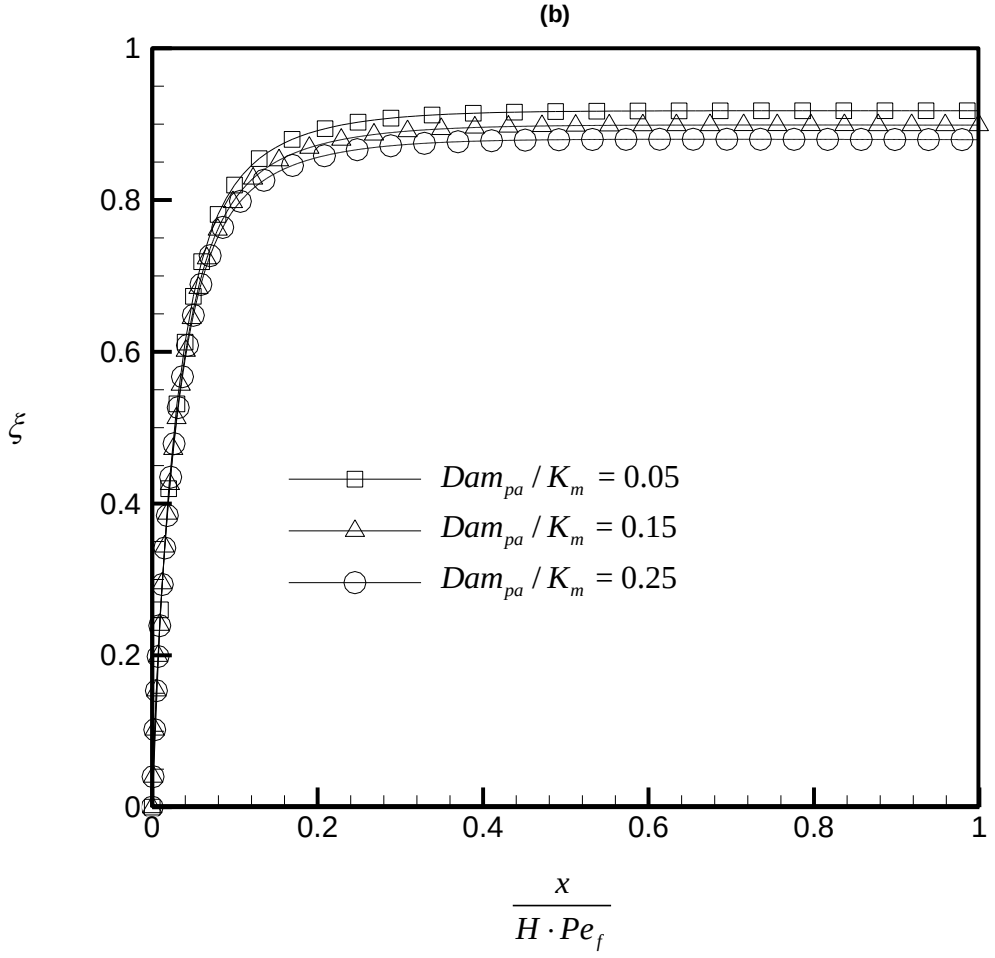


Figure 6.9 Effectiveness factor as function of effective distance parameter when $\varepsilon = 0.8$, $\beta = 0$ and $\beta_1 = 0$: (a) Michaelis-Menten reaction at different $a$ and $Dam_{pa}$ with $K_m$=0.128; (b) First order reaction at different $Dam_{pa} / K_m$.

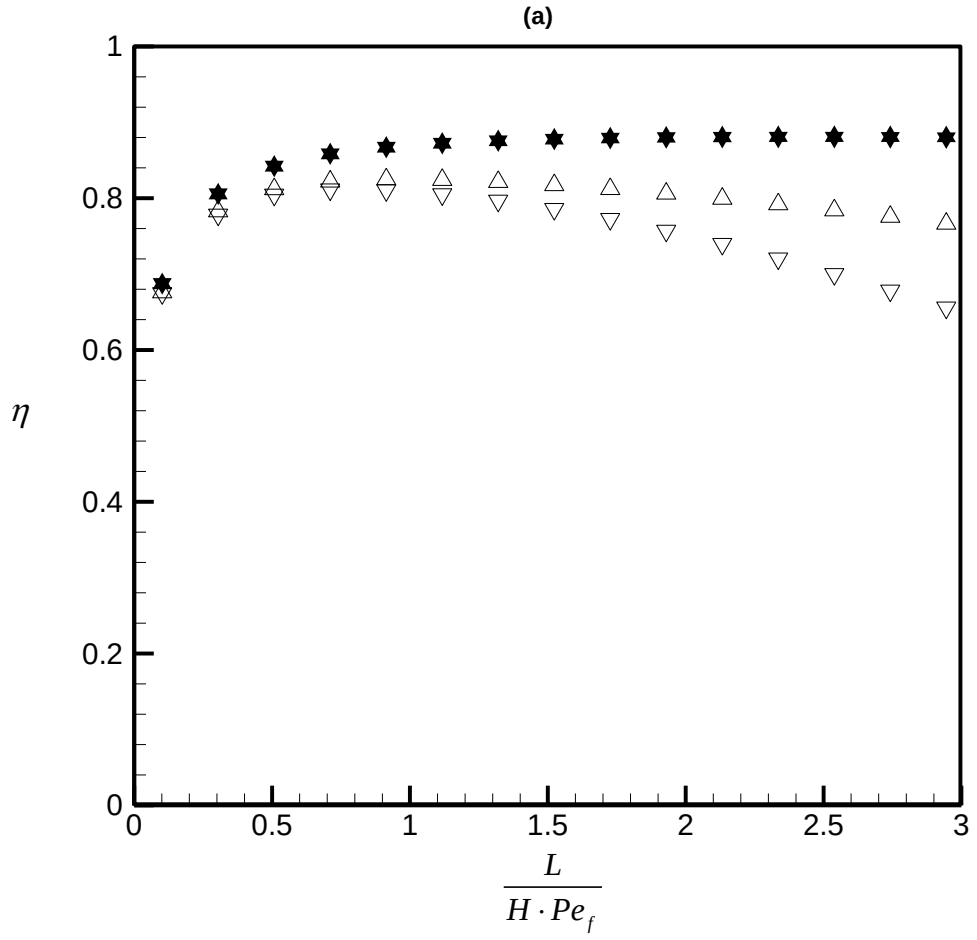
(a)
1
0.8
0.6
0.4
0.2
0
η
0
0.5
1
1.5
2
2.5
3
L / (H · Pe_f)
a =0.0
a =0.4
Dam_pa=0.1
a =0.0
a =0.4
Dam_pa=0.5

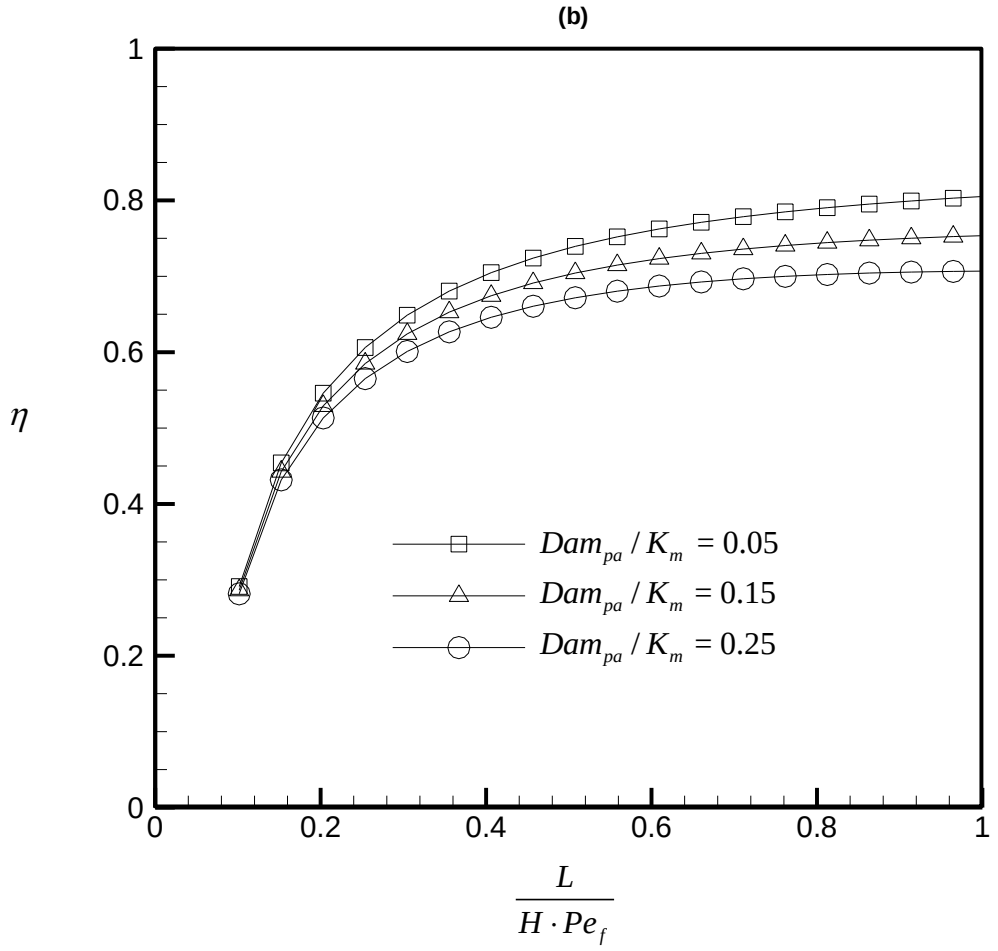


Figure 6.10 Reactor efficiency as function of effective distance parameter when $\varepsilon = 0.8$, $\beta = 0$ and $\beta_1 = 0$: (a) Michaelis-Menten reaction at different $a$ and $Dam_{pa}$ with $K_m$=0.128; (b) First order reaction at different $Dam_{pa} / K_m$.

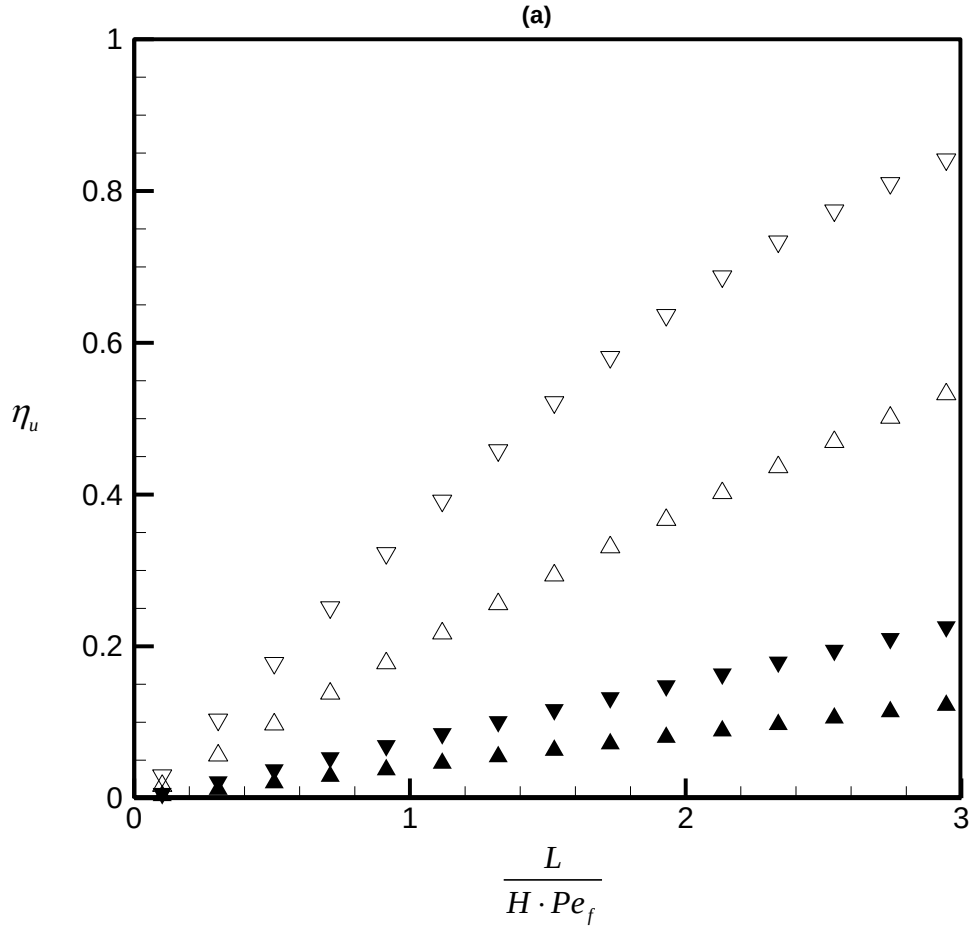


▼ $a$=0.0
▲ $a$=0.4
} $Dam_{pa}$=0.1

▽ $a$=0.0
△ $a$=0.4
} $Dam_{pa}$=0.5

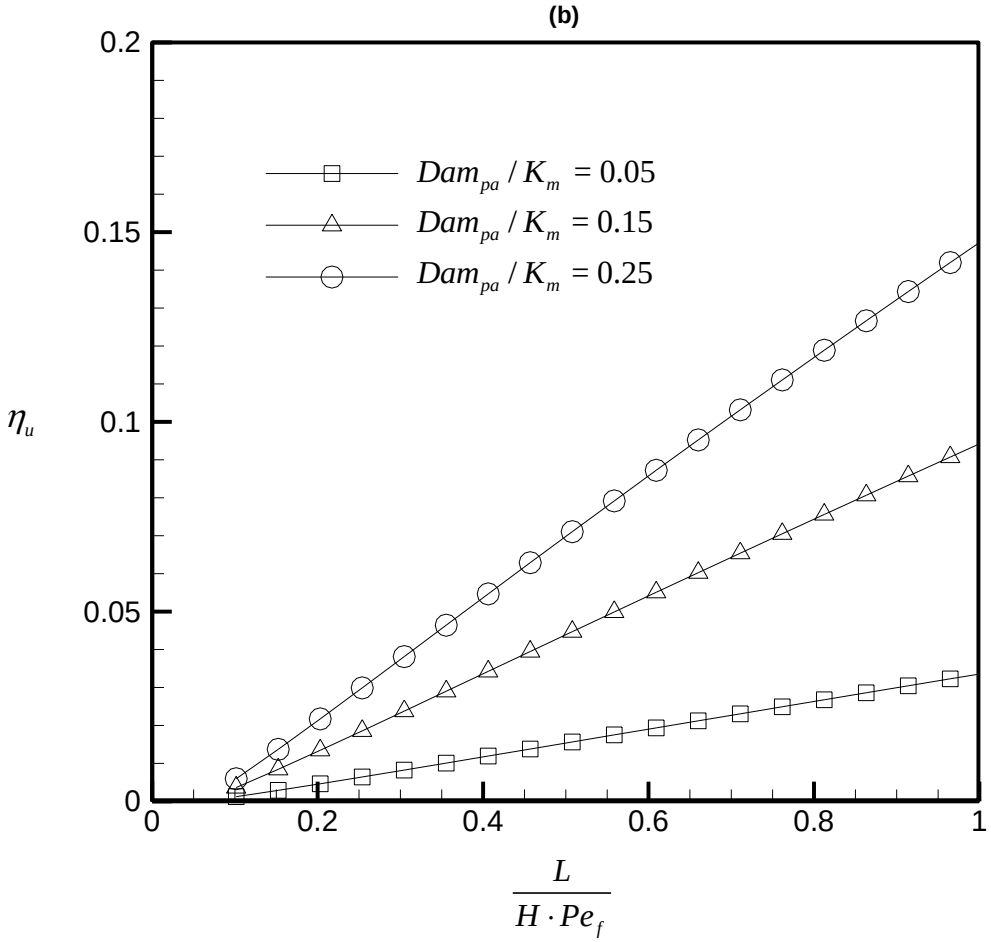


Figure 6.11 Utilization efficiency as function of effective distance parameter when $\varepsilon = 0.8$, $\beta = 0$ and $\beta_1 = 0$: (a) Michaelis-Menten reaction at different $a$ and $Dam_{pa}$ with $K_m$=0.128; (b) First order reaction at different $Dam_{pa} / K_m$.

# Chapter 7 Conclusions

## 7.1 Conclusions

A numerical study, using the BEM, was carried out on the flow through a channel partially filled with fibrous porous medium, which was modeled as a periodic, hexagonal array of cylinders. The low Reynolds number flow is studied in present work. The flow was transverse to the cylinders and the interfacial boundary conditions were analyzed. The slip coefficient was determined to vary from around 0.4 to 8.4 for the present range of permeability. Using the determined slip coefficients in the previous slip boundary model, the interfacial velocity was found to be less than the present BEM results by around 2–5 times. The effective viscosity varies from around 3.1 to 5 for the present permeability. The stress jump coefficient is of order one, which is consistent with previous literature. However, it is interesting that the present jump coefficients are negative in value. Note that Beavers-Joseph model has inherent defect of not having local geometry effects on slip coefficients. Hence it is difficult to compare present numerical results with those results deduced or matched from Beavers-Joseph model. The present results may give some indication of the range of values of the coefficients that are needed as empirical inputs to the various models of interfacial boundary conditions. The interfacial conditions noted from the present pore scale and REV scale modeling may be of interest to domain scale modeling of flow and heat transfer condition at the interface between fluid and porous

media.

A domain scale modeling based on the lattice Boltzmann equations was developed for flow systems with regions of homogenous fluid and porous medium. The two domains were coupled by the stress jump interfacial boundary condition of Ochoa-Tapia and Whitaker (1995a, 1995b, 1998). A treatment of the velocity and distribution functions at the interface was described. The interfacial velocity was calculated with the difference approximation of the velocity gradient derivatives in the stress jump condition. Then the updated interfacial velocity was used to update the distribution functions at the interface. This interfacial treatment was applied to simulate coupled flow problems such as channel flow, porous plug and cavity flow. These cases cover a variety of situations where the major flow is parallel, perpendicular and oblique to the interface. The stress jump parameter has more effect when the velocity is parallel to the interface. The results are in consistent with the analytical and/or finite-volume results.

The developed numerical method was then implemented to study a microchannel reactor with a porous wall. To characterize the mass transfer in the porous medium the porous Damkohler number $Dam_{pa}$ is defined as the ratio of consumption to diffusion of the substrates in the porous medium. The convective and diffusion time scales in the fluid region is characterized by an effective distance $\frac{x}{H}\frac{1}{Pe_f}$. The simplified analytical solutions indicate that the concentration should be normalized by the Damkohler number $Dam_{pa}$, Michaelis-Menten constant $K_m$ and release ratio $a$. The normalized numerical data, of the interface concentration and concentration

difference, show satisfactory correlation when presented as a function of the effective distance $\frac{x}{H}\frac{1}{Pe_f}$. To quantify the local mass transfer resistance along the length of the porous medium, an effectiveness factor is defined. The effectiveness factor varies from around 0.9 to 0.6 for reaction close to Michaelis-Menten type, and around 0.85, for reaction close to first order type. The reactor efficiency (averaged over length) is the ratio of actual reaction-rate over the maximum reaction rate (based on the inlet concentration). The reactor efficiency varies from around 0.85 to 0.6 for reaction close to Michaelis-Menten type, and around 0.7 for reaction close to first order type. The utilization efficiency (or conversion rate) is the ratio of actual utilized mass rate over the inlet mass rate. The utilization efficiency incorporates the effects of the porous medium, reactor length and fluid convection. The utilization efficiency varies from around 0 to 0.8 for reaction close to Michaelis-Menten type, and around 0 to 0.15 for reaction close to first order type. The results show that for both types of reactions, the utilization efficiencies are very low at small effective length $\frac{\mathrm{L}}{\mathrm{H}\cdot\mathrm{Pe}_f}$.

## 7.2 Recommendations

In the present study, because the boundary element method was employed to solve fibrous porous medium, the pore scale investigations were restricted to slow viscous flows. In the future work, the pore scale investigations could be extended to high Reynolds number flow system, which has wide applications in engineering, such as cooling fins, condenser, etc. This may be achieved by the lattice Boltzmann

method. A more complex three dimensional irregular but periodic pore structures could also be investigated using irregular granular pores and structures. A three dimensional combustion simulation in porous media using LBM had been presented by Yamamoto et al. (2005). The numerical results could be implemented to heat transfer applications, such as heat exchangers with fins. Several experiments can be designed to further study the interfacial conditions. These experiments could contribute on showing the physical characteristics of interfacial conditions. Fibrous porous medium modelled by titanic wires matrix with very small diameter (as thin as hair, practical and low cost), having specially designed structure to position titanic wires with capability for fine tuning of distance between wires. The porosity and permeability are changed by adjusting distance between wires. The low Reynolds number channel flow will be studied, and the constant inlet pressure maintained. The small and constant diameter titanic wires minimize effect of local geometry on interfacial conditions. The observed velocity will be nearly volume averaged. The titanic wire is highly corrosion resistant with little fouling and good for repeatable and reliable flow data collect.

# References


Abu-Hijleh, B., Convection heat transfer from a laminar flow over a 2-D backward facing step with asymmetric and orthotropic porous floor segments, *Numerical Heat Transfer A*, 31, pp. 25-335, 1997.

Abu-Hijleh, B., Heat transfer from a 2D backward facing step with isotropic porous floor segments, *International Journal of Heat and Mass Transfer*, 43, pp. 2727-2737, 2000.

Alazmi B. and Vafai K., Analysis of Fluid Flow and Heat Transfer Interfacial Conditions between a Porous Medium and a Fluid Layer, *Int. J. Heat Mass Transfer*; 44: 1735-1749, 2001

Al-Muftah A.E. and Abu-Reesh I.M., Effects of simultaneous internal and external mass transfer and product inhibition on immobilized enzyme-catalyzed reactor, *Biochem. Eng. J.* **27** (2), pp. 167–178. 2005

Anderson, E.J., Cooke, M.N., Savrin, J., Dean, D., and Knothe Tate, M.L. Performance evaluation of tissue engineering scaffolds—development of a novel tool for optimization of fluid flow & permeability. *Abstract presented at the Summer Bioengineering Conference, Vail, CO*, 2005.

Assato, M., Pedras, M. H. J. and Delemos, M. J. S., Numerical solution of turbulent channel flow past a backward-facing-step with a porous insert using linear and non-linear k-$\varepsilon$ models, *Journal of Porous Media*, 8, pp. 13-29, 2005.

Bai Huixing, Yu P, Winoto SH, and Low HT, Boundary conditions at the interface between fluid layer and fibrous medium, *International Journal for Numerical Methods in Fluids* 60, 809-825, 2009a

Bai Huixing, Yu P, Winoto SH, and Low HT, Lattice Boltzmann method for flows in porous and homogenous fluid domains coupled at the interface by stress jump, *International Journal for Numerical Methods in Fluids* 60, 691-708, 2009b.

Bancroft, G. N., Sikavitsas, V. I. and Mikos A. G., Design of a flow perfusion bioreactor system for bone tissue-engineering applications, *Tissue Engineering*, 9 (3), pp. 549-554, 2003.

Basu, A. J., and Khalili, A., Computation of flow through a fluid-sediment interface in a benthic chamber, *Physics of Fluids*, 11, pp. 1395-1405, 1999.

Beavers G. S., D. D. Joseph, Boundary conditions at a naturally permeable wall, *J. Fluid Mech*.; 30: 197-207, 1967

Bennacer, R., Beji, H. and Mohamad, A. A., Double diffusive convection in a vertical enclosure inserted with two saturated porous layers confining a fluid layer. *International Journal of Thermal Sciences*, 42, pp. 141-151, 2003.

Bera, P., Eswaran, V. and Singh, P., Numerical study of heat and mass transfer in an anisotropic porous enclosure due to constant heating and cooling, *Numerical Heat Transfer A*, 34, pp. 887-905, 1998.

Betchen L, Straatman AG and Thompson BE, A Nonequilibrium Finite-Volume Model for Conjugate Fluid/Porous/Solid Domains, *Numer. Heat Transfer A*,; 49: 543-565. 2006

Bhatia S., Long W.S. and Kamaruddin A.H., Enzymatic membrane reactor for the kinetic resolution of racemic ibuprofen ester: modeling and experimental studies, *Chem. Eng. Sci.* **59** (22–23), pp. 5061–5068. 2004

Bhattacharya, A. and Mahajan, R. L., Finned metal foam heat sinks for electronics cooling in forced convection, *Journal of Electronic Packaging*, 124, pp. 155-163, 2002.

Bhattacharyya, S., Dhinakaran, S. and Khalili, A., Fluid motion around and through a porous cylinder, *Chemical Engineering Science*, 61, pp. 4451-4461, 2006a.

Bhattacharyya, S., Maiti, D. K. and Dhinakaran, S., Influence of buoyancy on vortex shedding and heat transfer from a square cylinder in proximity to a wall, *Numerical Heat Transfer A*, 50, pp. 585-606, 2006b.

Barrere J, Gipouloux O, Whitaker S. On the closure problem for Darcy's law. *Transport in Porous Media*, **7**, 209–222, 1992

Boschetti, F., Raimondi, M. T., Migliavacca, F., and Dubini, G., Prediction of the Micro-Fluid Dynamic Environment Imposed to Three-Dimensional Engineered Cell Systems in Bioreactors, J. Biomech., **39**, pp. 418–425. 2006

Brinkman, H. C., A calculation of the viscous force exerted by a flowing fluid on a dense swarm of particles, *Applied Scientific Research, A1*, pp. 27-34, 1947a.

Brinkman, H. C., On the permeability of media consisting of closely packed porous particles, *Applied Scientific Research, A1*, pp. 81-86, 1947b.

Bruschke M. V. and Advani S. G., Flow of generalized Newtonian fluids across a periodic array of cylinders, *J. Rheol*.; 37 (3): 479-498. 1993

Cantini, Marco, Fiore, Gianfranco B.; Redaelli, Alberto; Soncini, Monica, Fluid flow through granular beds. *Tissue Engineering - Part A*, v 15, n 3, p 615-623, March 1, 2009

Carman, P. C., Fluid flow through granular beds. *Trans. Inst. Chem. Engrs*; 15: 150-166, 1937

Carslaw, H. S. and Jaeger, J. C., "Conduction of heat in solids", London, *Oxford University Press*. 1959.

Chandesris M., D. Jamet, Boundary conditions at a planar fluid-porous interface for a Poiseuille flow, *Int. J. Heat Mass Transfer*; 49 (13-14): 2137-2150. 2006

Chen Shiyi, Daniel Martinez and Renwei Mei, On boundary conditions in lattice Boltzmann methods, *Phys. Fluids*; 8(9): 2527-2536. 1996

Chen X.B., Y. Sui, H.P. Lee, H.X. Bai, P. Yu, S.H. Winoto and H.T. Low, Mass transport in a microchannel bioreactor with a porous wall, *J. Biomech. Eng.* 132 (6), p. 061001, 2010

Chen Yitung, Chen Huajun and Zhang Jinsuo, Numerical investigation on enhancement of oxygen transfer by forced convection in liquid lead-bismuth eutectic system, *Int. J. Heat and Mass Transfer***.** 50 (11), pp. 2139–2147. 2007

Chow D.C., L.A. Wenning, W.M. Miller and E.T. Papoutsakis, Modeling pO2 distributions in the bone marrow hematopoietic compartment. I. Krogh's model, *Biophys. J.* 81, pp. 675–684. 2001a

Chow D.C., L.A. Wenning, W.M. Miller and E.T. Papoutsakis, Modeling pO2 distributions in the bone marrow hematopoietic compartment. II. Modified Krogh's models, *Biophys. J.* 81, pp. 685–696. 2001b

Chung, C. A., Chen, C. W., Chen, C. P., and Tseng, C. S., Enhancement of Cell Growth in Tissue-Engineering Constructs Under Direct Perfusion: Modeling and Simulation, *Biotechnol. Bioeng.*, 97(6), pp. 1603–1616. 2007

Cioffi, M., Boschetti, F., Raimondi, M.T., and Dubini, G. Modeling evaluation of the fluid-dynamic microenvironment in tissue-engineered constructs: a micro-CT based model. *Biotechnol Bioeng* 93, 500, 2006.

Cooper, J. A., Lu, H. H., Ko, F. K., Freeman, J. W., and Laurencin, C. T., Fiber-Based Tissue-Engineered Scaffold for Ligament Replacement: Design Considerations and In Vitro Evaluation, *Biomaterials, 26, pp. 1523–1532.* 2005

Costa VAF, Oliveira LA, Baliga BR and Sousa ACM, Simulation of Coupled Flows in Adjacent Porous and Open Domains Using a Control-Volume Finite-Element Method, *Numer. Heat Transfer A*; 45: 675-697. 2004

De Vahl Davis, Natural convection of air in a square cavity: a bench mark solution. *International Journal of Methods of Fluids*, 3, 249-264, 1983

Dhanasekharan, K.M., Sanyal, J., Jain, A., and Haidari, A. A generalized approach to model oxygen transfer in bioreactors using population balances and computational fluid dynamics. *Chem Eng Sci* 60, 213, 2005.

Drott J., K. Lindstrom, L. Rosengren and T. Laurell, Porous silicon as the carrier matrix in microstructured enzyme reactors yielding high enzyme activities, *J. Micromech. Microeng.* **7** (1), pp. 14–23. 1997

Drott J., L. Rosengren, K. Lindstrom and T. Laurell, Porous silicon carrier matrices in micro enzyme reactors-influence of matrix depth, *Mikrochim. Acta* 131, pp. 115–120. 1999

Drummond J. E. and Tahir M. I., Laminar viscous flow through regular arrays of parallel solid cylinders. *Int. J. Multiphase Flow*; 10 (5): 515-540. 1984

Dusting, J., Sheridan, J. and Hourigan, K., A fluid dynamic approach to bioreactor design for cell and tissue culture, *Biotechnology and Bioengineering*, 94, pp. 1197–1208, 2006.

Dvir, T., Benishti, N., Shachar, M., and Cohen, S. A novel perfusion bioreactor providing a homogenous milieu for tissue regeneration. *Tissue Eng* 12, 2843, 2006.

Esterl S., Ozmutlu O., Hartmann C. and Delgado A., Three-dimensional numerical approach to investigate the substrate transport and conversion in an immobilized enzyme reactor. *Biotechnology and Bioengineering*, v 83, n 7, p 780-789, September 30, 2003

Ettefagh, J., Vafai, K., and Kim, S. J., Non-Darcian effects in open-ended cavities filled with a porous medium, *ASME Journal of Heat Transfer*, 113, pp. 747-756, 1991.

Ferziger, J. H. and Perić, M., Computational methods for fluid dynamics, 2nd ed., pp. 222-233, Springer, Berlin, 1999.

Forchheimer, P., Wasserbewegung durch Boden, Zeits. Ver. Deutsch. Ing., 45, pp. 1782-1788, 1901.

Fu, W.-S., Huang, H..-C. and Liou, W.-Y., Thermal enhancement in laminar channel flow with a porous block, *International Journal of Heat and Mass Transfer*, 39 (10), pp. 2165-2175, 1996.

Galbusera, F., Cioffi, M., Raimodi, M.T., and Pietrabissa, R. Computational modeling of combined cell population dynamics and oxygen transport in engineered tissue subject to interstitial perfusion. *Comput Methods Biomech Biomed Engin* 10, 279, 2007.

Gartling DK, Hickox CE and Givler RC, Simulation of Coupled Viscous and Porous Flow Problems, *Comp. Fluid Dyn.*; 7: 23-48. 1996

Gartling, D. K., A test problem for outflow boundary conditions flow over a backward-facing step, *International Journal for Numerical Methods in Fluids*, 11, pp. 953-967, 1990.

Gemmiti, C. V., and Guldberg, R. E., Fluid Flow Increases Type II Collagen Deposition and Tensile Mechanical Properties in Bioreactor Grown Tissue Engineered Cartilage, *Tissue Eng., 12, pp. 469–479.* 2006

Ghia, U., Ghia, K. N. and Shim, C. T., High-Re solutions for incompressible flow using the Navier-Stokes equations and a multigrid method, *Journal of Computational Physics*, 48, pp. 387-411, 1982.

Gilver R.C., Altobelli S.A., A determination of the effective viscosity for the Brinkman-Forchheimer flow model, *J. Fluid Mech.*; 258: 355-370. 1994

Gobin, D., Goyeau, B. and Neculae, A., Convective heat and solute transfer in partially porous cavities, *International Journal of Heat and Mass Transfer*, 48, pp. 1898-1908, 2005.

Goyeau B, Lhuillier D, Gobin D and Velarde MG, Momentum Transport at a Fluid-Porous Interface, *Int. J. Heat Mass Transfer*, vol. 46, pp. 4071-4081, 2003.

Greenkorn, R. A., Steady flow through porous media, *AICHE Journal*, 27, pp. 529-545, 1981.

Griffith, L. G., and Swartz, M. A., Capturing Complex 3D Tissue Physiology In Vitro, *Nat. Rev. Mol. Cell Biol., 7, pp. 211–224.* 2006

Guo Zhaoli and Shi Baochang and Wang Nengchao, Lattice BGK model for incompressible Navier-Stokes equation, *J. Computational. Physics*; 165: 288-306. 2000

Guo Zhaoli and Zhao T.S., Lattice Boltzmann model for incompressible flows through porous media, *Physical Review E.*; 66: 036304. 2002

Guo Zhaoli, Zheng Chuguang and Shi Baochang, Discrete lattice effects on the forcing term in the lattice Boltzmann method, *Physical Review E.*; 65: 046308. 2002

Guo Zhaoli, Zhao T. S. and Shi Yong, Preconditioned lattice-Boltzmann method for steady flows, *Physical Review E.*; 70: 066706. 2004

Guo Zhaoli and Zhao T.S., A lattice Boltzmann model for convection heat transfer in porous media, *Numerical Heat Transfer, Part B*; 47: 157-177. 2005

Happel, J., Viscous Flow Relative to Arrays of Cylinders, *AIChE J.*; 5: 174-177, 1959

Hasimoto, H., On the Periodic Fundamental Solutions of the Stokes Equations and their Application to Viscous Flow Past a Cubic Array of Cylinders, *J. Fluid Mech.*; 5 (2): 317-328, 1959

He X. Y., Chen S. Y. and Doolen G. D., A novel thermal model for the lattice Boltzmann method in incompressible limit, *J. Comput. Phys.*; 146: 282-300. 1998

Horta A., Alvarez J.R. and Luque S., Analysis of the transient response of a CSTR containing immobilized enzyme particles—Part I. Model development and analysis of the influence of operating conditions and process parameters, *Biochem. Eng. J.* 33 (1), pp. 72–87. 2007

Hou S., Zou Q., Chen S., G.D. Doolen, A.C. Cogley, Simulation of cavity flow by the Lattice Boltzmann method, *J. Comput. Phys.*; 118: 329-347. 1995

Hsu, C. T. and Cheng, P., Thermal dispersion in a porous medium, *International Journal of Heat and Mass Transfer*, 33, pp. 1587-1597, 1990.

Huang, P. C. and Vafai, K., Analysis of forced convection enhancement in a channel using porous blocks, *Journal of Thermophysics and Heat Transfer*, 8 (3), pp. 563-573, 1994a.

Huang, P. C. and Vafai, K., Internal heat transfer augmentation in a channel using an alternate set of porous cavity-block obstacles, *Numerical Heat Transfer A*, 25, pp. 519-539, 1994b.

James David F. and Davis Anthony M. J., Flow at the interface of a model fibrous porous medium, *J. Fluid Mech.*; 426: 47-72, 2001

Jue TC, Numerical Analysis of Vortex Shedding Behind a Porous Cylinder, *Int. J. Numer. Methods Heat Fluid Flow*; 14: 649-663. 2004

Kaviany M., Principles of Heat Transfer in Porous Media. Springer: New York, 1991

Keller, J.B., Viscous flow through a grating or lattice of cylinders, *J. Fluid Mech.*; 18 (1): 94-96. 1964

Kim SJ and Choi CY, Convection heat transfer in porous and overlying layers heated from below, *Int. J. Heat Mass Transfer*; 39: 319-329. 1996

Kozeny, C. F., Uber kapillare Leitung des Wassers im Boden. Sitz. Akad. Wissensh., 136: 271-306, 1927

Kuwabara, S., The Forces Experienced by Randomly Distributed Parallel Circular Cylinders or Spheres in a Viscous Flow at Small Reynolds Numbers, *J. Phys. See. Japan*; 14 (4): 527-532. 1959

Kuznetsov, A. V., Fluid mechanics and heat transfer in the interface region between a porous medium and a fluid layer: a Boundary Layer Solution, *Journal of Porous Media*, 2 (3), pp. 309-321, 1999.

Lapwood, E. R., Convection of a fluid in a porous medium, *Proceedings of Cambridge Philosophical Society*, 44, pp. 208-521, 1948.

Larson R. E. and J. L. Higdon, Microscopic flow near the surface of two-dimensional porous media. Part 2. Transverse flow, *J. Fluid Mech*.; 178: 119-136. 1987

Lee T. S., Early stages of an impulsively started unsteady laminar flow past tapered trapezoidal cylinders, *International Journal for Numerical Methods in Fluids*, 26, pp. 1181-1203, 1998a.

Lee, T. S., Numerical study of early stages of an impulsively started unsteady laminar flow past expanded trapezoidal cylinders, *International Journal of Numerical Methods for Heat and Fluid Flow*, 8, pp. 934-955, 1998b.

Lysenko V., Vitiello J., B. Remaki and D. Barbier, Gas permeability of porous silicon nanostructures. Part 2, *Phys. Rev. E* 70 (1) 017301. 2004

Ma, C.Y.J., Kumar, R., Xu, X.Y., and Mantalaris, A. A combined fluid dynamics, mass transport and cell growth model for a three-dimensional perfused bioreactor for tissue engineering of haematopoietic cells. *Biochem Eng J* 35, 1, 2007.

Mahmoudifar, N. and Doran, P. M., Tissue Engineering of human cartilage in bioreactors using single and composite cell-seeded scaffolds, *Biotechnology and Bioengineering*, 91 (3), pp. 338-55, 2005

Martin, I., Wendt, D., and Heberer, M. The role of bioreactors in tissue engineering. Trends, *Biotechnol* 22, 80, 2004.

McClelland, R. E., MacDonald, J. M., and Coger, R. N., Modeling $O_2$ Transport Within Engineered Hepatic Devices, *Biotechnol. Bioeng., 82(1), pp. 12–27.* 2003

Melander C., Bengtsson M., Schagerlof H., Tjerneld F., T. Laurell, and L. Gorton, Investigation of micro-immobilised enzyme reactors containing endoglucanases for efficient hydrolysis of cellodextrins and cellulose derivatives, *Analytica Chimica Acta* 550, 182–190. 2005

Melander C., Tüting W., Bengtsson M., T. Laurell, P. Mischnick and L. Gorton, Hydrolysis of maltoheptaose in flow through silicon wafer microreactors containing immobilised α-amylase and glycoamylase, *Starch-Stärke* 58, pp. 231–242. 2006

Mercier J, Weisman C, Firdaouss M and Quéré PL, Heat Transfer Associated to Natural Convection Flow in a Partly Porous Cavity, *ASME J. Heat Transfer*; 124: 130-143. 2002

Michael, L. S., and Fikret, K., *Bioprocess Engineering: Basic Concepts*, Prentice-Hall, Englewood Cliffs, NJ. 1992

Miyazaki M. and Maeda H., Microchannel enzyme reactors and their applications for processing, *Trends Biotechnol.* 24 (10), pp. 463–470. 2006

Neale G and Nader W, Practical Significance of Brinkman's Extension of Darcy's Law: Coupled Parallel Flows within a Channel and a Bounding Porous Medium, *Can. J. Chem. Engrg.*; 52: 475-478. 1974

Nicos S. Martys, Improved approximation of the Brinkman equation using a lattice Boltzmann method, *Physics of Fluids*; 13: 1807-1810. 2001

Nield DA, Discussion, *ASME J. Heat Transfer*; 119: 193-194. 1997

Nithiarasu P., Seetharamu K.N. and Sundararajan T., Natural convective heat transfer in a fluid saturated variable porosity medium. *Int. J. Heat Mass Transfer*. Vol. 40, NO. 16, pp3955-3967, 1997

Ochoa-Tapia J. A. and Whitaker S., Momentum Transfer at the Boundary between a Porous Medium and a Homogeneous Fluid I: Theoretical Development, *Int. J. Heat Mass Transfer*; 38: 2635-2646, 1995a

Ochoa-Tapia J. A. and Whitaker S., Momentum Transfer at the Boundary between a Porous Medium and a Homogeneous Fluid II: Comparison with Experiment, *Int. J. Heat Mass Transfer*; 38: 2647-2655. 1995b

Ochoa-Tapia, J. A. and Whitaker, S., Heat transfer at the boundary between a porous medium and a homogeneous fluid, *International Journal of Heat and Mass Transfer*, 40, pp. 2691-2707, 1997.

Ochoa-Tapia, J. A. and Whitaker, S., Heat transfer at the boundary between a porous medium and a homogeneous fluid: the One-equation model, *Journal of Porous Media*, 1, pp. 31-46, 1998a.

Ochoa-Tapia J.A. and Whitaker S., Momentum jump condition at the boundary between a porous medium and a homogeneous fluid: inertial effect, *J. Porous Media* **1**, pp. 201–217. 1998b

Pathi, P., Ma, T., and Locke, B. R., Role of Nutrient Supply on Cell Growth in Bioreactor Design for Tissue Engineering of Hematopoietic Cells, *Biotechnol. Bioeng., 89(7), pp. 743–758*. 2005

Pierre, J., Gemmiti, C. V., Kolambkar, Y. M., Oddou, C., and Guldberg, R. E., Theoretical Analysis of Engineered Cartilage Oxygenation: Influence of Construct Thickness and Media Flow Rate, *Biomech. Model. Mechanobiol., 7(6), pp. 497–510. 2*008

Porter, B., Zauel, R., Stockman, H., Guldberg, R., and Fyhrie, D., 3-D Computational Modeling of Media Flow Through Scaffolds in a Perfusion Bioreactor, *J. Biomech., 38(3), pp. 543–549*. 2005

Pozrikidis Costas., Boundary integral and singularity methods for linearized viscous flow, *Cambridge University Press*, Cambridge, 1992

Pozrikidis Costas., A practical guide to boundary element methods with the software library BEMLIB, *Chapman & Hall/CRC*, New York, 2002

Rayleigh, Lord. On the influence of obstacles arranged in rectangular order upon the properties of a medium. *Phil. Mag.*; 34: 481-502. 1892

Raimondi, M.T., Boschetti, F., Falcone, L., Fiore, G.B., Remuzzi, A., Marinoni, E., Marazzi, M., and Pietrabissa, R. Mechanobiology of engineered cartilage cultured under a quantified fluid-dynamic environment. *Biomech Model Mechanobiol* 1, 69, 2002.

Raimondi, M.T., Boschetti, F., Falcone, L., Migliavacca, F., Remuzzi, A., and Dubini, G. The effect of media perfusion on three-dimensional cultures of human chondrocytes: Integration of experimental and computational approaches. *Biorheology* 41, 401, 2004.

Sadiq T. A. K., Advani S.G. and Parnas R.S., Experimental investigation of transverse flow through aligned cylinders. *Int. J. Multiphase Flow*,; 21: 755-774. 1995

Sahraoui M. and Kaviany M., Slip and no-slip velocity boundary conditions at interface of porous, plain media, *Int. J. Heat Mass Transfer*; 35: 927-943. 1992

Sangani, A. S. and A. Acrivos, Slow Flow Through a Periodic Array of Spheres, *Int. J. Multiphase Flow*; 8 (4): 343-360. 1982

Sangani, A. S. and A. Acrivos, A Slow Flow Past Periodic Arrays of Cylinders with Application to Heat Transfer, *Int. J. Multiphase Flow*; 8 (3): 193-201. 1982

Sengers, B.G., van Donkelaar, C.C., Oomens, C.W., and Baaijens, F.P. Computational study of culture conditions and nutrient supply in cartilage tissue engineering. *Biotechnol Prog* 21, 1252, 2005.

Shi Yong, Zhao T. S. and Guo Zhaoli, Lattice Boltzmann method for incompressible flows with large pressure gradients, *Physical Review E*.; 73: 026704. 2006

Shu C., Peng Y. and Chew Y.T, Simulation of natural convection in a square cavity by Taylor series expansion- and least squares-based Lattice Boltzmann method, *Int. J. Modern Physics C*.; 13 (10): 1399-1414. 2002Silva RA and de Lemos MJS, Numerical Analysis of the Stress Jump Interface Condition for Laminar Flow Over a Porous Layer, *Numer. Heat Transfer A*; 43: 603-617. 2003

Singh, H., Teoh, S.H., Low, H.T., and Hutmacher, D.W. Flow modelling within a scaffold under the influence of uniaxial and bi-axial bioreactor rotation. *J Biotechnol* 119, 181, 2005.

Taylor G. I., A model for the boundary condition of a porous material. Part 1, *J. Fluid Mech*.; 49: 319-326, 1971

Tilles, A. W., Baskaran, H., Roy, P., Yarmush, M. L. and Toner, M., Effects of oxygenation and flow on the viability and function of rat hepatocytes co-cultured in a microchannel flat-plate bioreactor, *Biotechnol. Bioeng*. 73, pp. 379-389. 2001.

Tmej F., Limbergova Z. and Hasal P., Modelling and optimisation of enzymatic separating micro-reactor, *Bioprocess Biosyst. Eng*. 28 (2), pp. 123–130. 2005

Urban P.L., D.M. Goodall and N.C. Bruce, Enzymatic microreactors in chemical analysis and kinetic studies, *Biotechnol. Adv*. 24 (1), pp. 42–57. 2006

Vafai, K., and Tien, C. L., Boundary and Inertia Effects on Flow and Heat Transfer in Porous Media, *Int. J. Heat Mass Transfer, 24, pp. 195–203*. 1981

Vafai, K., and Tien, C. L., Boundary and Inertia Effects on Convective Mass Transfer in Porous Media, *Int. J. Heat Mass Transfer, 25, pp. 1183–1190*. 1982

Vafai, K and S. J. Kim, Fluid Mechanics of the Interface Region between a Porous Medium and a Fluid Layer – an exact solution, *Int. J. Heat Fluid Flow*; 11: 254-256. 1990

Vafai, K and R. Thiyagaraja, Analysis of flow and heat transfer at the interface region of a porous medium, *Int. J. Heat Mass Transfer*; 30: 1391-1405. 1987

Wang C. Y., Stokes flow through an array of rectangular fibers. *Int. J. Multiphase Flow*, 22 (1): 185-194. 1996

Wang C. Y., Longitudinal flow past cylinders arranged in a triangular array. *Applied Mathematical Modeling*; 23 (3): 219-230. 1999

Wang C. Y., Stokes flow through a rectangular array of circular cylinders, *Fluid Dynamics Research*; 29 (2): 65-80. 2001

Wang C. Y., Forced flow through a channel with longitudinal strips, *Mech. Res. Comm.* Vol. 36 , 735-741. 2009

Wang S., and Tarbell, J. M., Effect of Fluid Flow on Smooth Muscle Cells in a 3-Dimensional Collagen Gel Model, *Arterioscler., Thromb., Vasc. Biol*., 20, pp. 2220–2225. 2000

Williams K.A., Saini, S., and Wick, T.M. Computational fluid dynamics modeling of steady-state momentum and mass transport in a bioreactor for cartilage tissue engineering. *Biotechnol Prog* 18, 951, 2002.

Whitaker Stephen, The method of volume averaging, *KLUWER ACADEMIC PUBLISHERS*, Dordrecht / Boston / London, 1999

Wood B.D. and Whitaker S., Multi-species diffusion and reaction in biofilms and cellular media, *Chem. Eng. Sci.* **55**, pp. 3397–3418. 2000

Wood B.D., M. Quintard and S. Whitaker, Calculation of effective diffusivities for biofilms and tissues, *Biotechnol. Bioeng.* **77**, pp. 495–516. 2002

Yamamoto K., Takada N. and Misawa M., Combustion simulation with lattice Boltzmann method in a three-dimensional porous structure, *Proceedings of the Combustion Institute.* **30**, pp. 1509–1515. 2005

Ye H., D.B. Das, J.T. Triffitt and Z.F. Cui, Modelling nutrient transport in hollow fibre membrane bioreactors for growing three-dimensional bone tissue, *J. Membr. Sci.* **272** , pp. 169–178. 2006

Yin, C. S., Dynamics of nonhomogeneous fluids, Macmillan, New York, 1965.

Yu, P., Zeng, Y.; Lee, T.S.; Low, H.T. A numerical analysis of cell density effect on oxygen transport in a micro-bioreactor with a tissue engineering scaffold, *International Communications in Heat and Mass Transfer, v 36, n 6, p 569-73, July* 2009

Yu P., T. S. Lee, Y. Zeng and H. T. Low, A numerical method for flows in porous and homogenous fluid domains coupled at the interface by stress jump, *Int. J. Numer. Meth. Fluids*; 53: 1755-1775. 2007

Yu P, Zeng Y, Lee TS, Bai HX, and Low HT, Wake Structure for Flow past and through a Porous Square Cylinder, *International Journal of Heat and Fluid Flow*, 31, 141-153, 2010

Zeng Y., T.S. Lee, P. Yu and H.T. Low, Mass transport and shear stress in a microchannel bioreactor: numerical simulation and dynamic similarity, *J. Biomech. Eng*. 128, pp. 185–193. 2006

Zeng Y., T.S. Lee, P. Yu and H.T. Low, Numerical simulation on mass transport in a microchannel bioreactor for co-culture applications, *J. Biomech. Eng.* 129, pp. 365–373. 2007

Zeng Y., T.S. Lee, P. Yu and H.T. Low, Numerical simulation of mass transport in a microchannel bioreactor with cell micropatterning, *J. Biomech. Eng.* 130, pp. 1883–1900. 2008

Zhang Haifeng, Lattice Boltzmann method for solving the bioheat equation, *Physics in Medicine and Biology*. 53, pp. 15–23. 2008

Zhao, F., and Ma, T., Perfusion Bioreactor System for Human Mesenchymal Stem Cell Tissue Engineering: Dynamic Cell Seeding and Construct Development, *Biotechnol. Bioeng.*, 91(4), pp. 482–493. 2005

Zhao, F., Pathi, P., Grayson, W., Xing, Q., Locke, B. R., and Ma, T., Effects of Oxygen Transport on 3-D Human Mesenchymal Stem Cell Metabolic Activity in Perfusion and Static Cultures: Experiments and Mathematical Model, *Biotechnol. Prog.*, 21(4), pp. 1269–1280. 2005

Zhao, F., Chella, R., and Ma, T., Effects of Shear Stress on 3-D Human Mesenchymal Stem Cell Construct Development in a Perfusion Bioreactor System: Experiments and Hydrodynamic Modeling, *Biotechnol. Bioeng.*, 96(3), pp. 584–595. 2007